ENERGY ANALYTICS FOR ECO-FEEDBACK DESIGN IN MULTI-FAMILY RESIDENTIAL BUILDINGS

by

Sang woo Ham

A Dissertation

Submitted to the Faculty of Purdue University

In Partial Fulfillment of the Requirements for the degree of

Doctor of Philosophy

Lyles School of Civil Engineering

West Lafayette, Indiana

August 2021

THE PURDUE UNIVERSITY GRADUATE SCHOOL
STATEMENT OF COMMITTEE APPROVAL

Dr. Panagiota Karava, Chair
Lyles School of Civil Engineering

Dr. James E. Braun
School of Mechanical Engineering

Dr. Ilias Bilionis
School of Mechanical Engineering

Dr. Travis Horton
Lyles School of Civil Engineering

Approved by:
Dr. Dulcy M. Abraham
Chair of the Graduate Program

For my parents and brother.

ACKNOWLEDGMENTS

I am very privileged to have an opportunity to work in one of the best research institutions in the building industry, and I would like to express my sincere gratitude to my advisor, Professor Panagiota Karava to give me the opportunity with a relentless trust. I personally confronted various challenges in my life and research, but she helped me to overcome them in both direct and indirect ways based on her in-depth knowledge and experience. What I had in my life at Purdue with her is not just research, knowledge, or technical things. I am very lucky to meet someone like her to work with passion, insight, execution, and vision under common responsibility and trust.

I would like to thank Professor James E. Braun for helping us as a project mentor. His insight, experience, and passion in the building research are so valuable, and it is my personal honor to have an opportunity to work with him and see what the best practice of a project mentor is. I would like to thank Professor Ilias Bilionis for helping me learn and explore methodologies for my research. Life is working in a Bayesian way, and his comments and ways of thinking bring me to the Bayesian way, and this enhance my view of how to look at the problem in more meaningful way. I would like to thank Professor Travis Horton for his invaluable comments.

I would like to thank for all my colleagues at Purdue. It is my luck to meet Huijeong who can work with me more than 7 years with trust. I am also proud of us to move the project forward. I also thank for the project team members, Marlen, Hemanth, and Vanessa, for their relentless devotions. I appreciate Seungjae helping me out when I have troubles in my research and life. His brilliant and delicate attitude toward the research always motivate me. Also, I met great people in Herrick, Jaewan, Michael, Clare, and Kyeongsuk, and I thank the time with them at Purdue. I thank for all my friends at Purdue and PKTC. I cannot imagine how I survive here with my tennis friends. Also, I really appreciate my Korean friends, Yongjun, Sungwon, Daejong, and Seunghee to give me consolation and courage.

Finally, most importantly, I can never thank my parents, Seungjong, Youngsoon, and brother and my brother, Sanghun, enough. Our family does not have adorable personal characteristics, but we respect and trust each other, and they always support me with 100% trust. I am proud of myself to do my all responsibility toward their trust. I had so many coincidences in my life and research, so I never knows what will happen in the future, but I would like to thank everyone in my life that affect me.

TABLE OF CONTENTS

LIST OF TABLES

LIST OF FIGURES

ABSTRACT

The residential sector is responsible for approximately 21% of the total energy use in the U.S. As a result, there have been various programs and studies aiming to reduce energy consumption and utility burden on individual households. Among various energy efficiency strategies, behavior-based approaches have received considerable attention because they significantly affect operational energy consumption without requiring building upgrades. For example, up to 30% of heating and cooling energy savings can be achieved by having an efficient temperature setpoint schedule. Such approaches can be particularly beneficial for multi-family residential buildings because 88% of their residents are renters paying their own utility bills without being allowed to upgrade their housing unit.

In this context, eco-feedback has emerged as an approach to motivate residents to reduce energy use by providing information (feedback) on human behavior and environmental impact. This research has gained significant attention with the development of new smart home technology such as smart thermostats and home energy management systems. Research on the design of effective eco-feedback focuses on how to motivate residents to change their behavior by identifying and notifying implementable actions in a timely manner via energy analytics such as energy prediction models, energy disaggregation, etc.

However, unit-level energy analytics pose significant challenges in multi-family residential buildings tasks due to the inter-unit heat transfer, unobserved variables (e.g., infiltration, human body heat gain, etc.), and limited data availability from the existing infrastructure (i.e., smart thermostats and smart meters). Furthermore, real-time model inference can facilitate up-to-date eco-feedback without a whole year of data to train models. To tackle the aforementioned challenges, three new modeling approaches for energy analytics have been proposed in this Thesis is developed based on the data collected from WiFi-enabled smart thermostats and power meters in a multi-family residential building in IN, U.S.

First, this Thesis presents a unit-level data-driven modeling approach to normalize heating and cooling (HC) energy usage in multi-family residential buildings. The proposed modeling approach provides normalized groups of units that have similar building characteristics to provide the relative evaluation of energy-related behaviors. The physics-informed approach begins from a

heat balance equation to derive a linear regression model, and a Bayesian mixture model is used to identify normalized groups in consideration of the inter-unit heat transfer and unobserved variables. The probabilistic approach incorporates unit- and season-specific prior information and sequential Bayesian updating of model parameters when new data is available. The model finds distinct normalized HC energy use groups in different seasons and provides more accurate rankings compared to the case without normalization.

Second, this Thesis presents a real-time modeling approach to predict the HC energy consumption of individual units in a multi-family residential building. The model has a state-space structure to capture the building thermal dynamics, includes the setpoint schedule as an input, and incorporates real-time state filtering and parameter learning to consider uncertainties from unobserved boundary conditions (e.g., temperatures of adjacent spaces) and unobserved disturbances (i.e., window opening, infiltration, etc.). Through this real-time form, the model does not need to be re-trained for different seasons. The results show that the median power prediction of the model deviates less than 3.1% from measurements while the model learns seasonal parameters such as the cooling efficiency coefficient through sequential Bayesian update.

Finally, this Thesis presents a scalable and practical HC energy disaggregation model that is designed to be developed using data from smart meters and smart thermostats available in current advanced metering infrastructure (AMI) in typical residential houses without additional sensors. The model incorporates sequential Bayesian update whenever a new operation type is observed to learn seasonal parameters without long-term data for training. Also, it allows modeling the skewed characteristics of HC and non-HC power data. The results show that the model successfully predicts disaggregated HC power from 15-min interval data, and it shows less than 12% of error in weekly HC energy consumption. Finally, the model is able to learn seasonal parameters via sequential Bayesian update and gives good prediction results in different seasons.

1. INTRODUCTION

1.1 Background and motivation

The residential sector is responsible for approximately 21% of the total energy consumption in the U.S. (EIA, 2015). As a result, there have been various programs and studies (Better Buildings Initiative, 2019; Bourassa et al., 2012; Jones et al., 2015) aiming to reduce the energy consumption as well as the utility burden on individual households ($1850/year on average (EIA, 2015)). Studies report that $3.4 billion/year savings can be achieved for the 21 million households (1/6 of U.S. population) that live in multi-family residential buildings (Samarripas et al., 2017). Also, many low-income utility and public housing programs are designed for multi-family residential buildings (American Council for an Energy-Efficient Economy, 2020; Langevin et al., 2013; Reina & Kontokosta, 2017).

Since most multi-family buildings in metropolitan areas were built before the first energy code was adopted (Samarripas et al., 2017), many studies have focused on energy benchmarks (Energy Star, 2014b; Ghajarkhosravi et al., 2020) and simulation-based decision making (Malhortra et al., 2018; NREL, 2019) for building renovations (Salvalai et al., 2017) [13]. As a result, many successful case-studies are reported via weatherization (U.S. Department of Energy, 2018) and renovation (Salvalai et al., 2017) for multi-family residential buildings. However, approximately 88% of the residents in multi-family buildings in the US are renters who usually pay their own utility bill (Samarripas et al., 2017) and are not allowed to modify the building itself.

Recent studies emphasize that residents' energy-related behavior significantly affects operational energy consumption. It has been shown that up to 30% of heating and cooling (HC) energy savings are possible if residents adopt energy conserving behaviors such as efficient setpoint schedules (Rotondo et al., 2016). Furthermore, residents whose utility bills are included in their rent or subsidized tend to consume more energy than people who pay their own utility bills (Maruejols & Young, 2011; Reina & Kontokosta, 2017).

To address opportunities for reducing operational energy consumption in residences, two solutions have been examined: the automation of home energy systems (Nest Labs, 2015) and the provision of eco-feedback to motivate residents' energy efficient behavior (Froehlich et al., 2010). The most common practice in automation of home energy systems is to use a programmable

thermostat with an appropriate home/away/sleep setpoint schedule (CLEAResult, 2016; Energy Star, 2009). However, the benefits of programmable thermostats are often over-estimated because the energy use is compared with a fixed (and usually inefficient) setpoint scenario, which may not represent the actual thermostat adjustment behavior (Malinick et al., 2012). In addition, previous studies report that programmable thermostats are not often correctly used due to difficulties in usability (Meier et al., 2011) and a decrease in motivation (Sachs et al., 2012). This led to the development of smart thermostats that automatically set appropriate setpoint schedules based on data for household occupancy (G. Gao & Whitehouse, 2009; Kleiminger et al., 2014; Scott et al., 2011; Soltanaghaei & Whitehouse, 2018; Wörner et al., 2014) and residents' preferred setpoints (Nest Labs, 2015). However, this supervised type of home automation is often criticized because occupancy learning is difficult due to inherent randomness while residents express concerns with the loss of controllability and predictability (Pritoni et al., 2016; R. Yang et al., 2014, 2016; R. Yang & Newman, 2012).

Eco-feedback research follows a different approach by encouraging residents' energy conserving behavior. Based on intervention theory, when the gap between the current behavior and intervention-provided standards draws the attention of residents, they may regulate their behavior (Karlin et al., 2015). Eco-feedback hypothesizes that people usually do not have enough understanding and awareness about the linkage between their everyday behaviors and the environment. This lack of literacy can be addressed by providing appropriate energy-related information (Froehlich et al., 2010). Based on the type of information, time granularity, and delivery medium, different forms of energy analytics for eco-feedback have been proposed (Ehrhardt-Martinez et al., 2010; Froehlich et al., 2010; Jain et al., 2012; Mäkivierikko, 2019; Sussman & Chikumbo, 2016). Historic data consumption is used to provide self-evaluation (Jain et al., 2012) while disaggregated energy consumption helps residents identify where to save energy (Ehrhardt-Martinez, 2015; Kelly & Knottenbelt, 2016). In addition, peer-comparison (i.e., normative comparison) for a relative evaluation of energy consumption can be used for a small group of residents (Anderson et al., 2017; Jain et al., 2012) or large-scale utility programs (Allcott, 2011). Message framing (Asensio & Delmas, 2015) (e.g., monetary or environmental) or the way to express data (Chiang et al., 2014) (e.g., numerical or analogue) is widely investigated and customized or targeted feedback is emphasized (Khosrowpour et al., 2016; Strengers, 2014). Demand response program (e.g., real-time pricing, critical peak pricing, or time-of-use electricity

rates) delivers price information to customers to reduce or shift electricity usage during peak periods for peak demand reduction (Ehrhardt-Martinez et al., 2010; Hammerstrom et al., 2007; Harding & Lamarche, 2016). Social games are also utilized to actively motivate engagement while providing incentives as a reward (Konstantakopoulos et al., 2019).

The efficacy of eco-feedback depends on how to motivate and sustain residents' engagement and prevent from unintended consequences (Buchanan et al., 2015; Fogg, 2009). For example, actionable feedback provides residents information on accompanying benefits sometimes through an energy model and helps them choose specific actions among different alternatives (Buchanan et al., 2015; Ehrhardt-Martinez, 2015; Kimura et al., 2018; R. Yang et al., 2016). On the other hand, poorly designed normative comparison may bring unintended consequences such as adverse effects, loss of interest and trust toward the feedback, etc. (Allcott, 2011; Buchanan et al., 2015; Schultz, 2014). Specifically, the effect of weather and building needs to be normalized so that normative feedback can be directly used to evaluate the impact of behavior on the energy consumption.

While previous studies have shown successful eco-feedback applications mostly in single-family detached buildings, more attention is required for unit-level eco-feedback in multi-family residential buildings. This is because the inter-unit heat transfer (Siggelsten, 2014) makes the unit-level energy analytics such as HC energy prediction and normative comparison difficult. In addition, energy analytics need to i) consider various sources of uncertainty from unobserved variables (e.g., heat gain from appliances and occupants, infiltration); ii) infer the operational characteristics of HC systems (e.g., coefficient of performance) from limited data (e.g., power consumption without supply air temperature and flow rate); iii) be updated based on real-time data from smart thermostats and smart meters to reflect up-to-date conditions. Finally, the HC energy consumption data that used for the energy analytics needs to be inferred from currently available infrastructure (i.e., smart thermostats and smart meters) for scalable and practical implementation of proposed energy analytics.

1.2 Objectives

The main goal of this Thesis is to develop new approaches for energy analytics in multi-unit residential buildings within the context of eco-feedback design. These new approaches will enable energy savings through the lens of those most responsible for consumption: the occupants.

The main objectives of this thesis are:

1. To develop a data-driven building energy normalization model for normative comparison.
2. To develop a real-time modeling approach to predict unit-level heating and cooling energy consumption for actionable eco-feedback design.
3. To develop a scalable and practical heating and cooling energy disaggregation model by using smart thermostat and smart meter data.

All the proposed models are developed based on a Bayesian approach for the following reasons; it provides a flexible probabilistic framework to encode residential unit- and time-specific indexes for variables and parameters; it incorporates various unobserved stochastic disturbances such as inter-unit heat transfer, human body heat gain, infiltration, etc.; it allows the models to be updated through sequential Bayesian update when new data is obtained.

1.3 Document overview

Chapter 2 presents a literature review for energy prediction models suitable for eco-feedback research in multi-family residential buildings.

Chapter 3 presents the field study conducted in an actual multi-family residential building located in IN, U.S.

Chapter 4 presents a data-driven building energy normalization model.

Chapter 5 presents a real-time modeling approach to predict the HC energy consumption of an individual unit in multi-family residential building.

Chapter 6 presents a scalable and practical heating and cooling energy consumption disaggregation model by using smart thermostat and smart meter data.

Chapter 7 summarizes the conclusions and main achievements of this thesis and presents an outlook in continuation of this work.

2. LITERATURE REVIEW

2.1 Normalization models for normative comparison

2.1.1 Concept of normalization

Figure 2.1 shows a schematic diagram of factors affecting HC and non-HC energy consumption. Normative comparison, which is often called peer comparison, compares the energy consumption of a target residential unit with other residential units, and it is widely used in utility-scale studies (Allcott, 2011; Andor et al., 2020; Ayres et al., 2013; Khawaja & Stewart, 2014; Schultz et al., 2007). The energy comparison itself does not reveal how much the target unit's energy related behavior is good. Therefore, the energy consumption of a target unit should be relatively evaluated after normalizing the weather conditions and building characteristics.

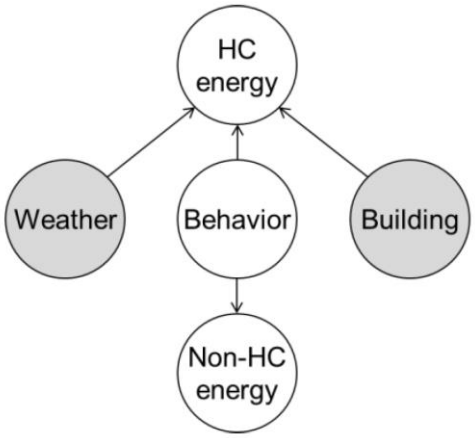

Figure 2.1. Factors affecting HC and Non-HC energy consumption in residential buildings.

2.1.2 Building-level normalization techniques

A common normalization method is to match units that have similar values for variables that explain their energy consumption such as geographical location, square footage, and heating and cooling (HC) systems (Allcott, 2011; Laskey & Kavazovic, 2011). Such units are considered a normalized group, and the energy comparison within the group is explained by variables that are not used for the matching process (e.g., human behavior). However, this matching-type of

normalization requires a large amount of data to have enough variation for all variables that are used for the matching process because the comparison is skewed or biased if the number of units in a group is too small or the energy consumption data does not show enough variation. In previous studies, units that have similar occupancy pattern (Anderson et al., 2017) or they are connected to a local social network (Jain et al., 2012; Mäkivierikko, 2019) are considered as a normalized group (i.e., peer group or neighbors). However, the normalization over building characteristics and HC systems is not considered in these studies while other experimental studies do not explain how the neighbors are chosen (Andor et al., 2020; Asensio & Delmas, 2015; Khawaja & Stewart, 2014; Schultz et al., 2007). Furthermore, studies reported that there is significant variation in energy consumption for units in a multi-family residential building despite of their similar building characteristics (e.g., similar geographical location, square footage, and mechanical system) and weather conditions, due to differences in inter-unit heat transfer (Moeller et al., 2020; Rouleau et al., 2018).

Accordingly, several data-driven normalization methods have been investigated in energy benchmark and retrofitting studies (U.S. Department of Energy, 2020; Yoshino et al., 2017). Although these methods are based on yearly energy consumption data, it is useful to understand how they are developed to overcome their limitations.

One of the most successful methods is a regression-based approach developed with national-level data such as the EnergyStar portfolio manager (Energy Star, 2014a, 2014b). In this tool, the source energy use intensity (EUI, i.e., energy usage divided by the floor area) is modeled as a function of several independent variables that represent building characteristics (e.g., weather (Energy Star, 2017), building operating hours, building type, etc.) by using a statistically sampled national-level database. The model does not use individual building technology parameters for windows, lighting, etc., but rather uses overall static building characteristics such as building-type, number of rooms, normal occupancy, presence of amenities, etc. The variance in the overall regression fit can be explained by unmodeled building technology variables and model outputs can be directly interpreted as the energy score of the implemented building technologies. Although EnergyStar provides the overall score of the building technology, it does not specify the expected economic benefits. Walter and Sohn used a similar approach based on a Building Performance Database (BPD) to overcome the limitation of the EnergyStar portfolio manager by including building technology variables in their regression model (Walter & Sohn, 2016). In addition, a more

complex probabilistic model was developed by Koetler and Ferreira based on a large database. In parallel efforts, several variations have been explored to improve the regression-based approaches (Kolter & Ferreira Jr., 2011). Stochastic frontier analysis was proposed to include skewness or a non-Gaussian shape of the data distribution in the benchmark (Amir & Ram, 2014; Z. Yang et al., 2018). Quantile regression was further developed to have relative scores even in cases of a skewed data distribution (Roth & Rajagopal, 2018). Recently, a method that uses regression with interaction terms and black-box models (Arjunan et al., 2020) applied to a publicly available dataset was developed for energy benchmarking (U.S. Energy Information Administration, 2018).

While the regression-based approach can be used for building groups partitioned by space-use types (e.g., residential commercial, schools), unsupervised clustering techniques can be implemented to identify normalized building groups that have similar characteristics across the space-use types. Through the feature selection process, this method finds features such as gross area, type of heating and cooling system, building operation hours, etc., that sufficiently explain building energy consumption. Buildings units that have similar values for these features form a normalized group through various clustering techniques (X. Gao & Malkawi, 2014; Schaefer & Ghisi, 2016). This unsupervised learning approach is convenient and suitable in the era of smart home technology (Ford et al., 2017) with a large amount of data. However, the quality and consistency of the model selection process in unsupervised clustering depends on the richness of data.

Lara et al. proposed a different normalization method for energy benchmarking that combines unsupervised clustering with a regression-based approach (Arambula Lara et al., 2015). In this approach, the authors assumed that the variance that is not captured by a multivariate regression model can be reduced once the data is clustered into several groups that have similar unmodeled characteristics. Therefore, the regression model for each group has less noise variance if the clustering successfully finds groups of similar buildings. Although the whole process of determining the number of clusters was manually conducted and evaluated, this study showed promise in terms of how unsupervised clustering can be fused with a knowledge-based benchmark model such as the regression method.

2.1.3 Challenges of unit-level normalization for multi-family residential buildings

Since the above-mentioned strategies are designed for building-level normalization, a new method is required for unit-level normalization within multi-family residential buildings to incorporate inter-unit heat transfer in the normalization method. Traditionally, energy simulation software is used to model the whole building and predict unit-level energy use (Jang & Kang, 2016, 2018). However, this whole building simulation approach requires detailed inputs and calibration, which entails a significant upfront effort. A simplified model was proposed by Siggelsten to reallocate heating costs based on a steady-state heat balance model which incorporates inter-unit heat transfer (Siggelsten, 2014). Although this model is practically useful due to its simple structure, it includes various assumptions for unobserved variables such as equal internal heat gains for all units, etc. Without considering the uncertainties from the stochastic nature of occupant behavior, these assumptions could result in inaccurate results.

2.2 Heating and cooling energy prediction models for actionable feedback

2.2.1 Single family houses

Actionable feedback helps residents to understand the relative importance between various energy-conserving behaviors based on the resulting benefits and motivates them to implement specific actions (Buchanan et al., 2015; Ehrhardt-Martinez, 2015; Kimura et al., 2018; R. Yang et al., 2016). Recently, the development of wireless technology allows homeowners to remotely control their smart home devices (Ford et al., 2017; von Bomhard et al., 2016). The availability of disaggregated energy usage data for heating or cooling systems which constitute a significant part of the residential energy consumption makes actionable feedback feasible. As a result, the literature on thermostat-related research is vast. However, only a few studies use data-driven energy models to provide reliable actionable feedback. For example, Rogers et al. (Rogers et al., 2013) present a scalable low-cost solution to provide heating-related feedback for a single-family detached house. They use a simple difference equation model to predict the indoor temperature and the feedback provides the energy savings per degree of setpoint difference without suggesting a specific action. Siemann (Siemann, 2013) develops a gray-box model for a single-family detached house to evaluate thermostat-control related energy saving strategies such as pre-cooling

and heating and smart setback but actionable feedback was not the focus of the study. Pisharoty et al. (Pisharoty et al., 2015) propose a personalized thermostat schedule recommender system based on occupancy data. The system provides recommendations to residents based on their descriptive settings for a comfort or energy efficient setpoint. It is a convenient tool as residents only need to choose one of the recommendations (R. Yang et al., 2016). However, the energy savings are calculated based on a simple rule of thumb (i.e., 1% of energy savings per 0.56℃ setback for an 8-hour period) and the resulting benefits are not explicitly presented to users.

2.2.2 Challenges for multi-family residential buildings

Energy modeling of each unit in a multi-family residential building poses significant challenges because the building thermal dynamic process depends on inter-unit heat transfer, outdoor air conditions, and stochastic occupant behavior for each household. Due to this complexity, physics-based computer simulation tools are widely used. Paiho et al. (Paiho et al., 2013) use building energy simulation software to predict the energy saving potential from building renovations. However, Jang and Kang (Jang & Kang, 2016) point out that variations in heating system control and activities between different households are hard to be captured in simulation software and proposed a Gaussian process classifier to estimate the distributions of model inputs such as heating setpoint ranges for an apartment to reduce the uncertainty in stochastic simulations. In a consecutive study from the same authors (Jang & Kang, 2018), polynomial regression was used to model the unit-level heating setpoint as a model input. In this way, the correlation of setpoints between different units was considered, and the simulation accuracy was increased.

Physics-based building energy simulation software requires a large number of inputs such as building layout, material properties, heating and cooling system specifications and control logic. This process is overly complicated for unit-level energy management and thus data-driven models have been proposed. Jain et al. (Jain et al., 2014) use a support vector regression model to predict the energy consumption of a multi-family residential building. This study investigates the applicability of the data-driven model for various spatial (unit, floor, building) and temporal (10 mins, hourly, daily) granularities. Although the model includes the dynamics of the building thermal process by having an autoregressive structure, it does not account for the inter-unit heat transfer and does not include an explicit occupant behavior term such as a setpoint schedule. For

unit-level modeling, the inter-unit heat transfer can be significant and there are large variations in heating and cooling energy consumption depending on each unit's boundary conditions (Moeller et al., 2020; Rouleau et al., 2018). For example, it has been reported that a unit adjacent to conditioned spaces (such as other units) may require small amounts of energy due to "free" heating or cooling from its adjacent units (Siggelsten & Olander, 2013). Siggelsten (Siggelsten, 2014) proposes a cost effective approach to offset the effect of heat transfer from adjacent units in energy bills, but this method is based on a steady-state heat balance (i.e., static model) and it is not suitable for unit-level energy prediction. On the other hand, gray-box models (Ellis & Alanqar, 2018) are widely studied for control applications in single-family detached houses. Such models are developed based on dynamic thermal processes and can predict energy consumption from various resident behavior scenarios, but they are not suitable for multi-family residential buildings because of the inter-unit heat transfer.

2.2.3 Real-time update

A HC prediction model needs to handle streaming data for real-time eco-feedback applications. When an energy model is used as decision-making tool for energy retrofits, historic data can be used for the model calibration. However, real-time eco-feedback should be provided based on updated building information and real-time (streaming) data considering the following two issues. First, some model parameters are time-varying or season-specific (e.g., cooling and heating system efficiencies). While building materials and heating and cooling system performance could degrade with time. These model parameters require training for different seasons or updating with streaming data. Second, the model needs to include unobserved stochastic disturbances such as occupant behavior (e.g., window opening, portable heater use, internal heat gains, etc.) and infiltration. These two considerations imply that model parameters need to be updated with streaming data, and the model structure needs to include unobserved disturbances in a probabilistic form.

Several real-time models have been developed but they have non-probabilistic structures. Omar et al. (Omar et al., 2017) use a seven-day sliding window of training data to consider seasonal variations. Wang et al. (J. Wang et al., 2019) propose a simplified form of a state-space model that has an analytical format to estimate model parameters in real-time based on a simple Euler

discretization. However, these models have non-probabilistic structures and do not include unobserved disturbances. A probabilistic state-space model (called augmented state-space model) can easily include unobserved disturbance terms (Ellis & Alanqar, 2018). Several studies present real-time parameter-learning with the state-space structure via a non-linear Kalman filter, such as extended or unscented Kalman filter. Radecki and Hencey (Radecki & Hencey, 2017) develop an augmented state-space model for a multizone building and validate it with data from a simulation model. As the augmented model no longer is a non-linear system, various discretization schemes are investigated by Baldi et al (Baldi et al., 2016). However, this augmented model could induce over-dispersion in parameters because the model parameters are updated when the filtering proceeds by adding random noise in every time step, and this noise would accumulate (Liu & West, 2001).

2.3 Energy disaggregation for eco-feedback design

2.3.1 Advanced metering infrastructure for energy efficiency and demand response

Recently, the U.S. government launched the Smart Grid Investment Grant (SGIG) program (U.S. Department of Energy, 2016) to achieve grid modernization (i.e., smart grid via advanced metering infrastructure (AMI)). By integrating smart meters, communication networks, and data management systems, AMI provides various approaches such as automatic billing, fault/outage detection, time- or incentive-based utility rate programs for energy efficiency (EE) and demand response (DR) (Gold et al., 2020; York et al., 2019) by enabling the two-way communication between customers and utility companies. It is reported that advanced metering infrastructure (AMI) is available for about 60% of U.S. households, and it provides low-resolution (i.e., 5-, 15-, 30-, or 60-minute interval data) electricity consumption data to utility companies via smart meters. Furthermore, the prevalence of smart phones and smart home devices (e.g., a smart thermostat) (Ford et al., 2017) provides new opportunity to provide interactive utility programs for behavior change, often called eco-feedback (Ehrhardt-Martinez et al., 2010; Froehlich et al., 2010), by integrating building systems, residents, utility companies without complex commercial-level building automation platforms (Ford et al., 2017; Northeast Energy Efficiency Partnerships, 2015).

2.3.2 Energy disaggregation for eco-feedback design

With the development of smart home devices and AMI, the design of effective eco-feedback for EE and DR (i.e., behavior change programs) have become active research topics (Batalla-Bejerano et al., 2020; Sussman & Chikumbo, 2016; York et al., 2019). Specifically, motivated residents would change their behavior when they have enough ability to implement and are triggered in a timely manner (Fogg, 2009; Froehlich et al., 2010). Disaggregated energy information is essential because it helps residents to identify where to save energy (Ehrhardt-Martinez, 2015; Kelly & Knottenbelt, 2016) and provide what to do with accompanied benefits through a dynamical model of HC energy consumption (Ham & Karava, 2020; Pisharoty et al., 2015; Rogers et al., 2013; Siemann, 2013). Furthermore, disaggregated HC energy consumption (i.e., thermostatically controllable load) can be used to design DR programs by analyzing HC demand characteristics of customers to find someone who have a high potential to shift HC energy consumption to reduce peak demand (Asadinejad et al., 2018; Gold et al., 2020; Kwac & Rajagopal, 2016; Qi et al., 2020; Smith et al., 2012). Although there have been several efforts to reduce the cost (Cutler et al., 2019) and engineering efforts (Sparn et al., 2017), individual circuit monitoring is still expensive and requires engineering efforts for installation and data collection (Northeast Energy Efficiency Partnerships, 2015).

2.3.3 Non-intrusive energy disaggregation for eco-feedback

Energy disaggregation, which is often called non-intrusive load monitoring (NILM), provides appliance-level energy consumption from net energy consumption, and it is a promising research area for eco-feedback design such as a personalized actionable feedback based on appliance-level energy consumption (Batra et al., 2015; Carrie Armel et al., 2013; Gopinath et al., 2020; Kimura et al., 2018). The main advantage of this technique is that it does not require appliance- or circuit-level power sensors and expensive data collection infrastructure. Various NILMs (e.g., event-based/event-less or supervised/unsupervised) have been proposed (Gopinath et al., 2020; Kelly & Knottenbelt, 2016; Pereira & Nunes, 2020). While NILM research has shown some success in academic field based on dataset obtained in laboratories, there are several challenges for field application. For example, a supervised method requires several steps of engineering works such as data labeling, event detection, feature extraction, and disaggregation

(Giri & Bergés, 2015; Gopinath et al., 2020). An unsupervised method needs to be validated with a few weeks of operation in coordination with residents (Gopinath et al., 2020). In other words, both methods require labeled observations during the training stage. In addition, most NILMs are developed based on high-resolution power, voltage, current, and phase information (Carrie Armel et al., 2013; Gopinath et al., 2020).

On the other hand, some studies have focused on the HC energy disaggregation from low-resolution smart meter data (e.g., 5-, 15-, 30-, or 60-min) (Albert & Rajagopal, 2015; Asadinejad et al., 2018; Culière et al., 2020; Liang et al., 2019; Qi et al., 2020). This is practically useful because low-resolution data is currently being collected from current AMI. In some studies, net energy consumption (hourly or daily) is modeled as a function of outdoor air temperature by using a piecewise linear regression and divided by consumption in HC period or non-HC period (Culière et al., 2020; Kwac & Rajagopal, 2016; Qi et al., 2020). This approach does not explicitly split HC energy consumption, but it can be used to identify homes that have more variability in energy consumption to outdoor air temperature (i.e., more potential to shift HC energy consumption) for DR. A few studies have attempted to explicitly disaggregate HC energy consumption. Lee and Zhang propose a random forest based autoregressive model to disaggregate HC energy consumption for residential model predictive control (Lee & Zhang, 2021). In this approach, HC energy consumption needs to be monitored to train the model for several months to capture seasonal characteristics of HC system, which may require the installation of sub-circuit power meter for the HC system. Liang et el. proposed a computationally efficient model to sequentially disaggregate HC energy consumption (Liang et al., 2019). However, this method relies on various rule-of-thumb values, requires several months of data (e.g., 6 months), and does not include operation specific energy consumption such as auxiliary heating, heat pump heating, etc. that would be required for developing a dynamic model for HC energy consumption (Ham et al., 2021).

3. ENERGY CONSUMPTION IN A MULTI-FAMILY RESIDENTIAL BUILDING

3.1 Overview

This chapter presents a field study from an actual multi-family residential building located in IN, U.S. This study facilitates our understanding of the energy consumption trends in multi-family residential buildings and helps us identify challenges in energy analytics. This chapter includes (i) the overview of the testbed multi-family residential building and the data collection method with the list of installed sensors (Section 3.2), (ii) the yearly end-use energy consumption (Section 3.3), (iii) the HC energy consumption by season (Section 3.4), (iv) the heating energy consumption by building characteristics (Section 3.5), (v) the HC energy consumption data for an entire year (Section 3.6), and (vi) the HC energy consumption by operation (Section 3.7).

3.2 Building overview

Our testbed is a remodeled multi-family residential building, located in Indiana, United States (Figure 3.1). It includes 50 apartment units (40 one-bedroom and 10 two-bedroom). The residential units are located on the 2nd, 3rd, and 4th floors while the1st floor includes all amenities (e.g., laundry, multi-purpose, PC, and storage rooms). The building was originally used as a factory, and the main concrete slabs and pillars were reused during the remodeling process. Except for the south wall façade on 2nd and 3rd floor that were kept from the old building, all other exterior and interior walls were completely replaced. 6-in fiberglass insulation (R19) was used on the exterior and some of the interior walls. 5-inch poly-iso insulation (R30) was installed on the roof. The slabs between floors consist of 12-in recycled concrete with an interior finish and no insulation. The restored south wall façade consists of old brick without additional insulation. The residential units are aligned along the east and west side of the building with windows facing east or west. Units located on the west-side have balconies in the living room. Units on the 2nd floor have a back yard since the 2nd floor is on the ground-level of the west side. On the other hand, units on 3rd and 4th floors have non-protrusion balconies, and their floor area is smaller than the units on the 2nd floor Units located on the east-side have operable awning windows in the living room. All units on both west and east side of the building have operable awning windows in the bedrooms.

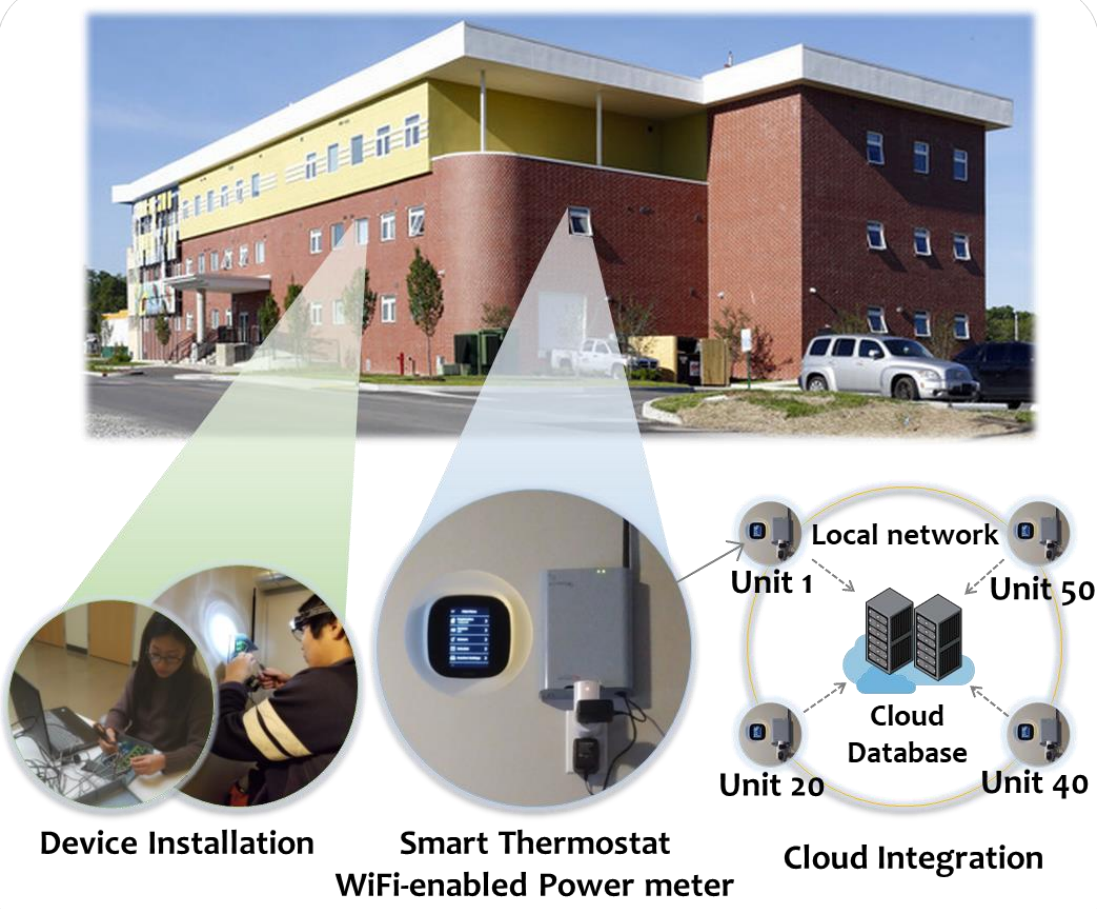

Figure 3.1. Testbed building and data collection.

Figure 3.2 shows the floor plan of two adjacent units. Each unit has a dedicated air handler and a heat pump which are controlled by a thermostat. The air handler is in a mechanical room between two units, and the outdoor unit of heat pump is on the rooftop. The return air from each unit flows without a dedicated duct into the mechanical room through the return grilles. In the mechanical room it is mixed with return air from the adjacent unit. Some common spaces (e.g., hallway, computer room, laundry room, etc.) have thermostats controlled by the building manager, but other non-occupied spaces (e.g., storage, loading deck) are not conditioned except for emergency electric heaters.

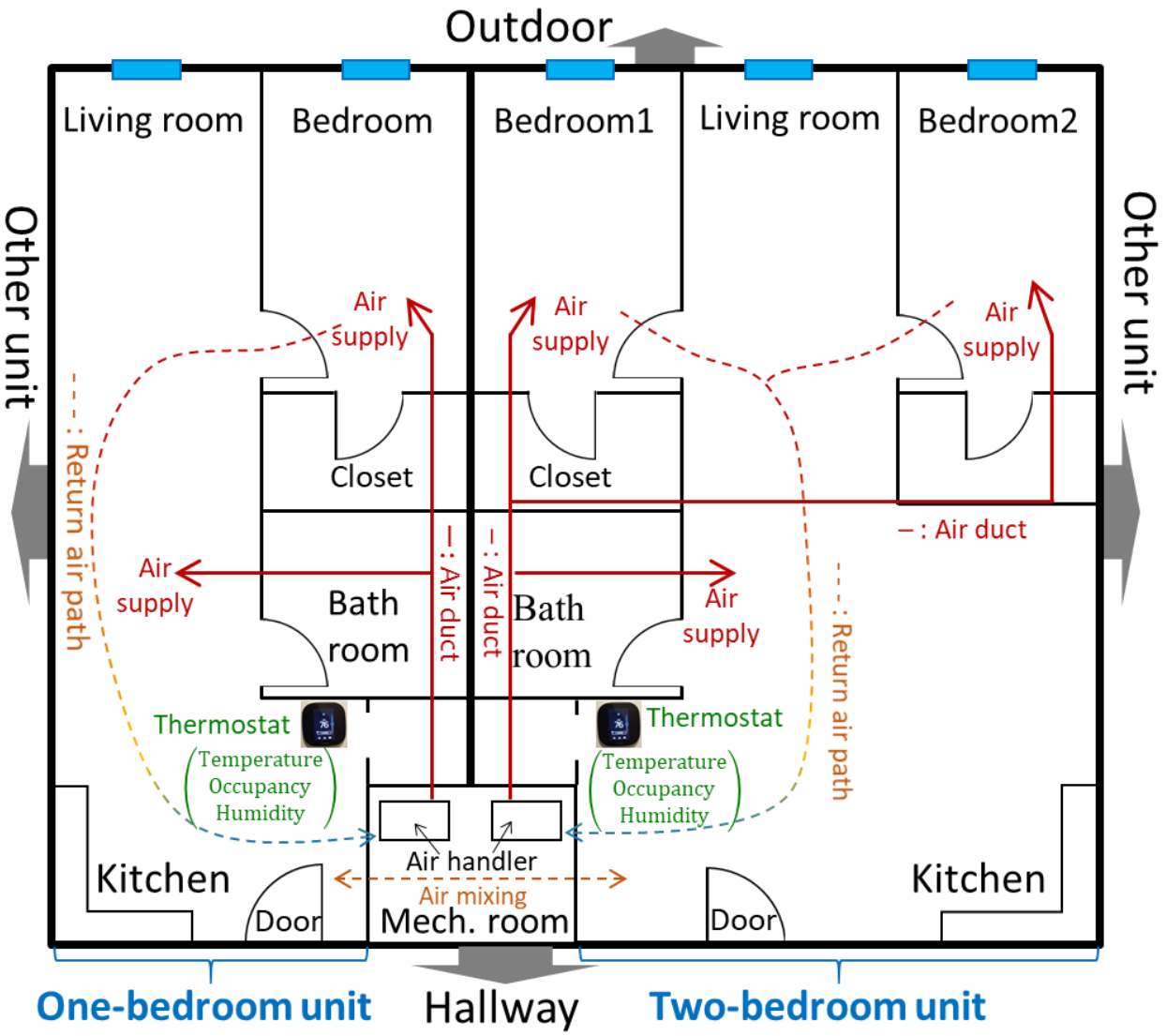

Figure 3.2. Room and heating/cooling system layout.

Wi-Fi-enabled smart thermostats (Ecobee3 (Ecobee, 2021)) and sub-circuit power meters (GreenEye Monitor (Brultech, 2021)) were installed inn each residential unit to collect thermostat and disaggregated energy usage data every 5 minutes through their web-based application program interfaces (APIs) (Figure 3.1). The thermostat measures indoor air temperature (± 0.5℃ accuracy), indoor relative humidity ($\pm 5\%$ accuracy), proximity, and HC system operation signals (Figure 3.2). The sub-circuit power meter measures all powers of main and hot wires (i.e., lights, fridge, air handler, heat pump, room plugs, water heater, etc. as shown in Figure 3.3). Current transformers with maximum capacity 200 A and $\pm 1\%$ accuracy are used for the main wires. Current

transformers with ±1% accuracy with maximum capacity 50 A are used for the hot wires. Weather information such as outdoor air temperature and global solar radiation is collected via a weather station installed on the rooftop (Davis Vantage Pro2 (Davis Instruments, 2021)). This study was approved by the Institutional Review Board (IRB Protocol #: 1702018811).

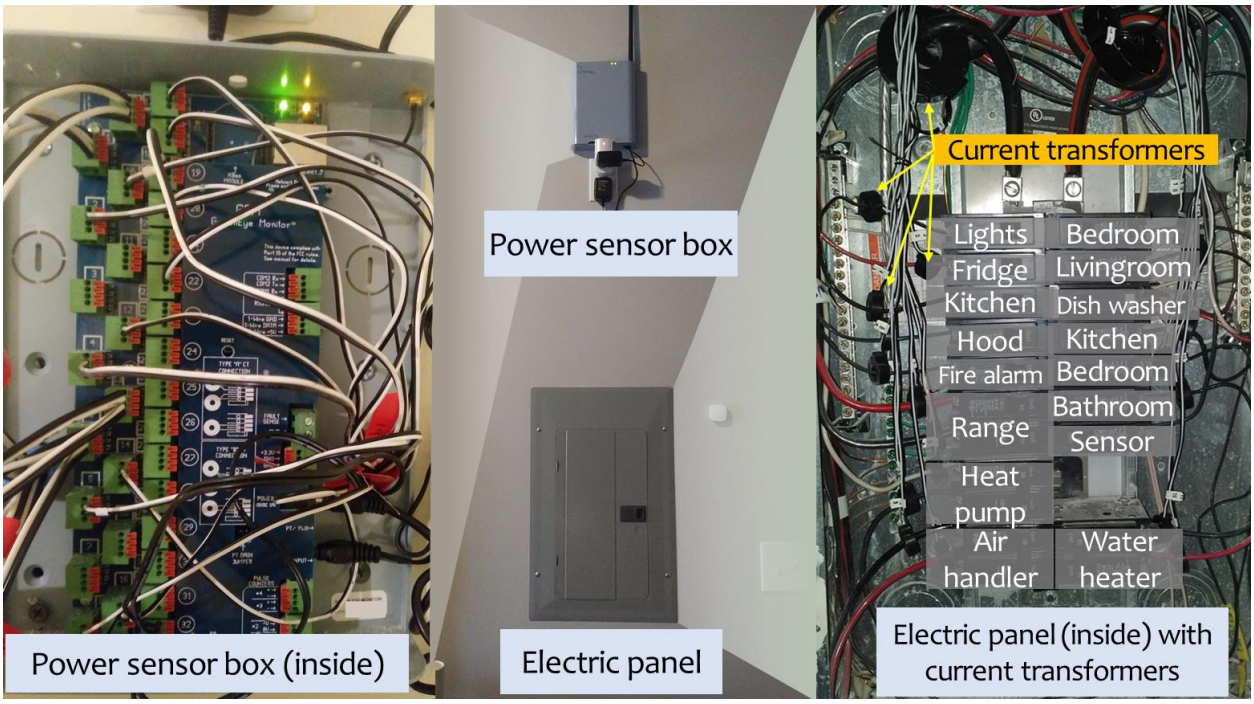

Figure 3.3. Sub-circuit power meter.

3.3 Overall energy consumption

Figure 3.4 shows area-normalized end-use energy consumption in each unit for a year, and the percentage of heating and cooling consumption in total consumption is also presented. Throughout the year, units have different end-use consumption composition. Specifically, it is shown that HC consumption accounts for 56% of total energy consumption in average, and it ranges from 30% to 80%. From this investigation, it is still shown that HC consumption is the main target of energy management in this newly constructed multi-family residential building.

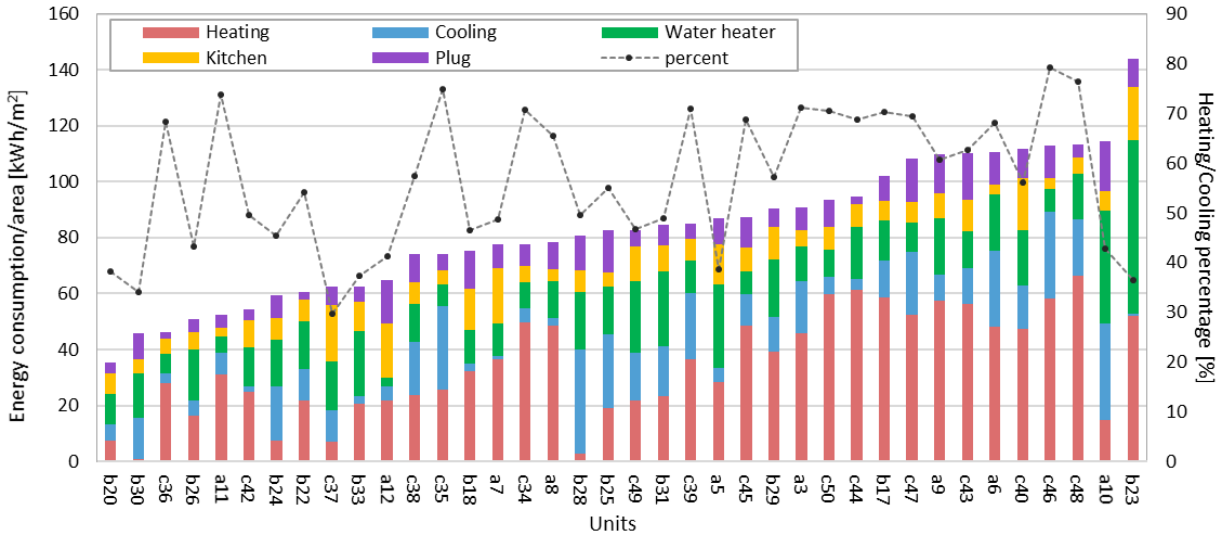

Figure 3.4. Area-normalized end-use energy consumption, and percentage of heating and cooling consumption in total consumption for each unit (Jan 2018 – Dec 2018).

3.4 Heating and cooling energy consumption by seasons

Figure 3.5 shows the area-normalized total HC energy consumption and average heating and cooling setpoints for all units during the (a) heating, (b) transition, and (c) cooling season. For each season, all data are ordered according to the total HC energy consumption. The HC energy consumption is higher during the heating season because the climate in this area is heating dominant. Although all units are in the same building under the same weather conditions, their total heating energy consumption varies from almost 0 (b30) to 2900 kWh (45 kWh/m^2) (c34) for three heating season months, and such variations can be explained by differences in building characteristics (e.g., exterior walls, windows) and occupant behavior (e.g., occupancy schedule, setpoint, internal heat gains).

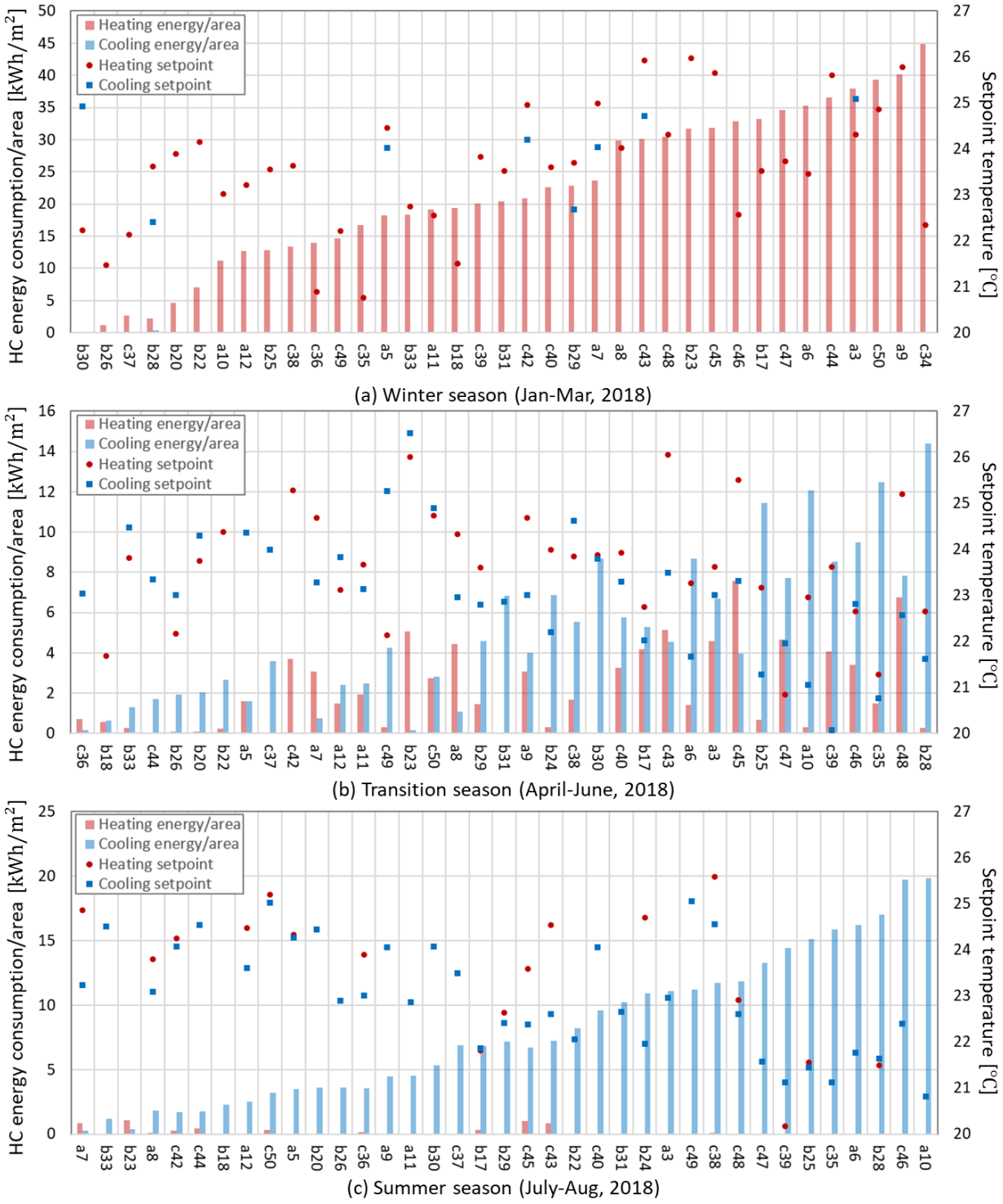

Figure 3.5. Area-normalized heating and cooling energy consumption and average heating and cooling setpoints in different seasons (setpoints are omitted for units that there is no heating or cooling operation).

Figure 3.6 shows non-heating and cooling (non-HC) energy consumption per floor area of units by season. In this building, non-HC energy consumption is the sum of all appliances (i.e., dish washer, refrigerator, fridge, etc.), all plug loads, a water heater, and an electric range in each unit. In the most units, it is shown that the non-HC energy consumption of each unit show similar values over different seasons but large variations over different units. In other words, non-HC electricity consumption is mostly explained by behavior as shown in Figure 2.1.

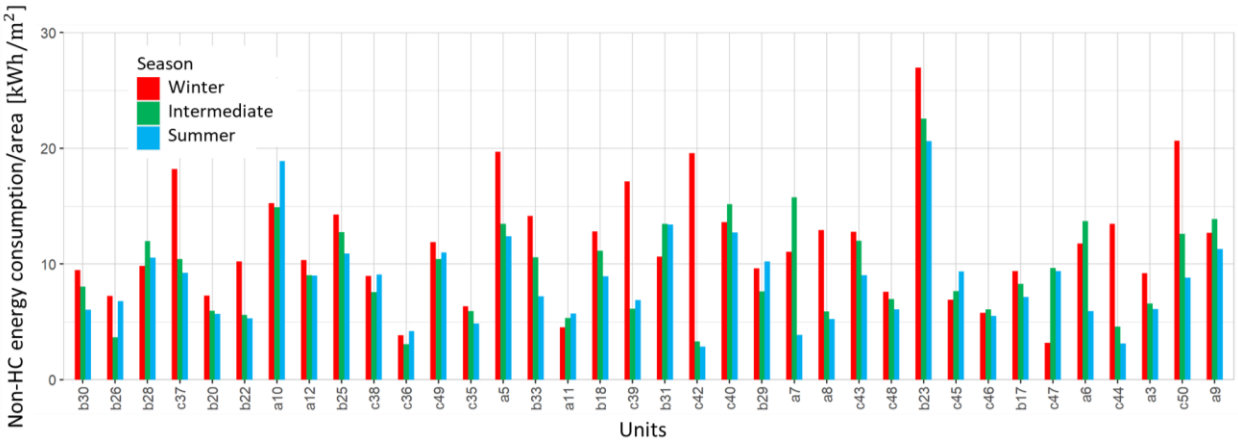

Figure 3.6. Area-normalized non-heating and cooling energy consumption of units by seasons.

3.5 Heating energy consumption by building characteristics

In Figure 3.7, heating electricity consumption per floor area for units with different building characteristics is presented for a winter week (outdoor air temperature ranging from −12℃ to 12℃), and the results show large variations. Units on the top floor (4th floor) are expected to have higher consumption due to the larger exposure to the outdoor weather, but no distinctive differences are observed. Units with balconies located at the corner are marked as B and C in the top figure, respectively. We would expect that the heating energy consumption would be correlated with the indoor temperature of the units when other factors such as weather, unit location in a building, etc. are normalized. Units located at the building corners (marked as C in Figure 3.7) generally show high energy consumption because they have larger exterior wall area than non-corner units. However, unit c35 shows less energy consumption than unit c36 (non-corner unit with balcony) though their temperatures are similar. Most units with a balcony have a tendency to

show higher energy consumption than units without a balcony. However, it is challenging to quantify the effect of building characteristics (e.g., corner, balcony) on energy consumption through this descriptive analysis. Unit c46 and unit c44 are located on the same floor and have similar energy consumption, but their indoor temperatures are quite different. From this analysis, we could confirm that normalization over major building characteristics such as existence of balcony, floor-level, location with respect to building corner is not enough because of unobserved factors such as inter-unit heat transfer. In summary, this empirical analysis is helpful to understand the complex variations in unit-level energy consumption and highlights the need to develop an appropriate normalization method for a multi-family residential building.

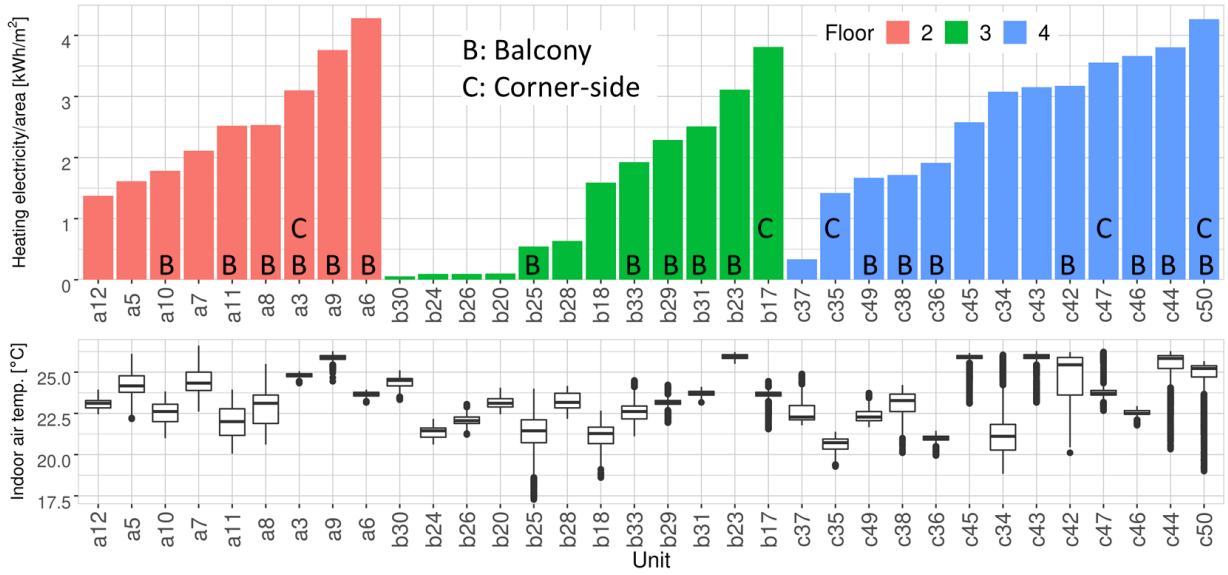

(a) Area-normalized heating energy consumption (top) and indoor air temperature (bottom)

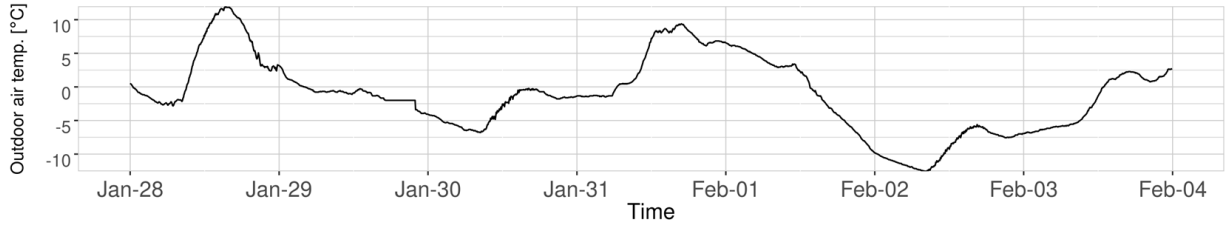

(b) Outdoor air temperature

Figure 3.7. Area-normalized heating energy consumption, indoor and outdoor air temperature during a winter week (2018/01/28–2018/02/04).

3.6 Heating and cooling energy consumption data for an entire year

Figure 3.8 presents the area-normalized heating and cooling energy consumption for each unit over an entire year (2018) sorted in increasing magnitude for heating or cooling consumption. The averages of temperature difference between heating or cooling setpoint and outdoor air temperature during the heating or cooling operation are also shown. Although all units are in the same building and use the same type of heating devices, no clear correlation between indoor air temperature and heating energy consumption per floor area is found. Instead, units with similar setpoint temperatures show large differences in energy use, even those located on the same floor. For example, unit c38 is located right next to c40, and they are both 1-bedroom units on the 4th floor with the same average setpoint temperature of 24℃. But the heating energy consumption for c40 is two times of that for c38. This can be attributed to the different building envelope characteristics and heat transfer to adjacent spaces. For any given unit, if there is a single factor that affects heating and cooling consumption per area, the heating and cooling consumption should follow a certain correlation. For example, when the outdoor air temperature is a significant factor, a unit that has large heating energy consumption should also have large cooling energy consumption. On the other hand, if the effect of the heat transfer from adjacent units is the major factor, then a unit with high heating energy use attributed to a low setpoint temperature of an adjacent unit should have low energy consumption for cooling. In this figure, there is no clear correlation between the cooling and heating energy consumption per floor area, illustrating its complex nature in a multi-family residential building.

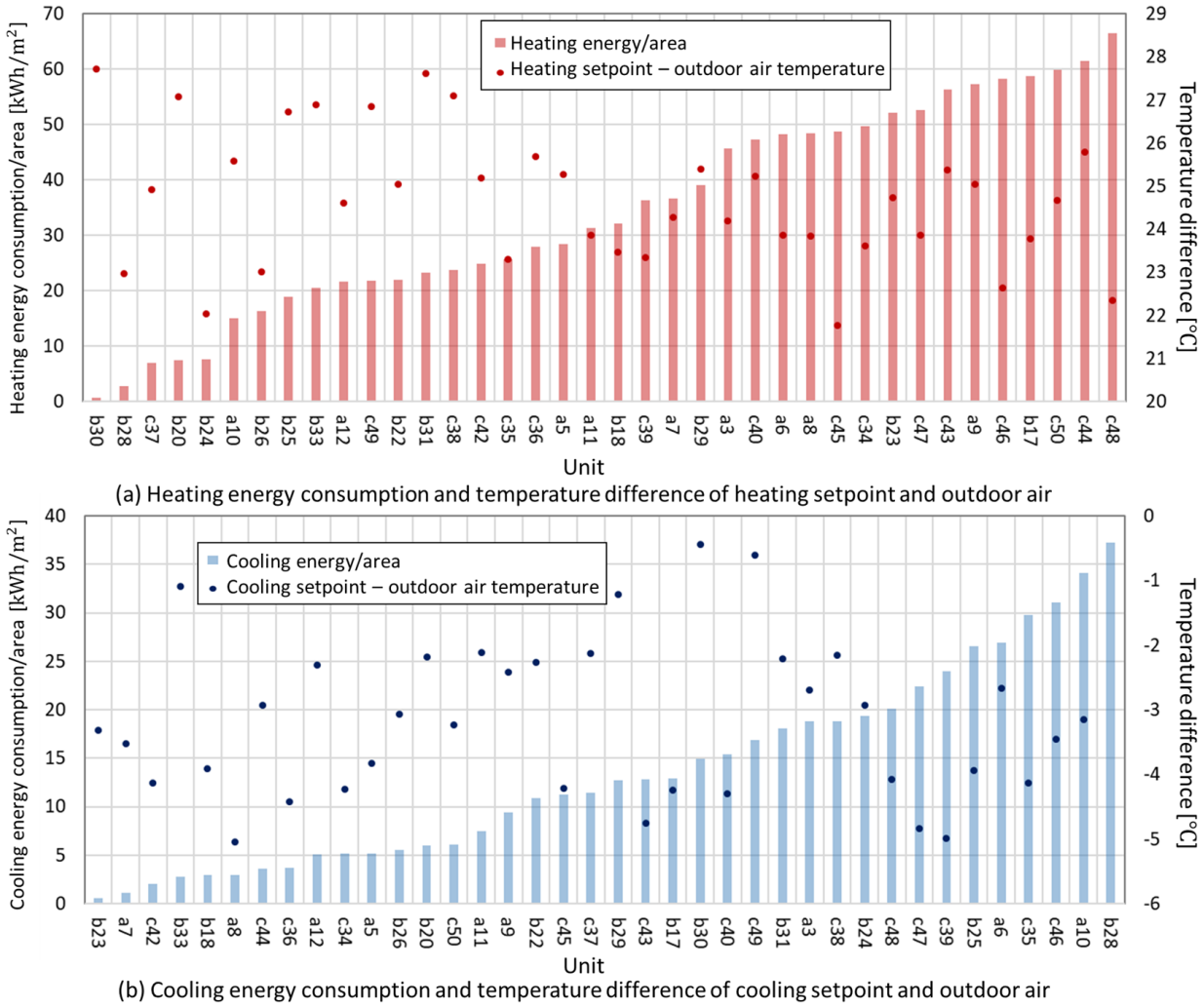

Figure 3.8. Area-normalized heating and cooling energy consumption and temperature difference between setpoint and outdoor air in each unit (Jan 2018 – Dec 2018).

To understand the inter-unit heat transfer, four units with almost identical setpoint control at different locations in the building (Figure 3.9 (b)) are selected. The corresponding heating energy consumption per floor area is shown in Figure 3.9 (c) for four consecutive days in March 2018 with outdoor air temperature ranging from −4℃ to 10℃. Unit a3 is located on the west-corner of the 2nd floor. Unit a12 is also on the 2nd floor but on the east side and not in the corner. Unit b22 is similar to a12 but located on the 3rd floor. Finally, c47 is located on the east-corner of the 4th floor. Figure 3.9 (a) shows the indoor temperature of each unit. Units a3, b22, and c47 had an average heating setpoint of 23.9℃ during the selected period. The four units show very different

heating energy consumption per floor area with unit a3 showing the highest (1.33 kWh/m^2) and b22 the lowest (0.18 kWh/m^2) value. Several reasons cause these differences. In this building, most of west-side units have large balconies with large glazing while east-side units have small awning windows. The spaces with amenities on the 1st floor are partially conditioned, therefore, the 2nd floor units may require more heating than the 3rd floor units. When comparing a3 and a12, a3 has larger exterior walls than a12 due to the balcony and corner-location. However, both a3 and a12 lose heat through the floor slab to the non-conditioned storage on the 1st floor. Although a12 and b22 have similar building envelope characteristics (no balcony and non-corner units), the floor slab of b22 faces another residential unit, so it loses less heat than unit a12, in which the floor slab faces the partially conditioned laundry room. As a result, b22 consumed the least energy consumption (0.18 kWh/m^2) and its room air temperature was sometimes higher than the setpoint without any heating. c47 is located on the top floor, so it is expected to show the highest consumption due to the heat loss from the roof. However, the roof is well-insulated, and c47 does not have a balcony, which results in less energy consumption than a3. In addition, it could be possible that the heat pump of c47 is more efficient than that of a3 because all the outdoor units of the heat pumps are on the rooftop, so the shorter refrigerant piping results in lower heat loss.

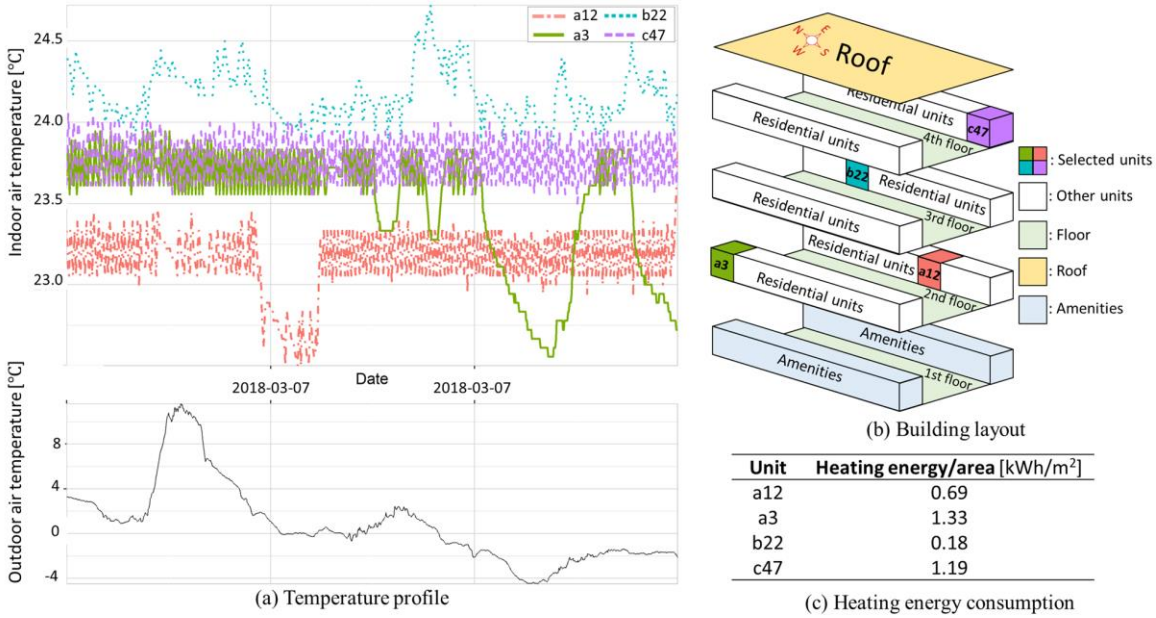

(a) Temperature profile

(b) Building layout

Unit	Heating energy/area [kWh/m^2]
a12	0.69
a3	1.33
b22	0.18
c47	1.19

(c) Heating energy consumption

Figure 3.9. Comparison of area-normalized heating energy use among different units with similar setpoints.

3.7 Heating and cooling energy consumption by operation

In Figure 3.10, the distributions of HC and non-HC power in different units and seasons are visualized. The data is sampled every 5 minutes, and 9-month of data is visualized. Each month is classified as three different seasons (i.e., heating: Jan, Feb, Mar, transition: Apr, May, June, and cooling: July, Aug, Sep). During the heating season, units a10, a11, and b17 shows bimodal distribution because there are two types of heating operation: heat pump heating (about 1000 W) and auxiliary heating (about 4000 W). While unit c37 did not use the auxiliary heater at all, unit c49 only used the auxiliary heater. During the transition and cooling season, most of HC power consists of heat pump.

Although the heat pumps in this building have single stage operation (i.e., either heating or cooling), their distributions are right-skewed. It could be attributed to the data sampling interval (5 minutes) because heat pumps show smaller power than normal operation during the on/off period. Furthermore, bimodal shapes are observed during heat pump heating operation, and it can be explained by the defrost control (see next paragraph and Figure 3.11). On the other hand, it is noted that the non-HC power distributions are consistent over different seasons in same unit, but different units show different distributions. Non-HC power shows bimodal shape for some units because of large consuming appliances such as microwave, oven, water heater, etc. Overall, their consumptions are highly left-skewed distributions for the most of time.

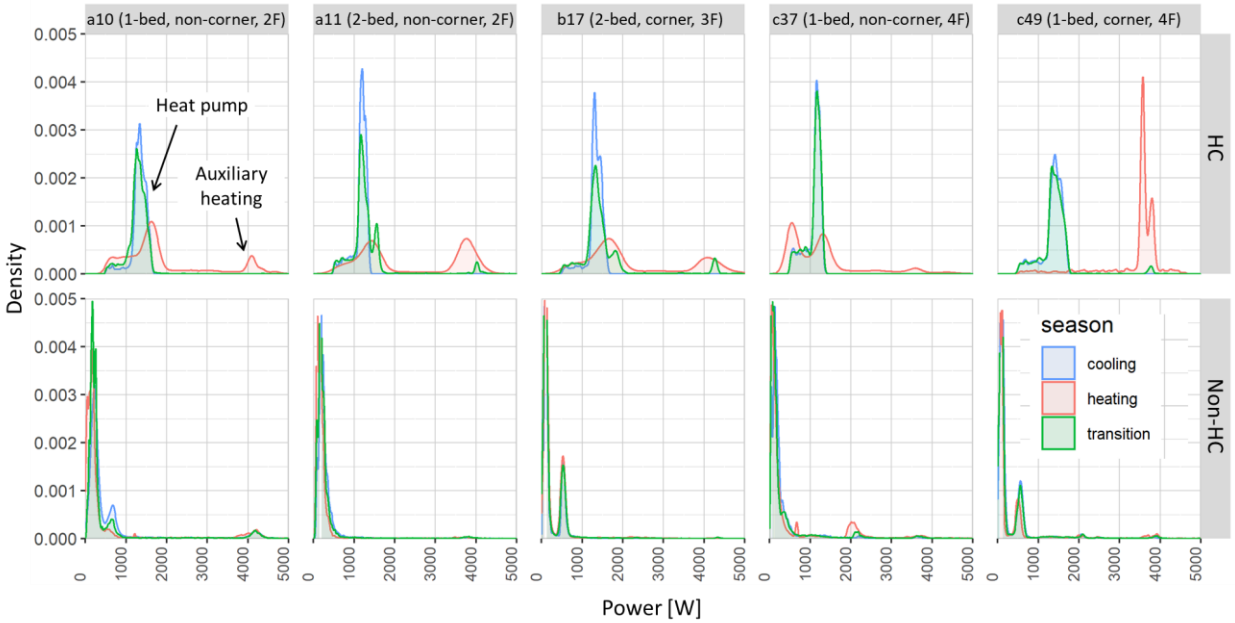

Figure 3.10. HC and non-HC power distribution by different units and seasons (2018/01/01 - 2018/09/30).

HC power, HC operation signal, and outdoor air temperature of one unit during a winter week is visualized in Figure 3.11. The data is sampled in every 15 minutes. In this thermostat setting, when the indoor temperature does not reach heating setpoint in 30 minutes with the heat pump heating, the auxiliary heating is used. For example, after 30 minutes of heat pump heating (a), the auxiliary heating is used (b). The simultaneous operation of heat pump heating and auxiliary heating is disabled in this thermostat. After (b) period, the heat pump heating with defrost control (c) is used. When the outdoor air temperature is relatively mild (e.g., higher than 0°C), heat pump heating without defrost control activates during (d) period. For the defrost control, auxiliary heating sometimes activates to compensate the reduced heat pump heating due to defrost cycle. Since the control logic of auxiliary heating during the defrost control is embedded in the heat pump system, it is difficult to explicitly model this logic unless it is modeled as a stochastic random variable. For this reason, we use data sampled every 15-minute to model HC power during defrost control by smoothing the auxiliary heating power (see Section 6.2.1).

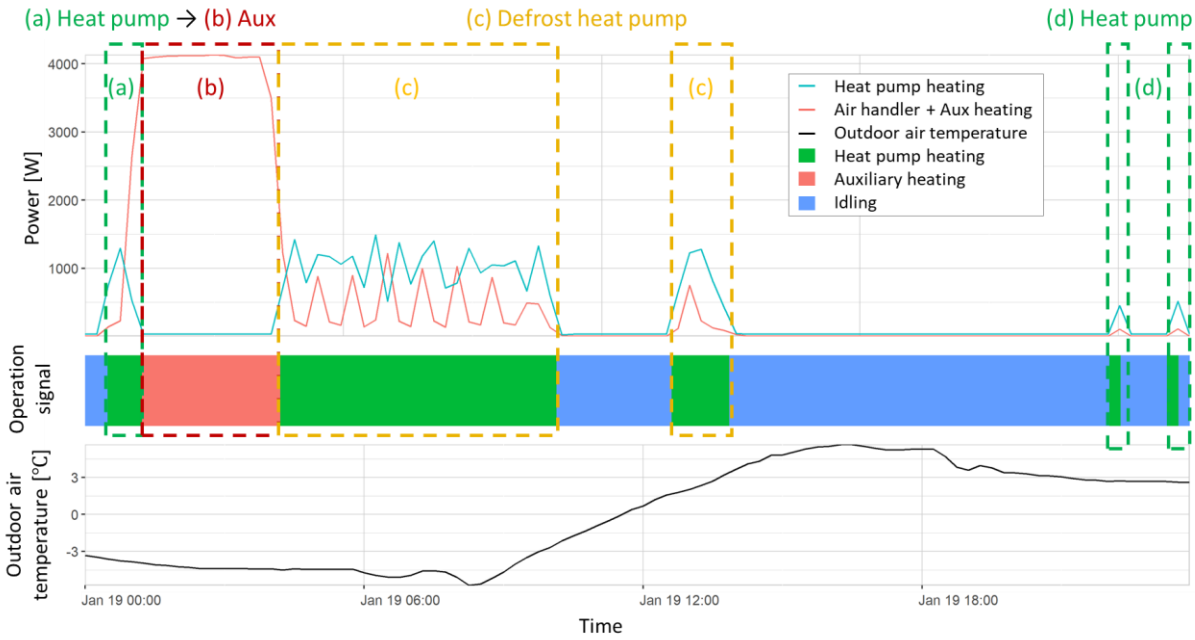

Figure 3.11. Various heating operations in a winter week (a10).

4. DATA-DRIVEN BUILDING ENERGY NORMALIZATION MODEL FOR ECO-FEEDBACK DESIGN

4.1 Overview

This chapter presents a data-driven building energy normalization model for normative comparison in a multi-family residential building. It includes (i) a Bayesian mixture model for normalization that considers inter-unit heat transfer and unobserved variables (Section 4.2.1 and 4.2.2); (ii) a sequential Bayesian update approach (Section 4.2.3); the normalized group identification (Section 4.2.4), and the normative comparison (Section 4.2.5). The model performance is discussed in Section 4.3, and the limitations and recommendations for future work in Section 4.4.

4.2 Modeling approach

A conceptual diagram for our normalization method is shown in Figure 4.1. The HC energy use for each unit in a multi-family residential building (HC energy a, b, c, d in the figure) depends on building characteristics (Bldg. char. a, b, c, d) and occupant behavior (Occ Behav. a, b, c, d). Starting with a unit-level heat balance equation, a linear regression model is developed to represent the effect of building characteristics and occupant behavior on HC energy consumption while considering inter-unit heat transfer and unobserved variables. Then, a normalization model is formed to identify groups of units that have similar values for building characteristics in the regression model (i.e., normalized group). Within each group, the HC energy consumption of different units is directly comparable for the evaluation of occupant behavior.

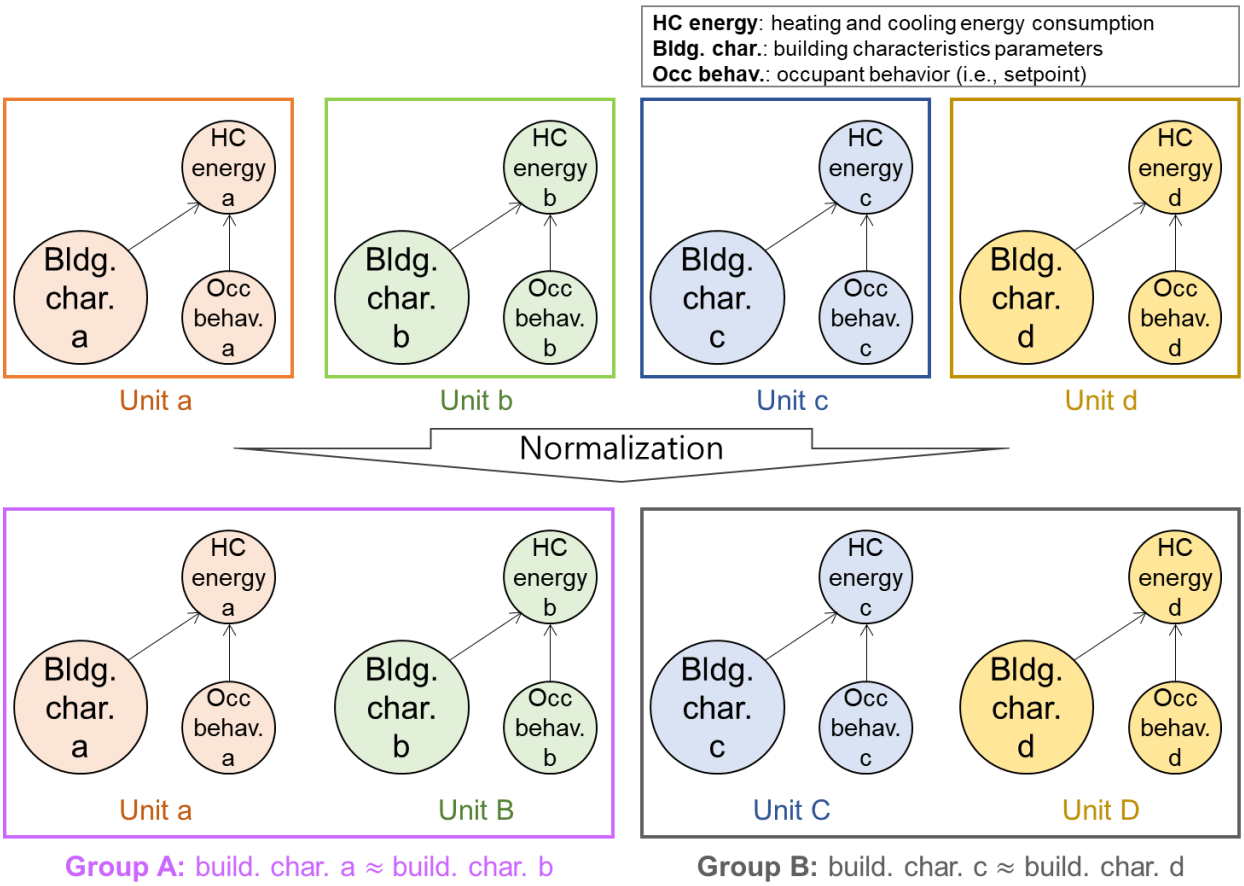

Figure 4.1. Conceptual diagram of the normalization model.

The implementation process for the normalization model consists of three steps. The first step is **Model inference**. Using data collected during the previous week and prior distributions, the posterior distributions of the model parameters are inferred. The inferred parameters are used to identify normalized groups of residential units for normative comparison (**Application**). Finally, the posterior distributions are used as prior distributions for the next week (**Model update**).

4.2.1 Unit-level heat balance equation

We assume that a typical residential unit conditioned by a single thermostat in a multi-family residential building can be represented as a single zone thermal network. The sensible energy balance of a single zone residential unit is written as Eq. 4.1 (Mitchell & Braun, 2012):

$$C_{\text{unit},h}\frac{dT_{\text{unit},h,t}}{dt} = \dot{Q}_{\text{ex},h,t} + \dot{Q}_{\text{win},h,t} + \dot{Q}_{\text{adj},h,t} + \dot{Q}_{\text{hc},h,t} + \dot{Q}_{\text{inf},h,t} + \dot{Q}_{\text{vent},h,t} + \dot{Q}_{\text{appl},h,t} + \dot{Q}_{\text{occu},h,t}, \quad (4\text{-}1)$$

where $C_{\text{unit},h}$, $T_{\text{unit},h,t}$, $\dot{Q}_{\text{ex},h,t}$, $\dot{Q}_{\text{win},h,t}$, $\dot{Q}_{\text{adj},h,t}$, $\dot{Q}_{\text{hc},h,t}$, $\dot{Q}_{\text{inf},h,t}$, $\dot{Q}_{\text{vent},h,t}$, $\dot{Q}_{\text{appl},h,t}$, and $\dot{Q}_{\text{occu},h,t}$ are the lumped capacitance, indoor temperature, heat flow through exterior walls, heat flow through glazing, inter-unit heat transfer from adjacent spaces through interior walls, heat flow from the HC device, heat gain from infiltration, heat gain from ventilation, heat gain from appliances, and heat gain from occupants, respectively, for unit h and time t.

The heat flow through an opaque wall ($\dot{Q}_{\text{ex},h,t}$) can be written as Eq. 4.2 (Mitchell & Braun, 2012):

$$\dot{Q}_{\text{ex},h,t} = UA_{\text{ex},h}\left[T_{\text{out},t} + \frac{\alpha_{\text{ex},h}}{\kappa_{\text{eq,ex},h}}G_{\text{T}_\text{s},\text{ex},h,t} - \frac{em_{\text{ex},h}}{\kappa_{\text{eq,ex},h}}\left(T_{\text{out},t}^4 - T_{\text{rad},t}^4\right) - T_{\text{unit},h,t}\right], \quad (4\text{-}2)$$

where $UA_{\text{ex},h}$, $T_{\text{out},t}$, $\alpha_{\text{ex},h}$, $\kappa_{\text{eq,ex},h}$, $\text{em}_{\text{ex},h}$, $G_{\text{T}_\text{s},\text{ex},h,t}$, and $T_{\text{rad},t}$ are the overall heat transfer coefficient times the exterior wall area, outdoor air temperature, solar absorptivity of the exterior wall, summation of radiative and convective heat transfer coefficient at the outer surface of the exterior wall (i.e., $\kappa_{\text{eq,ex},h} = \kappa_{\text{rad,ex},h} + \kappa_{\text{conv,ex},h}$), solar emissivity of the exterior wall, incident solar radiation on the exterior wall, and radiant temperature of the surroundings, respectively.

The heat flow through the glazing ($\dot{Q}_{\text{win},h,t}$) can be written as Eq. 4.3 (Mitchell & Braun, 2012):

$$\dot{Q}_{\text{win},h,t} = UA_{\text{win},h}\left(T_{\text{out},t} - T_{\text{unit},h,t}\right) + G_{\text{T}_\text{s},\text{win},h,t}A_{\text{win},h}\left(\tau_{\text{win},h} + \frac{\alpha_{\text{win},h}U_{\text{win},h}}{\kappa_{\text{eq,win},h}}\right), \quad (4\text{-}3)$$

where $UA_{\text{win},h}$, $G_{\text{T}_\text{s},\text{ex},h,t}$, $\tau_{\text{win},h}$, $\alpha_{\text{win},h}$, $U_{\text{win},h}$, and $\kappa_{\text{eq,win},h}$ are the overall heat transfer coefficient times the glazing area, incident solar radiation on the external glazing surface, transmissivity of the glazing, absorptivity of the glazing, overall heat transfer of the glazing, and summation of the radiative and convective heat transfer coefficient at the glazing outer surface (i.e., $\kappa_{\text{eq,win},h} = \kappa_{\text{rad,win},h} + \kappa_{\text{conv,win},h}$), respectively.

The inter-unit heat transfer ($\dot{Q}_{\text{adj},h,t}$) is expressed as Eq. 4.4:

$$\dot{Q}_{\text{adj},h,t} = UA_{\text{adj},h}\left(T_{\text{adj},h,t} - T_{\text{unit},h,t}\right), \quad (4\text{-}4)$$

where $UA_{\mathrm{adj},h}$ and $T_{\mathrm{adj},h,t}$ are the overall heat transfer coefficient of the interior wall and average temperature of the adjacent spaces.

The heat gain from infiltration ($\dot{Q}_{\mathrm{inf},h,t}$) can be written as Eq. 4.5:

$$\dot{Q}_{\mathrm{inf},h,t} = \dot{m}_{\mathrm{inf},h,t} c_p \left(T_{\mathrm{out},t} - T_{\mathrm{unit},h,t}\right), \tag{4-5}$$

where $\dot{m}_{\mathrm{inf},h,t}$ and c_p are the infiltration air mass flow rate and specific heat of air, respectively.

Using Eqs. 4.2–5, Eq. 4.1 can be written as:

$$\begin{aligned}
C_{\mathrm{unit},h} \frac{dT_{\mathrm{unit},h,t}}{dt}
&= UA_{\mathrm{ex},h}\left[T_{\mathrm{out},t} + \frac{\alpha_{\mathrm{ex},h}}{\kappa_{\mathrm{eq,ex},h}} G_{\mathrm{T_s,ex},h,t} - \frac{em_{\mathrm{ex},h}}{\kappa_{\mathrm{eq,ex},h}}\left(T_{\mathrm{out},t}^4 - T_{\mathrm{rad},t}^4\right)\right. \\
&\left. - T_{\mathrm{unit},h,t}\right] + UA_{\mathrm{win},h}\left(T_{\mathrm{out},t} - T_{\mathrm{unit},h,t}\right) \\
&+ G_{\mathrm{T_s,win},h,t} A_{\mathrm{win},h}\left(\tau_{\mathrm{win},h} + \frac{\alpha_{\mathrm{win},h} U_{\mathrm{win},h}}{\kappa_{\mathrm{eq,win},h}}\right) \\
&+ UA_{\mathrm{adj},h}\left(T_{\mathrm{adj},h,t} - T_{\mathrm{unit},h,t}\right) + \dot{Q}_{\mathrm{hc},h,t} + \dot{Q}_{\mathrm{appl},h,t} \\
&+ \dot{m}_{\mathrm{inf},h,t} c_p \left(T_{\mathrm{out},t} - T_{\mathrm{unit},h,t}\right) + \dot{Q}_{\mathrm{vent},h,t} + \dot{Q}_{\mathrm{occu},h,t} \\
&= \dot{Q}_{\mathrm{hc},h,t} + T_{\mathrm{out},t}\left(UA_{\mathrm{ex},h} + UA_{\mathrm{win},h} + \dot{m}_{\mathrm{inf},h,t} c_p\right) \\
&+ T_{\mathrm{unit},h,t}\left(-UA_{\mathrm{ex},h} - UA_{\mathrm{win},h} - UA_{\mathrm{adj},h} - \dot{m}_{\mathrm{inf},h,t} c_p\right) \\
&+ UA_{\mathrm{ex},h} \frac{\alpha_{\mathrm{ex},h}}{\kappa_{\mathrm{eq,ex},h}} G_{\mathrm{T_s,ex},h,t} - UA_{\mathrm{ex},h} \frac{em_{\mathrm{ex},h}}{\kappa_{\mathrm{eq,ex},h}}\left(T_{\mathrm{out},t}^4 - T_{\mathrm{rad},t}^4\right) \\
&+ A_{\mathrm{win},h}\left(\tau_{\mathrm{win},h} + \frac{\alpha_{\mathrm{win},h} U_{\mathrm{win},h}}{\kappa_{\mathrm{eq,win},h}}\right) G_{\mathrm{T_s,win},h,t} + UA_{\mathrm{adj},h} T_{\mathrm{adj},h,t} \\
&+ \dot{Q}_{\mathrm{vent},h,t} + \dot{Q}_{\mathrm{appl},h,t} + \dot{Q}_{\mathrm{occu},h,t}.
\end{aligned} \tag{4-6}$$

To make this simple, we parameterize the variables and parameters according to unit- and season-specific dependencies:

$$
\begin{aligned}
&\theta_{0,h,t} = \eta_{\mathrm{hc},h,t} \text{ from } \dot{Q}_{\mathrm{hc},h,t} = \eta_{\mathrm{hc},h,t} i_{\mathrm{hc},h,t} P_{\mathrm{hc},h,t},\\
&\theta_{1,h} = UA_{\mathrm{ex},h} + UA_{\mathrm{win},h},\\
&\theta_{2,h,t} = \dot{m}_{\mathrm{inf},h,t} c_p,\\
&\theta_{3,h} = UA_{\mathrm{ex},h} + UA_{\mathrm{win},h} + UA_{\mathrm{adj},h},\\
&\theta_{4,h}\theta_{5,h,t} = UA_{\mathrm{ex},h} \frac{\alpha_{\mathrm{ex},h}}{\kappa_{\mathrm{eq,ex},h}} G_{\mathrm{T_s,ex},h,t},\\
&\theta_{6,h}\theta_{7,h,t} = UA_{\mathrm{ex},h} \frac{em_{\mathrm{ex},h}}{\kappa_{\mathrm{eq,ex},h}} \left(T^4_{\mathrm{out},t} - T^4_{\mathrm{rad},t}\right),\\
&\theta_{8,h}\theta_{9,h,t} = A_{\mathrm{win},h} \left(\tau_{\mathrm{win},h} + \frac{\alpha_{\mathrm{win},h} U_{\mathrm{win},h}}{\kappa_{\mathrm{eq,win},h}}\right) G_{\mathrm{T_s,win},h,t},\\
&\theta_{10,h,t} = UA_{\mathrm{adj},h} T_{\mathrm{adj},h,t},\\
&\theta_{11,h,t} = \dot{Q}_{\mathrm{vent},h,t} + \dot{Q}_{\mathrm{appl},h,t} + \dot{Q}_{\mathrm{occu},h,t}.
\end{aligned}
\tag{4-7}
$$

For example, building characteristic parameters such as the overall heat coefficient (e.g., $UA_{\mathrm{ex},h}$) have a unit-specific dependency while weather-related variables such as solar radiance (i.e., $G_{\mathrm{T_s,ex},h,t}$) have both dependencies. In Eq. 4.7, the heat flow from the HC device is expressed as a multiplication of the efficiency, device operation signal, and power consumption (i.e., $\dot{Q}_{\mathrm{hc},h,t} = \eta_{\mathrm{hc},h,t} i_{\mathrm{hc},h,t} P_{\mathrm{hc},h,t}$). When the device is in heating, cooling, and idling mode, the $i_{\mathrm{hc},h,t}$ is 1, -1, and 0, respectively.

Eq. 4.6 can be rewritten after a 1st order Euler discretization:

$$
\begin{aligned}
&C_{\mathrm{unit},h} \left(T_{\mathrm{unit},h,t+\Delta t} - T_{\mathrm{unit},h,t}\right)/\Delta t\\
&\quad = i_{\mathrm{hc},h,t} P_{\mathrm{hc},h,t}\left(\theta_{0,h,t}\right) + T_{\mathrm{out},t}\left(\theta_{1,h} + \theta_{2,h,t}\right) - T_{\mathrm{unit},h,t}\left(\theta_{3,h} + \theta_{2,h,t}\right)\\
&\quad + \theta_{4,h}\theta_{5,h,t} + \theta_{6,h}\theta_{7,t} + \theta_{8,h}\theta_{9,h,t} + \theta_{10,h,t} + \theta_{11,h,t},
\end{aligned}
\tag{4-8}
$$

where Δt is a 5-minute interval in our dataset.

In Eq. 4.8, the behavior term ($\theta_{11,h,t}$) accounts for unmeasured human behaviors such as ventilation (i.e., operation of mechanical fans or windows), appliance use, human body heat generation. Our analysis (Appendix A) shows that the non-HC energy consumption (i.e., all electricity consumption except for HC energy), which is related to human behaviors, shows weekly time dependency instead of complete random noise. Therefore, we assume that the unmeasured behavior term ($\theta_{11,h,t}$) follows a household specific random noise in a weekly time interval

because typical residential units have a weekly schedule and behavior. Therefore, we integrate the discretized Eq. 4.8 for a week as shown in Eq. 4.9:

$$\begin{aligned}&\frac{C_{\mathrm{unit},h}}{\Delta t}\sum_{t_k=1}^{n_{\mathrm{week}}}\left(T_{\mathrm{unit},h,t_k+1}-T_{\mathrm{unit},h,t_k}\right)\\&=\sum_{t_k=1}^{n_{\mathrm{week}}}i_{\mathrm{hc},h,t_k}P_{\mathrm{hc},h,t_k}\left(\theta_{0,h,t_k}\right)+\sum_{t_k=1}^{n_{\mathrm{week}}}\left[T_{\mathrm{out},t_k}\left(\theta_{1,h}+\theta_{2,h,t_k}\right)+\theta_{4,h}\theta_{5,h,t_k}+\theta_{6,h}\theta_{7,h,t_k}+\theta_{8,h}\theta_{9,h,t_k}+\theta_{10,h,t_k}\right]\\&\quad-\sum_{t_k=1}^{n_{\mathrm{week}}}T_{\mathrm{unit},h,t_k}\left(\theta_{3,h}+\theta_{2,h,t_k}\right)+\sum_{t_k=1}^{n_{\mathrm{week}}}\theta_{11,h,t_k},\end{aligned}\tag{4-9}$$

where t_k is discrete time index (i.e., $t_k = 1,2,\dots,n_{\mathrm{week}}W$), and $n_{\mathrm{week}} = 2016$ is the number of data points in a week with 5-min interval data. $w = 1,2,\dots,W$ is weekly index. Eq. 4.9 shows the integration for the first week ($w = 1$). For different weeks, $t_k = 1,\dots,n_{\mathrm{week}}$ for $w = 1$, $t_k = n_{\mathrm{week}}+1,\dots,2n_{\mathrm{week}}$ for $w = 2$, and $t_k = Wn_{\mathrm{week}}-2015,\dots,Wn_{\mathrm{week}}$ for $w = W$.

The left-side of Eq. 4.9 is approximately zero (i.e., $\sum_{t_k=1}^{n_{\mathrm{week}}}T_{\mathrm{unit},h,t_k+1}-T_{\mathrm{unit},h,t_k}\approx 0$) because the indoor temperature difference between the beginning and end of a week is a few degrees at maximum. After averaging the terms on the right-side of Eq. 4.9 over all time steps, it can be written as Eq. 4.10 with weekly index w:

$$\theta_{12,h,w}i_{\mathrm{hc},h,w}P_{\mathrm{hc},h,w}=\theta_{13,h,w}+\theta_{14,h,w}T_{\mathrm{unit},h,w}+\theta_{15,h,w},\tag{4-10}$$

where

$$\theta_{12,h,w}=\frac{-1}{n_{\mathrm{week}}}\sum_{t=1}^{n_{\mathrm{week}}}\left(\theta_{0,h,t_k}\right),$$

$$i_{\mathrm{hc},h,w}=\frac{1}{n_{\mathrm{week}}}\sum_{t=1}^{n_{\mathrm{week}}}\left(i_{\mathrm{hc},h,t_k}\right),$$

$$P_{\mathrm{hc},h,w}=\frac{1}{n_{\mathrm{week}}}\sum_{t=1}^{n_{\mathrm{week}}}\left(P_{\mathrm{hc},h,t_k}\right),$$

$$\theta_{13,h,w}=\frac{1}{n_{\mathrm{week}}}\sum_{t=1}^{n_{\mathrm{week}}}\left[T_{\mathrm{out},t_k}\left(\theta_{1,h}+\theta_{2,h,t_k}\right)+\theta_{4,h}\theta_{5,h,t_k}+\theta_{6,h}\theta_{7,h,t_k}+\theta_{8,h}\theta_{9,h,t_k}+\theta_{10,h,t_k}\right],$$

$$\theta_{14,h,w}=\frac{-1}{n_{\mathrm{week}}}\sum_{t=1}^{n_{\mathrm{week}}}\left(\theta_{3,h}+\theta_{2,h,t_k}\right),$$

$$T_{\mathrm{unit},h,w}=\frac{1}{n_{\mathrm{week}}}\sum_{t=1}^{n_{\mathrm{week}}}\left(T_{\mathrm{unit},h,t_k}\right),$$

$$\theta_{15,h,w}=\frac{1}{n_{\mathrm{week}}}\sum_{t=1}^{n_{\mathrm{week}}}\left(\theta_{11,h,t_k}\right).$$

After dividing Eq. 4.10 by $\theta_{12,h,w}$, all terms are rewritten in a form typically used in a standard linear regression:

$$y_{h,w}=\beta_{0,h,w}+\beta_{1,h,w}x_{h,w}+\varepsilon_{h,w},\tag{4-11}$$

where $y_{h,w} = i_{\mathrm{hc},h,w} P_{\mathrm{hc},h,w}$, $\beta_{0,h,w} = \frac{\theta_{13,h,w}}{\theta_{12,h,w}}$, $\beta_{0,h,w} = \frac{\theta_{14,h,w}}{\theta_{12,h,w}}$, $x_{h,w} = T_{\mathrm{unit},h,w}$, and $\varepsilon_{h,w} = \frac{\theta_{15,h,w}}{\theta_{12,h,w}}$.

Eq. 4.11 is a simplified linear regression equation based on a unit-level energy balance and employs two assumptions for application. The weekly overall HC equipment efficiency coefficient ($\theta_{12,h,w}$) is assumed to be the same for different units within a normalized group. Although the defrost control and auxiliary heating are not same for units in a group if they have different heating and cooling operation time in a week, this cycling operation is very short (e.g., 30 minutes or 1 hour) when considering the entire week. Therefore, this should not affect the overall HC equipment efficiency if there are sufficient heating and cooling operation hours within a week. Finally, the behavior term ($\theta_{15,h,w}$) divided by the efficiency term is assumed to follow a unit specific noise ($\Pr(\varepsilon_{h,w}|\sigma_h) = \mathrm{HalfNormal}(\varepsilon_{h,w}|0, \sigma_h^2)$) as discussed in Eqs. 4.8-9 and Appendix A.

4.2.2 Bayesian mixture model for normalization

Our goal is to simultaneously fit the unit-specific parameters of Eq. 4.11 and cluster the units according to their energy consumption characteristic. To this end, we embed Eq. 4.11 within a Bayesian mixture framework. In Eq. 4.11, the two unit-specific and time-varying parameters ($\beta_{0,h,w}, \beta_{1,h,w}$) represent the effect of building characteristics and inter-unit heat transfer. Therefore, units that have similar values for these two parameters can be viewed as a group of units normalized over building characteristics, and a group-specific index $k \in \{1, \dots, K\}$ is assigned instead of unit-specific index ($h \in \{1, \dots, H\}$), i.e., $\beta_{0,k,w}$ and $\beta_{1,k,w}$. The total number of groups may vary in different seasons. For example, during the transition season, there is little heating and cooling operation, and the left-hand side of Eq. 4.11 will be almost 0. In this case, the total number of identified groups is less than the groups in cold or hot seasons. For this reason, we also include a season specific index $c \in \{1, \dots, C\}$ for the parameters (i.e., $\beta_{0,k,w}$ and $\beta_{1,k,c,w}$).

The problem is to find K linear regressions ($y_{h,w} = \beta_{0,1,\dots K,w} + \beta_{1,1,\dots K,c,w} x_{h,w} + \varepsilon_{h,w}$) given the data in week w of season c. A Bayesian mixture model is used to encode these group and season indices. The complete model structure is shown in Eq. 12 and expressed using the plate notation (Bishop, 2006) in Figure 4.2 for the first week ($w = 1$). There are two reasons we formulate this problem in a probabilistic format based on a Bayesian approach: (1) the unit- and season-specific parameters have different prior information; (2) the model is implemented in an

real-time form through sequential Bayesian updating without requiring a large amount of data from each season.

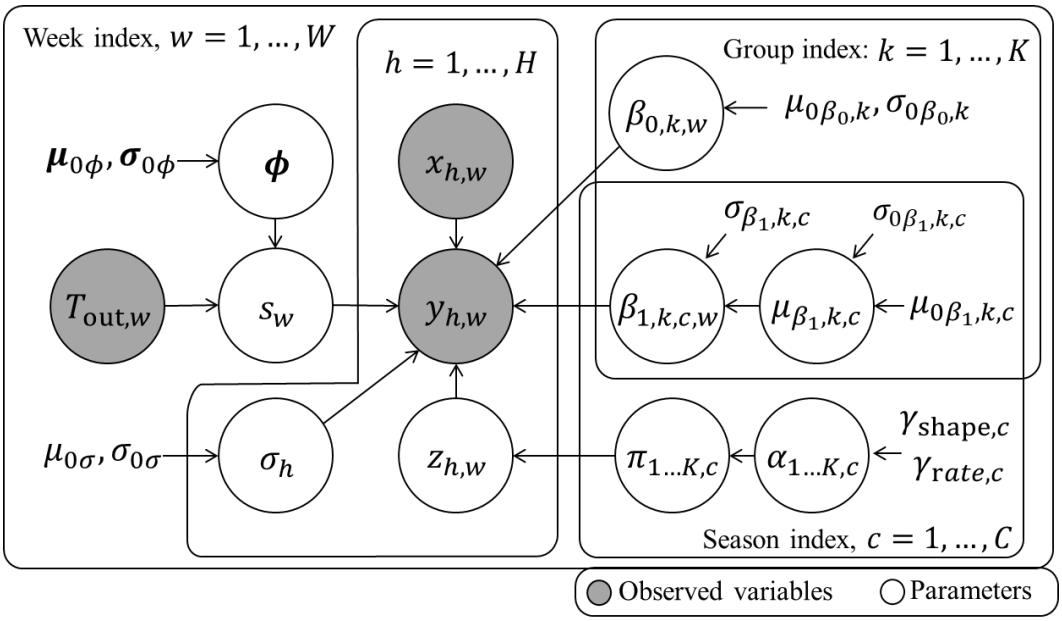

Figure 4.2. Plate notation of normalization model.

The prior knowledge, parameter constraints, unit- and season-specific indexing utilized in this probabilistic formulation are explained below. For the first week ($w = 1$), there is data $\{x_{1:H,1}, y_{1:H,1}, T_{\text{out},1}\}$ from all units ($h \in 1, 2, \dots, H$). The weekly average of outdoor air temperature, $T_{\text{out},w}$ does not have a unit-specific indicator h because all units are located in the same building. The model inference includes the following steps. First, the probability ($\boldsymbol{\lambda}_w = [\lambda_{1,w}, \lambda_{2,w}, \lambda_{3,w}]$) of being in the heating, transition, and cooling season respectively ($c \in \{1, 2, 3\}$) given $T_{\text{out},w}$ is estimated by an ordered logit classified (McElreath, 2020) as shown in Eq. 4.12:

$$\lambda_{1\dots C,w}: \begin{cases} \lambda_{1,w} = 1 - \text{softmax}(T_{\text{out},w} - \phi_{\text{heating}}) \\ \lambda_{2,w} = \text{softmax}(T_{\text{out},w} - \phi_{\text{heating}}) - \text{softmax}(T_{\text{out},w} - \phi_{\text{cooling}}), \\ \lambda_{3,w} = \text{softmax}(T_{\text{out},w} - \phi_{\text{cooling}}) \end{cases} \quad (4\text{-}12)$$

where ϕ_{heating} and ϕ_{cooling} are cut-point parameters that divide heating to transition and transition to cooling seasons, respectively.

These parameters follow normal distributions:

$$\begin{aligned}\Pr(\phi_{\text{heating}}) &= \text{Normal}\left(\phi_{\text{heating}}|\mu_{0\phi_{\text{heating}}}, \sigma_{0\phi_{\text{heating}}}\right),\\ \Pr(\phi_{\text{cooling}}) &= \text{Normal}\left(\phi_{\text{cooling}}|\mu_{0\phi_{\text{cooling}}}, \sigma_{0\phi_{\text{cooling}}}\right),\end{aligned} \tag{4-13}$$

where $\mu_{0\phi_{\text{heating}}}$, $\mu_{0\phi_{\text{cooling}}}$, $\sigma_{0\phi_{\text{heating}}}$, and $\sigma_{0\phi_{\text{cooling}}}$ are set to 10℃, 18.3℃, 3℃, and 3℃, respectively, based on heating and cooling degree-day temperatures defined by ASHRAE (ASHRAE, 2013b).

Based on $\lambda_{1\ldots C,w}$, the season-specific index ($s_w = c$) follows a categorical distribution:

$$\Pr(s_w|\lambda_{1\ldots C,w}) = \text{Categorical}(s_w|\lambda_{1\ldots C,w}). \tag{4-14}$$

For example, when $T_{\text{out},w}$ is lower than ϕ_{heating}, this is a heating season week ($s_w = 1$). Likewise, when $T_{\text{out},w}$ is in between two cut-points, it is a week in transition season ($s_w = 2$). Otherwise, it is a week in cooling season ($s_w = 3$).

To identify the group index ($z_{h,w}$), a Bayesian mixture model with finite-dimensional mixture weights is utilized (Bishop, 2006), in which $z_{h,w}$ follows a categorical distribution at given $s_w = c$:

$$\Pr(z_{h,w}|\pi_{1\ldots K,c}) = \text{Categorical}(z_{h,w}|\pi_{1\ldots K,c}), \tag{4-15}$$

where $k \in \{1,2,\ldots,K\}$ is the group index, and the maximum number of possible groups is K.

The probability of being in a specific group ($\pi_{1\ldots K,c}$) follows a Dirichlet distribution (i.e., $P(\pi_{1\ldots K,c}) = \text{Dirichlet}(\alpha_{1\ldots K,c})$). We assign a hyper prior Gamma distribution (i.e., $\text{Gamma}(\gamma_{\text{shape},c}, \gamma_{\text{rate},c})$) for $\alpha_{1\ldots K,c}$ so that the number of groups is automatically determined through Bayesian inference by having small values for the elements of $\pi_{1\ldots K,c}$ that correspond to unnecessary groups (Corduneanu & Bishop, 2001). For example, if there are $K-1$ groups in a week, the Kth elements of $\pi_{1\ldots K,\text{c}}$ would be near zero. The shape ($\gamma_{\text{shape},c}$) and rate ($\gamma_{\text{rate},c}$) of the Gamma prior are set to 2 and 4, respectively, for the first week as a hyper prior to have uniformly most values less than 1.

The intercept term ($\beta_{0,k,w}$) follows a normal distribution:

$$\Pr(\beta_{0,1\ldots K,w}) = \text{Normal}(\beta_{0,1\ldots K,w}|\mu_{0\beta_0,1\ldots K}, \sigma^2_{0\beta_0,1\ldots K}), \tag{4-16}$$

where $\mu_{0\beta_0,1\ldots K}$ and $\sigma^2_{0\beta_0,1\ldots K}$ are means and variances.

There are several treatments for the intercept term. To identify mixtures of distinct linear regressions, we utilize an ordered transform (Stan Development Team, 2020a) that forces $\beta_{0,1,w} > \beta_{0,2,w} > \cdots > \beta_{0,K,w}$ during the inference. Specifically, it is possible that K numbers of similar linear regressions with large variance can be identified. In this case, the identified groups are meaningless because they are almost identical lines. The ordered transform helps to prevent this problem from occurring. Through this approach, while there are K numbers of distinct intercept values, only meaningful linear regressions are identified by having effective values for the mixing weights ($\pi_{k,c}$). For the data scaling, min-max normalization (Han et al., 2012) is used for $x_{h,w}$ and for $y_{h,w}$ so that their values are in $[-0.5,0.5]$. The scaling is conducted on a weekly basis. After data scaling, $\mu_{0\beta_0,1\ldots K}$ are set to K numbers of linearly distributed values from -0.1 to 0.1. $\sigma_{0\beta_0,1\ldots K}$ is set to 0.5 for $k = 1,2,\ldots,K$ in each week as they are independently estimated every week. We want to have ordered intercepts but similar values for $\mu_{0\beta_0,1\ldots K}$ to identify distinct groups even if intercepts have small differences. Also, we assign large standard deviation ($\sigma_{0\beta_0,1\ldots K}$) values to allow adequate exploration of the space.

Two factors are considered for the slope term ($\beta_{1,k,c,w}$). First, this term shares a hyper prior ($\mu_{\beta_1,k,c}$) over different weeks because it is mainly affected by non-time varying terms such as building wall characteristics. In other words, $\beta_{1,k,c,w}$ for different weeks is generated from a shared hyper prior distribution. The hyper prior follows a normal distribution:

$$\Pr\left(\mu_{\beta_1,1\ldots K,1\ldots C}\right) = \text{Normal}\left(\mu_{\beta_1,1\ldots K,1\ldots C} | \mu_{0\beta_1,1\ldots K,1\ldots C}, \sigma^2_{0\beta_1,1\ldots K,1\ldots C}\right), \quad (4\text{-}17)$$

where $\mu_{0\beta_1,1\ldots K,1\ldots C}$ and $\sigma^2_{0\beta_1,1\ldots K,1\ldots C}$ are means and variances, respectively.

Second, a LogNormal distribution is used for $\beta_{1,k,c,w}$ because it is composed of positive terms such as heat transfer coefficients:

$$\Pr\left(\beta_{1,k,c,w} | \mu_{\beta_1,k,c}\right) = \text{LogNormal}\left(\beta_{1,k,c,w} | \mu_{\beta_1,k,c}, \sigma^2_{\beta_1,k,c}\right), \quad (4\text{-}18)$$

where $\mu_{\beta_1,k,c}$ and $\sigma^2_{\beta_1,k,c}$ are means and variances, respectively.

For $\mu_{\beta_1,k,c}$, we use ordered transform (Stan Development Team, 2020a) for $\mu_{\beta_1,1,c}$, $\mu_{\beta_1,2,c}$, $\ldots\mu_{\beta_1,K,c}$ because a group with higher energy consumption also has a steeper slope. $\mu_{0\beta_1,k,c}$ is set to equally separated values in [0.05, 2.0], and $\sigma_{0\beta_1,k,c}$ is set to 1 to enable adequate exploration after scaling the data. $\sigma_{\beta_1,k,c}$ is set to 0.2.

The behavior term in each unit is modeled as a unit-specific noise variance (σ_h^2), and it follows a half-normal distribution:

$$\Pr(\sigma_{1\dots H}^2) = \text{HalfNormal}\left(\sigma_{1\dots H}^2 | \mu_{0\sigma,1\dots H}, \sigma_{0\sigma,1\dots H}^2\right), \quad (4\text{-}19)$$

where $\mu_{0\sigma,1\dots H}$ and $\sigma_{0\sigma,1\dots H}^2$ are means and variances, respectively. Each unit has a different lifestyle that corresponds to weekly behavioral disturbances such as ventilation, appliance usage, human body heat gain, etc. $\mu_{0\sigma,h}$ and $\sigma_{0\sigma,h}$ are set to 0 and 0.5, respectively.

Finally, the likelihood of $y_{h,w}$ follows a normal distribution:

$$\Pr\left(y_{h,w} | \beta_{0,k,w}, \beta_{1,k,c,w}, x_{h,w}, \sigma_h^2, z_{h,w}, s_w\right) = \text{Normal}\left(y_{h,w} | \beta_{0,k,w} + \beta_{1,k,c,w} x_{h,w}, \sigma_h^2\right). \quad (4\text{-}20)$$

4.2.3 Inference and sequential Bayesian update

To estimate posterior distributions of parameters and latent variables of this model, we use automatic differentiation variational inference (ADVI) (Kucukelbir et al., 2017). ADVI is a type of variational inference that uses automatic differentiation and stochastic optimization and can be applied to various probabilistic models without conjugacy assumptions through various transformations of distributions. ADVI is a fast but sufficiently accurate approximation, and it is particularly convenient for use in sequential Bayesian update (see next paragraph). However, automatic differentiation does not support discrete variables from a categorical distribution, and therefore, the latent discrete variables for the group ($z_{h,w}$) and season (s_w) indices need to be marginalized (Stan Development Team, 2020b). The marginalization of our mixture model is shown in Appendix B. In this study, we use PyMC3 library for ADVI (Salvatier et al., 2016), and mean-field ADVI (a factorized Gaussian variational approximation (Kucukelbir et al., 2017)) is used by assuming the parameters are independent.

This model is designed to update the posterior distribution of parameters with incoming data. Specifically, at week $w = W$, the prior distributions of time-varying parameters can be written as $\Pr\left(\boldsymbol{\phi} | T_{\text{out},1:W-1}\right)$, $\Pr\left(\sigma_h | y_{h,1:W-1}\right)$, $\Pr\left(\boldsymbol{\pi}_c | y_{h,1:W-1}\right)$, and $\Pr\left(\mu_{\beta_1,k,c} | y_{h,1:W-1}\right)$. These distributions are posterior distributions of parameters obtained with all the previous data before the current week (i.e., weeks $w = 1, \dots, W-1$). In general, in Bayesian inference methods such as Markov Chain Monte Carlo (MCMC), the posterior distributions are represented by a large number of samples, and it is not possible to use the samples for Bayesian update unless they are approximated by certain distributions or the MCMC sampler uses all historic data for the update.

In ADVI, the posterior distributions are approximated by normal distributions with fixed parameters (i.e., $\mu_{0\phi_{\text{heating}}}|T_{\text{out},1:W-1}$, $\sigma_{0\phi_{\text{heating}}}|T_{\text{out},1:W-1}$, $\mu_{0\phi_{\text{cooling}}}|T_{\text{out},1:W-1}$, $\sigma_{0\phi_{\text{cooling}}}|T_{\text{out},1:W-1}$, $\mu_{0\sigma,h}|y_{1:W-1}$, $\sigma_{0\sigma,h}|y_{1:W-1}$, $\mu_{0\beta_1,k,c}|y_{1:W-1}$, $\sigma_{0\beta_1,k,c}|y_{1:W-1}$, and $\boldsymbol{\alpha}_c|y_{1:W-1}$). Therefore, the approximated posterior distributions with data collected before the current week can be directly used as prior distributions for the model update. An example of the proposed model with synthetic data is presented in the author's repository (Ham, 2020). Also, there is a notebook with model training codes and visualization.

4.2.4 Normalized group identification

The first step in our approach is to find the normalized group assignment for the target unit. The model is composed of two mixtures. The first mixture is the season index (s_w), and it is determined based on the outdoor air temperature for the current week. From the ordered logit classifier, we get the probability of being in a specific season ($\boldsymbol{\lambda}_w$). In a real-world application, the highest value of median sample of $\boldsymbol{\lambda}_w$ determines the season. For example, if $\lambda_{2,w} > \lambda_{3,w} > \lambda_{1,w}$, then $s_w = 2$ (transition season). The second mixture is the group index. The probability of a unit being in a group k (i.e., $\Pr(z_{h,w} = k|y_{h,w})$) at season c can be obtained from Eq. 4.21:

$$\Pr(z_{h,w} = k, s_w = c|y_{h,w}) = \frac{\pi_k \lambda_{c,w} \text{Normal}(y_{h,w}|\beta_{0,k,w} + \beta_{1,k,c,w} x_{h,w}, \sigma_h^2)}{\sum_{j=1}^{K}\sum_{d=1}^{C} \pi_j \lambda_{d,w} \text{Normal}(y_{h,w}|\beta_{0,j,w} + \beta_{1,j,c,w} x_{h,w}, \sigma_h^2)}. \quad (4\text{-}21)$$

The unit's group and season index in real-world application are set to k and c that maximize Eq. 4.21. from the median samples. In our study, groups that had less than 4 units were removed because this number is too small for a meaningful comparison and possibly caused by outliers, and these units were included in the second most probable group k that gives the second largest value of Eq. 4.21.

4.2.5 Normative comparison – counterfactual scenario

Once the season and group indices are obtained, the typical scenario for the normative comparison is to sort the energy consumption of the units within a group and assign a ranking or quantile for each unit (Figure 4.3 (a)). However, in some cases, when the consumptions of all units

in a specific group are similar, the comparison in this group does not provide enough information with respect to the behavior. To overcome this problem, we adopt a counterfactual scenario, i.e., "*how good the energy consumption of a target unit would have been if all units in the building had similar building characteristics with the target unit?*". In Figure 4.3, the difference between typical and counterfactual scenarios is presented. In the counterfactual scenario (Figure 4.3 (b)), it is assumed that all units in the building have the same building characteristics as the target unit. This is encoded in our model by assigning the values of $\beta_{0,k,w}$ and $\beta_{1,k,c,w}$ for the target unit to all other units. Specifically, to enable this comparison, the energy consumption of all units in the counterfactual scenario is calculated by using posterior predictive simulation (Gelman et al., 2013). This predicts observable $\tilde{y}$ from the observed y with same process including all uncertainties of parameters. Practically, this is obtained through Eq. 4.22:

$$\Pr(\tilde{y}|y) = \int \Pr(\tilde{y}|\theta)\Pr(\theta|y)\,d\theta \approx \frac{1}{n_{\text{sample}}}\sum_{s=1}^{n_{\text{sample}}} \Pr\left(\tilde{y}|\theta^{[s]}\right), \tag{4-22}$$

where θ, n_{sample}, and $\theta^{[s]}$ are parameters, number of samples that approximate the posterior distribution, and each sample of posterior distribution, respectively.

In other words, for this calculation, the predicted values from the estimated posterior distribution (i.e., parameters) and input variable (i.e., $x_{h,w}$) are used. For the counterfactual scenario, the observed input variable ($x_{h,w}$) of each unit is used, with the parameters of the target unit (i.e., $\beta_{0,k,w}$ and $\beta_{1,k,w}$). Through this approach, it is possible to utilize all samples in a multi-family residential building for normative comparisons.

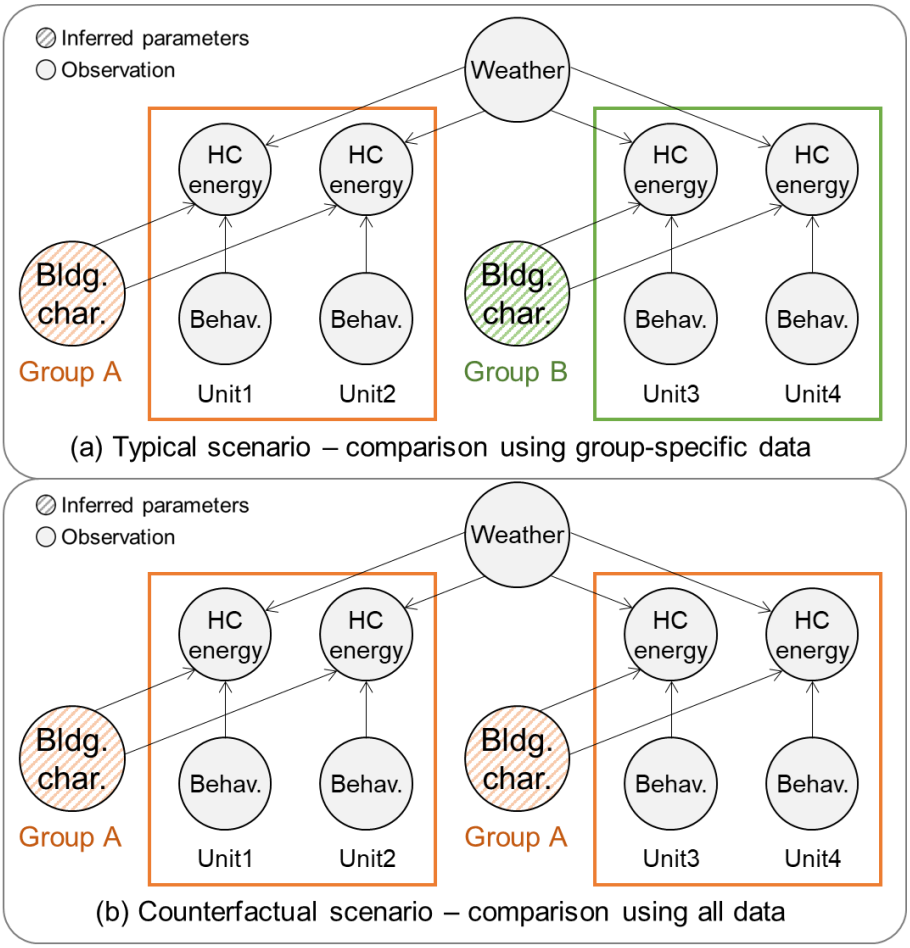

Figure 4.3. Difference between typical and counterfactual scenario.

4.3 Results

Figure 4.4 presents identified normalized groups for two weeks during the heating season. The x-axis is the weekly average indoor air temperature of each unit ($x_{h,w}$ in Eq. 4.11), and the y-axis is the weekly average HC power use ($y_{h,w}$ in Eq. 4.11 with positive and negative values for heating and cooling, respectively). In addition, the household unit identifiers (e.g., a11, c46) are shown near the data points. In this study, the maximum number of groups (K) was set to four. Three normalized groups (high-, mid-, and low-consuming groups) are practically useful for comparisons in a multi-family residential building with 50 units and an additional group was added since it is possible that some units may not fit with any group due to device malfunction, abnormal thermostat settings (e.g., auxiliary electric heating only mode), or vacation. For the specific week considered (2018/01/21–2018/01/27), the model identified three normalized groups (group A, B,

and C) through Bayesian inference (Corduneanu & Bishop, 2001) as shown in Figure 4.4 (a). 95% highest density intervals (HDI) (Kruschke, 2014) and median lines of posterior predictive distributions of all groups are shown using colored areas and dotted lines, respectively. Most units except for two (a6 and a7) are located within the HDIs for the three groups. From the model, these units were classified as a separate group, since they had atypical operation due to fixed auxiliary heating override settings in their thermostat during this week, resulting in high energy consumption compared to other units with similar behaviors. However, as shown in Figure 4.4 (b), when their thermostat settings were normal (i.e., heat pump and auxiliary heating together), they were assigned to Group C and were located within the given uncertainty range. As a result, the group that had these outliers was discarded for normative comparisons. The results confirm that the group identification model successfully explains the data. Each unit is assigned to each group based on its median value of group assignment probability (Eq. 4.21). Groups were assigned labels of A, B, and C according to increasing values for slopes and intercepts, which also correspond to increasing order of heating energy consumption for the same behavior. For example, unit b29, which is mostly surrounded by conditioned spaces and residential units but has one exterior wall, had 153 kWh (2.35 kWh/m^2) of heating energy consumption during this week, but other units in different groups such as b33 and c46 had significantly greater consumption of 449 kWh (6.9 kWh/m^2) and 786 kWh (12.1 kWh/m^2), respectively, even though their average indoor temperatures were similar.

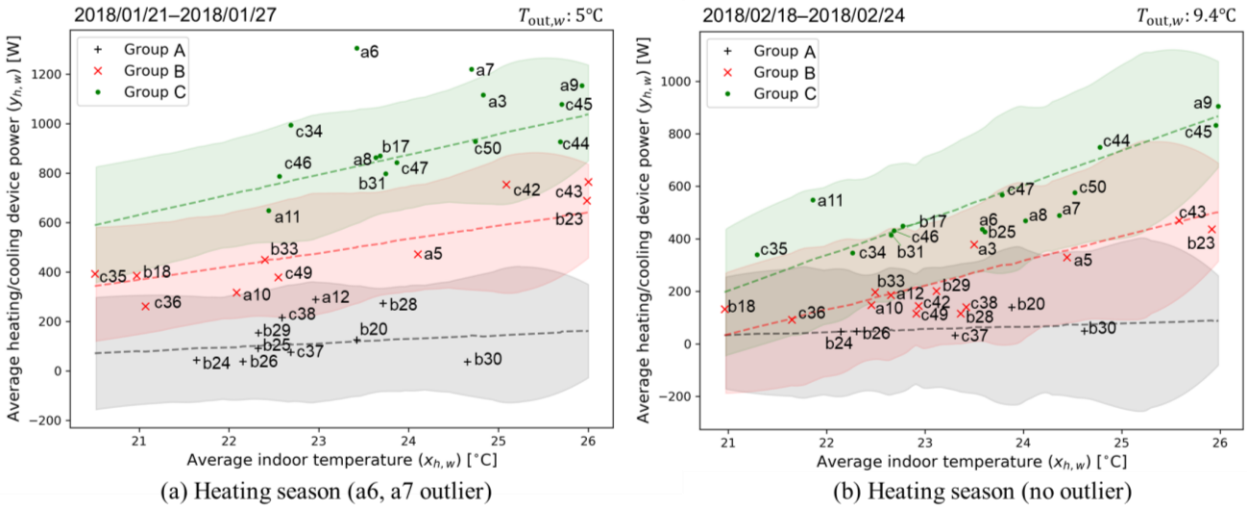

(a) Heating season (a6, a7 outlier) (b) Heating season (no outlier)

Figure 4.4. Normalized groups for two weeks during the heating season.

Figure 4.5 shows the normalization groups for two consecutive weeks from the heating to transition season. As shown in Figure 4.5 (a), three groups were identified for the heating season. However, as the weather became milder, the following week was classified as a transition season because the mean outdoor temperature (12.2℃) was higher than the estimated posterior mean of the heating season cutoff (ϕ_{heating}) value (10.04℃). For this weather, the variation in HC energy consumption between groups decreased and a smaller number of groups was enough to explain the data (Figure 4.5).

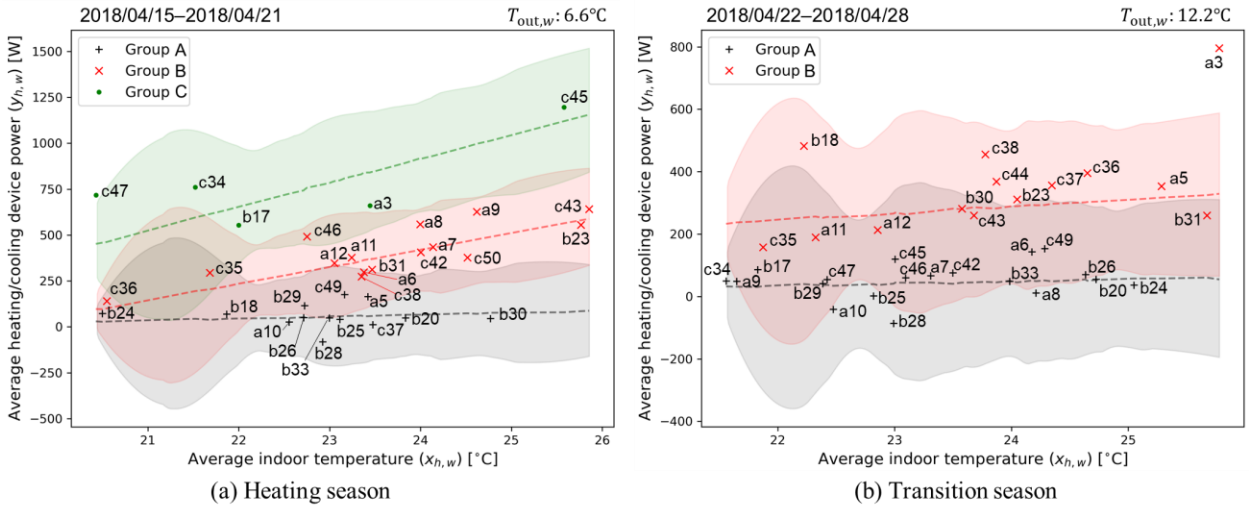

Figure 4.5. Normalized groups for two consecutive weeks during the heating (left) and transition (right) seasons.

Normalization results for a week during the cooling season are presented in Figure 4.6. This week was classified as a cooling season week since the mean outdoor temperature (23.8℃) was higher than the estimated posterior mean of the cooling season cutoff (ϕ_{cooling}) value (18.5℃). Although higher energy consumption is observed compared to the transition season, only one group was identified. This building is located in a heating dominant climate, so the effect of building characteristics on HC energy consumption is more apparent in heating season. However, in the cooling season, the amount of cooling demand from disturbances is larger than that from outdoor air, so there is no distinctive difference in cooling demand due to building characteristics, which resulted in a single group.

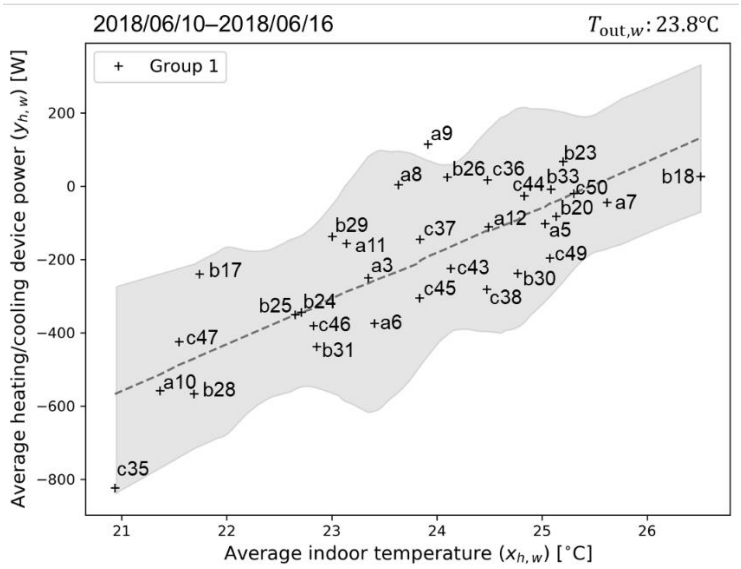

Figure 4.6. Normalized group for a week during the cooling season.

In addition to season-specific parameters, such as the intercept ($\beta_{0,k,w}$), that are estimated every week, other unit-specific parameters such as the unit noise variance (σ_h) and hyper prior of the slope ($\mu_{\beta_1,k,c}$) are updated with new data through Bayesian update. Therefore, it is important that group identification results are consistent over different weeks to confirm the validity of the model update. In general, most units show consistent group assignments (Figure 4.7), but some units sometimes move between groups. Two scenarios can explain the changes in group assignment. The parameters of the model include unobserved terms such as adjacent space temperatures and infiltration, and the same unit could have different values for these parameters in different weeks. Thus, the group assignment could change in different weeks. Another case is zero energy consumption due to vacancy, such as the units that were assigned to group A as shown in Figure 4.4. Consider unit b25 that was normally in group B but sometimes in group C. During two periods 2018/01/21–2018/02/03 and 2018/03/11–2018/03/24, there were no people in the unit and the thermostat was turned off. During these periods, this unit was assigned to group A because of very little heating energy consumption.

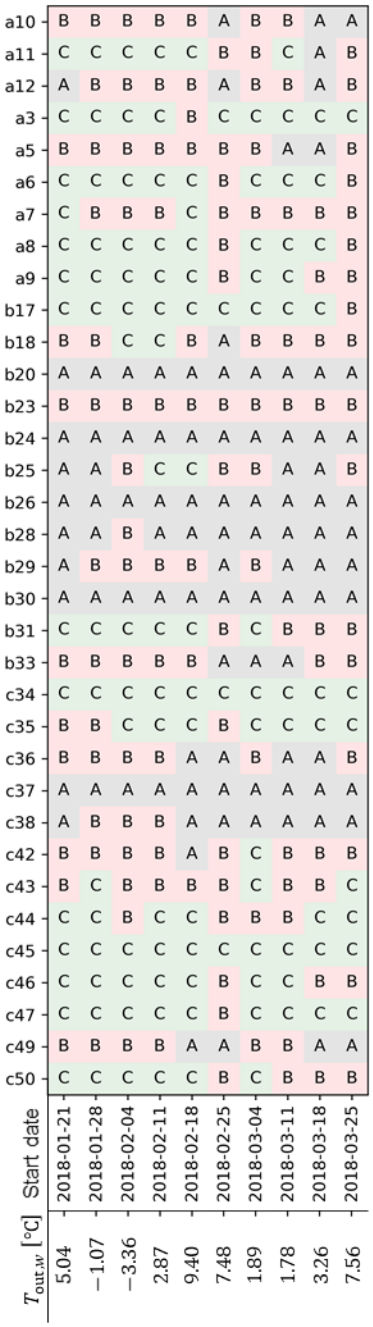

Figure 4.7. Changes in group assignment over different weeks in winter.

A counterfactual scenario for normative comparisons is illustrated in Figure 4.8. As discussed in Section 4.2.5, in a counterfactual scenario, all the units in the multi-family residential building are assumed to have similar building characteristics with a target unit (a3 in this case). In the model, this is realized by assigning the target unit values of $\beta_{0,k,w}$ and $\beta_{1,k,c,w}$ to all other units.

This procedure is graphically illustrated in Figure 4.8 (a). All units are mapped into group C (the group of a3), and posterior predictive distributions are used to create an empirical distribution as shown in Figure 4.8 (b). Each unit's data points are connected to the median of the posterior predictive distributions. The target unit a3 is located at 0.05 quantile of the distribution, meaning this unit is within the top 5% of energy efficiency among all units in the building.

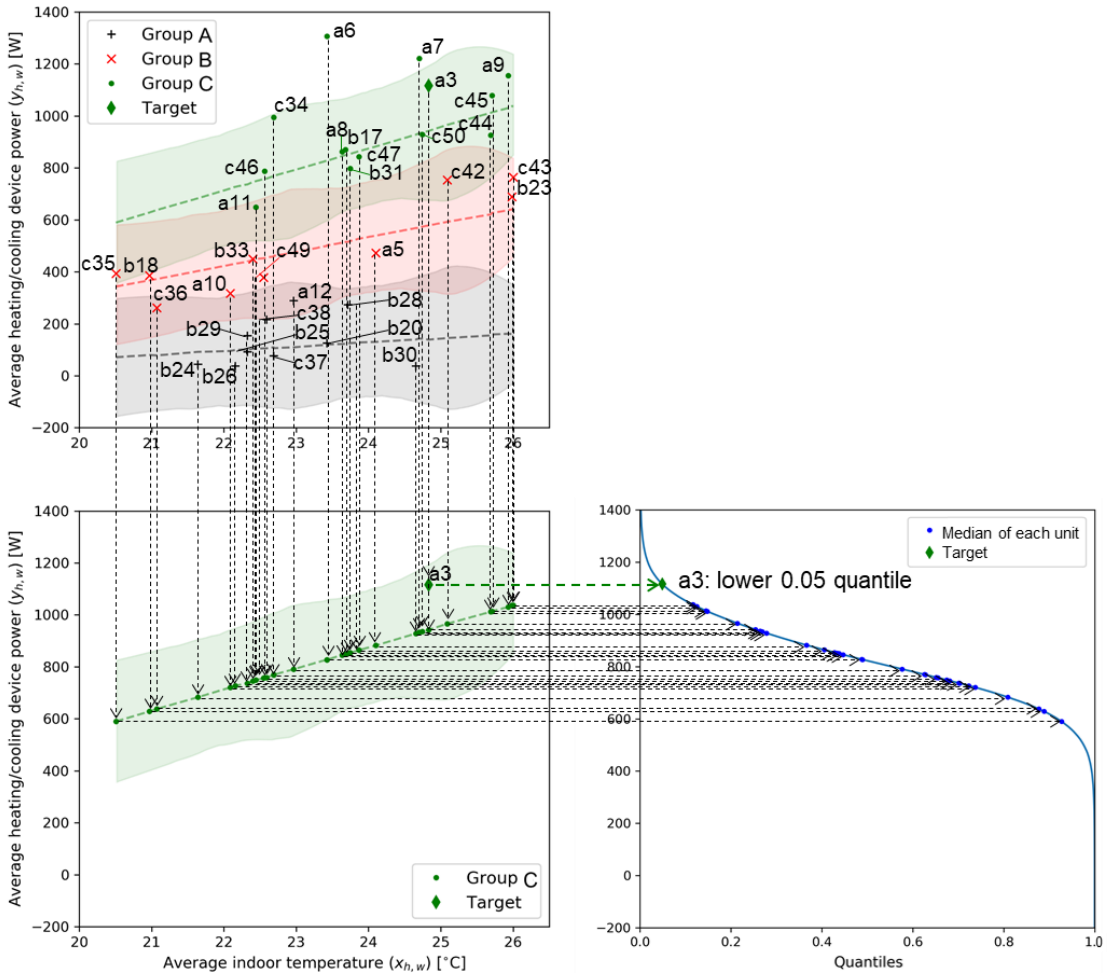

Figure 4.8. Counterfactual scenario – (a) mapping all units into the target group and (b) calculating quantiles from the empirical distribution.

To demonstrate the significance of normalization, comparisons without (a) and with normalization (b, c, d) are presented in Figure 4.9. Three units that have almost identical setpoint behaviors but were assigned to different groups were selected (a10 from group B, b31 from group

C, and c37 from group A). Their temperature profiles for the specific heating season week used for the analysis (2018/03/04–2018/03/10), are shown in Figure 4.10. It is observed that units c37, b31, and a10 had average heating setpoints of 22.2℃ (72°F), 22.8℃ (73°F), and 22.8℃ (72.8°F), respectively. The results without normalization (Figure 4.9 (a)) were determined by creating an empirical distribution of the HC energy consumption for all units. Although the units had similar behavior, each unit would have received three significantly different eco-feedback messages. For example, unit c37 consumed less than the community median by 463 kWh during this week, which corresponds to approximately $55 considering the electricity price in the specific building location (Indiana, U.S. (Indianapolis Power & Light Company, 2018)). Also, for unit b31, the heating energy consumption was more than the community median by 151 kWh during this week, which has a value of approximately $18. However, with normalization and a counterfactual scenario (Figure 4.9 (b, c, d)), unit c37 would consume only 12 kWh less than the median of all the other units in the building. The rank of this unit's energy efficiency would be in the top 46% among all units with normalization, but it was in the top 21% without normalization. Likewise, the energy consumption of unit b31 was less than the median of group C by 155 kWh. The rank of this unit's energy efficiency would be in the top 23% in all units with normalization while it was in the top 62% without normalization.

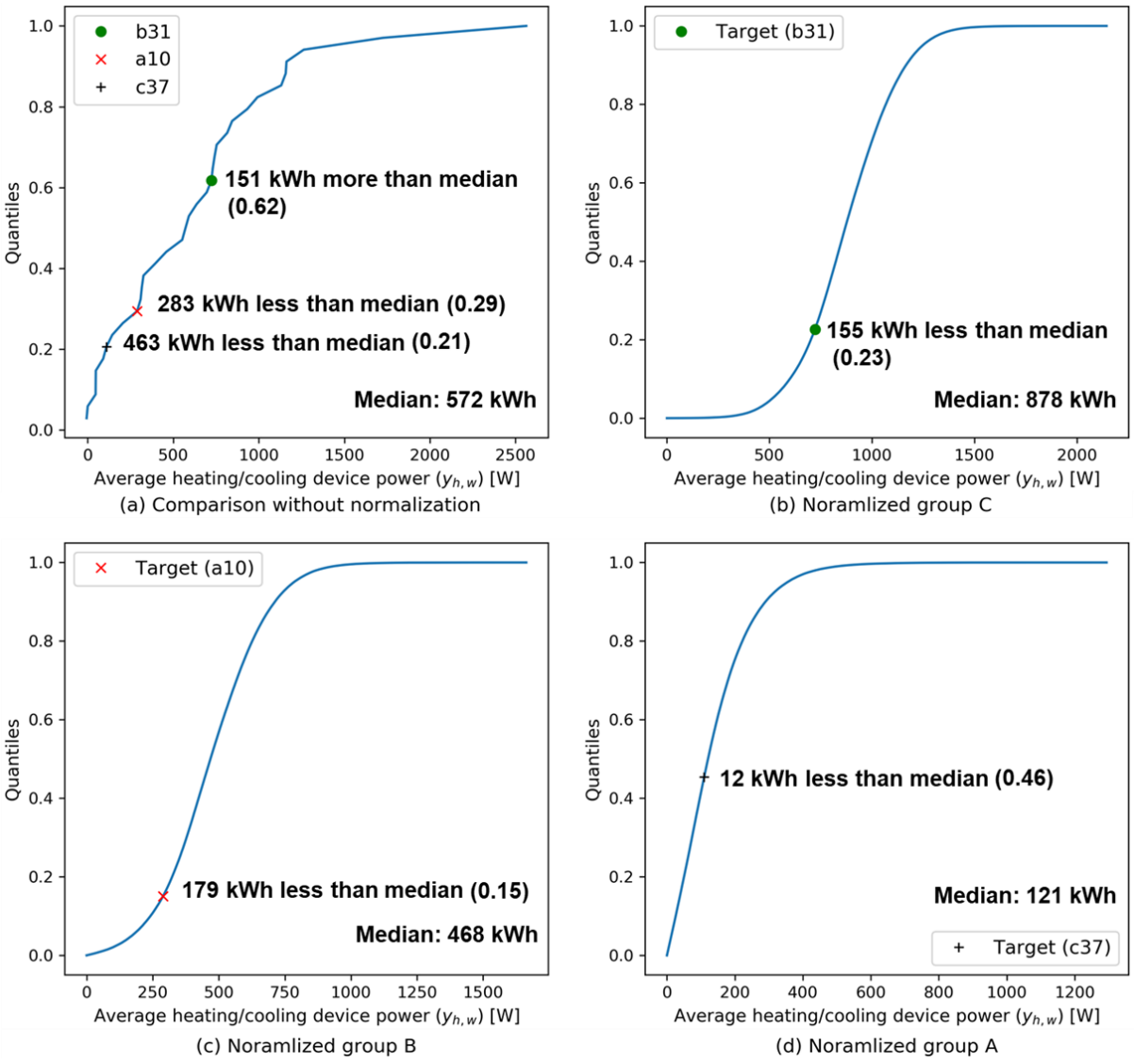

Figure 4.9. Normative comparison without (a) and with normalization (b, c, d).

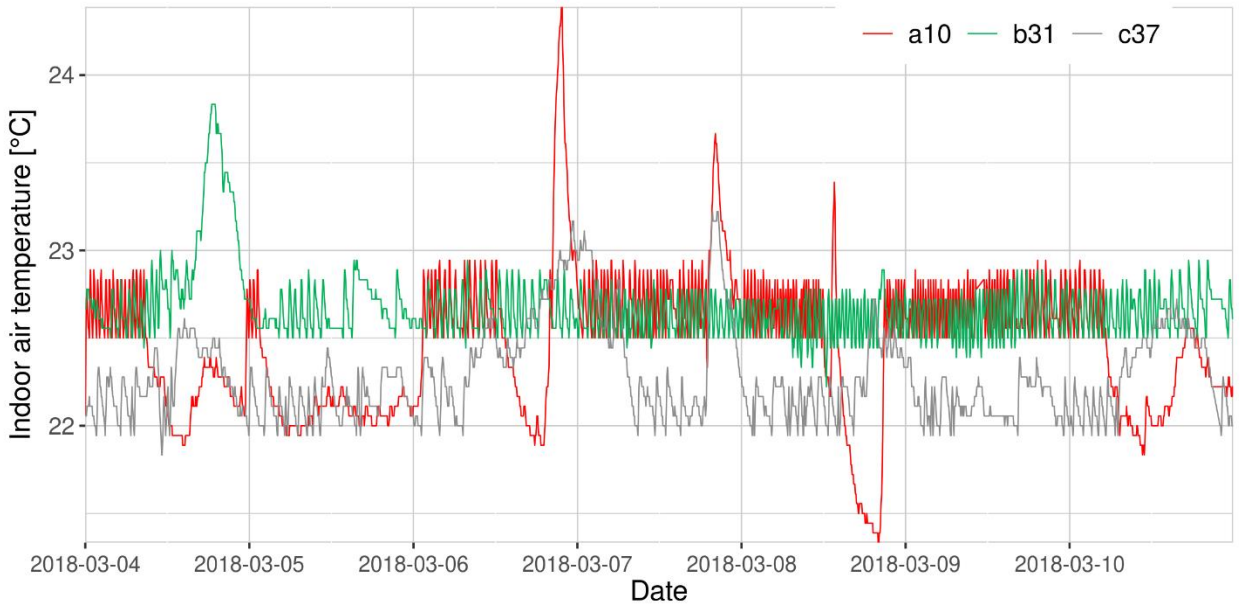

Figure 4.10. Indoor air temperature profiles of units a10, b31, and c37 in a heating season week.

In Table 4.1, we present the expected HC savings estimated based on the following counterfactual scenario: *"how much energy would a unit have saved if the unit had the setpoint schedule of the best (energy efficient) unit in the group?"*. This represents the ideal (i.e., maximum) energy saving potential estimated through a normative comparison assuming all units in each group behave like the most energy efficient peer. The results show that the expected HC savings per unit are 108.7-220.8kWh/month, and this is equivalent to $13.2-26.7/month savings based on the electricity rates of the utility company in IN (Indianapolis Power & Light Company, 2018). During the heating season, the average setpoints of the best peer are 20.3-22.9℃ while they are 24.1-25.8℃ for the cooling season.

Table 4.1. Estimated HC savings per unit for each month in 2018.

Month	1	2	3	4	5	6	7	8	9	10	11	12
HC saving [kwh]	158.4	200.7	170.7	113.5	203.9	191.8	220.8	199.5	146.6	108.7	196.4	150.6
HC saving [%]	32.4	40.9	48.5	49.9	83.0	74.0	79.3	70.8	63.7	52.4	54.1	33.8
Dollar saving [$]	15.5	20.5	18.0	13.7	24.6	23.0	26.7	24.9	18.7	13.2	20.6	15.2
Avg. setpoint of the best peer [℃]	22.1	21.0	20.3	23.1	23.6	25.8	25.7	24.1	23.8	23.7	22.9	22.3

4.4 Chapter conclusion and discussions

In this chapter, a data-driven building energy normalization model was presented. The model is designed to provide a reliable comparison of the impact of behavior on HC energy consumption by normalizing the effect of building characteristics in multi-family residential buildings. The model utilizes easily accessible data from smart thermostats and WiFi-enabled power meters. A physics-informed approach was used starting from a heat balance equation to derive a simplified linear regression model that represents the effect of building characteristics and occupant behavior on HC energy consumption while considering inter-unit heat transfer. Several groups of linear regressions are identified through a Bayesian mixture model that forms normalized groups of units. Furthermore, a Bayesian approach is used to assign unit- and season-specific prior information for parameters. From a practical viewpoint, sequential Bayesian update is applied so that the model can be used in a real-time form without the need for a large amount of data from different seasons.

The model was developed and demonstrated using data collected in a multi-family residential building located in Indiana, U.S. The results show that there were three, two, and one distinct normalized groups during the heating, transition, and cooling seasons, respectively. While HC energy comparison without normalization provides totally different rankings for units that have similar behavior, the proposed method captures the effect of behavior on HC energy consumption by normalizing the effect of building characteristics. In addition, the model successfully identifies different normalized groups for different seasons through sequential Bayesian update by capturing the changes in the HC demand due to weather. This structure allows the model to be implemented in a real building without the need for long-term measured data for model training. The formulation of model including unobserved variables was shown to successfully explain the data through an investigation of the predictive uncertainty of the model. Also, the model can be used to estimate the expected energy savings from a counterfactual scenario based on normative comparison to design energy efficiency programs.

Although the model is designed to be applicable for any multi-family residential building, there are limitations to be considered for general field implementation. First, the linear regression model is derived from a single-zone sensible energy balance equation under the assumption that all spaces in a unit are conditioned by a single thermostat and HC system. It is also necessary that there are several units that have similar layouts and HC system configurations. The building thermal parameters in the sensible energy balance equation such as capacitances, resistances, etc.

are lumped into two parameters in a linear regression to account for different levels of exposure to the exterior environment (e.g., envelope area) and the inter-unit heat transfer. In the unlikely event that a unit has completely different layout such as (i.e., two-story) it may need to be excluded from the analysis. Also, unit-specific indoor air temperature and power consumption data for HC devices need to be monitored for the linear regressions. However, the model includes an overall efficiency coefficient for the HC device in the regression parameters, so various types of HC devices for different units could be normalized together. Furthermore, the unit-level inter-unit heat transfer is not explicitly quantified in this model. Although it is included in the parameters of the linear regression, the model is designed to capture the lumped impact of building characteristics and inter-unit heat transfer on HC energy consumption. Therefore, it is not possible to split the effect of inter-unit heat transfer in this model. In addition, when there are non-periodic and atypical unobserved variables such as a device malfunction, incorrect thermostat settings, window opening during vacation, etc., the unit-specific noise may not sufficiently explain the unobserved variables in the model uncertainty. Finally, unobserved human behaviors such as appliance use, windows opening, etc. are modeled as unit-specific noise in weekly time interval by assuming weekly time dependency, so the model can be used for a longer time interval such as bi-weekly or monthly. However, the model parameters have different estimations in different seasons, and therefore, longer time interval than a month may fail to capture the effect of season change. With consideration of these limitations, the model is considered to be useful for implementation in an eco-feedback framework for any multi-family residential building. Furthermore, the model could be extended for application in multiple buildings from multiple locations by including an outdoor air temperature term in the linear regression. The recent increase of smart meters and thermostats and their data communication provide a new opportunity of utility-scale energy management such as thermostat behavior analysis (Huchuk et al., 2018; Ueno & Meier, 2020), power outage detection (Meier et al., 2019), customer segmentation and load shape analysis for demand management (Beckel, 2016; Kwac & Rajagopal, 2016; McLoughlin et al., 2015). By leveraging this infrastructure, the model could also be scaled up for utility level energy efficiency and demand management programs in future work.

5. REAL-TIME MODEL FOR UNIT-LEVEL HEATING AND COOLING ENERGY USE PREDICTION IN MULTI-FAMILY RESIDENTIAL HOUSING FOR ECO-FEEDBACK DESIGN

5.1 Overview

This chapter presents a real-time modeling approach to predict the HC energy consumption of individual units in multi-family residential housing. It includes (i) the development of a unit-level model (Section 5.2.1), (ii) the formulation of a Bayesian modeling framework to evaluate the effect of unobserved boundary conditions and unobserved disturbances on prediction uncertainty and to sequentially update model with new data (Section 5.2.2), (iii) the application of the model for counterfactual HC energy prediction in eco-feedback design (Section 5.2.4). The model performance along with limitations and recommendations for future work are discussed in Sections 5.3 and 5.4.

5.2 Real-time unit-level model

5.2.1 Model structure

The unit-level building thermal dynamics is modeled with a simple R-C model as shown in Figure 5.1 and all variables are described in Table 5.1. The model structure is selected through a system identification approach as described in Appendix C. It includes three temperature nodes representing the exterior wall ($x_{\mathrm{e},t}$), indoor air ($x_{\mathrm{i},t}$), and indoor mass ($x_{\mathrm{m},t}$). Each node has a thermal capacitance (C_{e}, C_{i}, and C_{m}, respectively) and they are connected through thermal resistances (R_{ie} and R_{im}). The exterior wall node is connected to the outdoor air node ($x_{\mathrm{a},t}$). The thermostat sensor is modeled with a separate node ($x_{\mathrm{s},t}$) with capacitance (C_{s}) because the thermostat in each unit is located near the entrance (Figure 3.2). The inter-unit heat transfer is modeled with a node representing the overall temperature of all adjacent spaces ($x_{\mathrm{n},t}$). $\psi_{\mathrm{n},t}$ is an unobserved disturbance modeled as an augmented state (i.e., stochastic random process) and naturally includes all the other unobserved disturbances such as windows opening, infiltration, etc., when the posterior of $x_{\mathrm{n},t}$ is estimated with data (see Section 5.2.2).

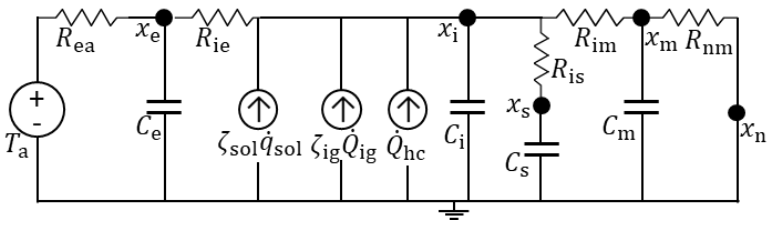

Figure 5.1. R-C diagram of unit-level model.

Table 5.1. State and input variables and model parameters.

Name	Description
x_a [°C]	Outdoor air temperature
x_i [°C]	Indoor air temperature
x_e, x_m, x_s [°C]	Exterior wall, interior mass, and thermostat sensor temperature
x_n [°C]	Overall temperature of adjacent spaces
y_{x_s}[°C]	Measured thermostat sensor temperature
$R_{ea}, R_{ie}, R_{in}, R_{nm}, R_{is}$ [k/W]	Thermal resistance between temperature nodes
C_e, C_i, C_m, C_s [J/K]	Thermal capacitance of each node
$\dot{q}_{sol}$ [W/m^2]	Global horizontal solar irradiance at the weather station
$\dot{Q}_{ig}$ [W]	Total power consumed by all appliances and devices in the unit
$\dot{Q}_{cal,hc}$ [W]	Calculated HC supply rate of heat pump system based on the measured power.
ζ_{sol}	Ratio of solar heat gain divided by the global horizontal solar irradiance
η_{hc}	Efficiency of HC supply rate of heat pump system
ζ_{ig}	Ratio of total internal heat gain (due to appliances, devices and occupants) divided by the corresponding power consumption

Therefore, we utilize a probabilistic approach to capture the stochastic process. Among the six temperature nodes, only two of them ($x_{a,t}$ and $x_{s,t}$) are observed in our field study. The thermal dynamics of all nodes (Figure 5.1) can be expressed as a set of differential equations of the states ($\mathbf{x}_t = \{x_{e,t}, x_{i,t}, x_{m,t}, x_{s,t}, x_{n,t}\}$) transition (Eqs. 5.1–5) with state noise variance $\boldsymbol{\sigma}_x^2 = \{\sigma_e^2, \sigma_i^2, \sigma_m^2, \sigma_s^2, \sigma_e^2\}$:

$$dx_{\mathrm{e},t} = \left(\frac{\left(x_{\mathrm{i},t} - x_{\mathrm{e},t}\right)}{R_{\mathrm{ie}}C_{\mathrm{e}}} + \frac{\left(x_{\mathrm{a},t} - x_{\mathrm{e},t}\right)}{R_{\mathrm{ea}}C_{\mathrm{e}}}\right)dt + \sigma_{\mathrm{e}}dw_{\mathrm{e},t}, \tag{5-1}$$

$$dx_{\mathrm{i},t} = \left(\frac{\left(x_{\mathrm{e},t} - x_{\mathrm{i},t}\right)}{R_{\mathrm{ie}}C_{\mathrm{i}}} + \frac{\left(x_{\mathrm{m},t} - x_{\mathrm{i},t}\right)}{R_{\mathrm{im}}C_{\mathrm{i}}} + \frac{\left(x_{\mathrm{s},t} - x_{\mathrm{i},t}\right)}{R_{\mathrm{is}}C_{\mathrm{i}}} + \eta_{\mathrm{hc}}\dot{Q}_{\mathrm{cal,hc}} + \zeta_{\mathrm{ig}}\dot{Q}_{\mathrm{ig}} + \zeta_{\mathrm{sol}}\dot{q}_{\mathrm{sol}}\right)dt + \sigma_{\mathrm{i}}dw_{\mathrm{i},t}, \tag{5-2}$$

$$dx_{\mathrm{m},t} = \left(\frac{\left(x_{\mathrm{i},t} - x_{\mathrm{m},t}\right)}{R_{\mathrm{im}}C_{\mathrm{m}}} + \frac{\left(x_{\mathrm{n},t} - x_{\mathrm{m},t}\right)}{R_{\mathrm{rm}}C_{\mathrm{m}}}\right)dt + \sigma_{\mathrm{m}}dw_{\mathrm{m},t}, \tag{5-3}$$

$$dx_{\mathrm{s},t} = \left(\frac{\left(x_{\mathrm{i},t} - x_{\mathrm{s},t}\right)}{R_{\mathrm{is}}C_{\mathrm{s}}}\right)dt + \sigma_{\mathrm{s}}dw_{\mathrm{s},t}, \tag{5-4}$$

$$dx_{\mathrm{n},t} = \sigma_{\mathrm{n}}dw_{\mathrm{n},t}, \tag{5-5}$$

where $\mathbf{w}_t = \{w_{\mathrm{e},t}, w_{\mathrm{i},t}, w_{\mathrm{m},t}, w_{\mathrm{s},t}, w_{\mathrm{n},t}\}$ are standard Wiener processes for the states ($\mathbf{x}$).

The continuous observation equation ($y_t = \int_t^{t+\Delta t} x_{\mathrm{s},\tau}d\tau + \int_t^{t+\Delta t} \sigma_y dw_{y,\tau}$) can be approximated as a discrete form (Eq. 5.6). There is only one observation state (y_{x_{s},t_k}) from $x_{\mathrm{s},t}$ with an error term following a normal distribution $\Pr(\varepsilon_{y,t_k}|\sigma^2_{\mathrm{d},y}) = \mathrm{Normal}(\varepsilon_{y,t_k}|0, \sigma^2_{\mathrm{d},y})$:

$$y_{x_s,t_k} = x_{\mathrm{s},t_k} + \varepsilon_{y,t_k}. \tag{5-6}$$

Since this is a continuous linear stochastic differential equation, we can calculate the states in the next timestep without integration through discretization (Rouchier et al., 2019; Särkkä & Solin, 2019). A 15-minute timestep is used in this study to increase the calculation speed and capture the building thermal dynamics. After discretization (noted with subscript d), the system can be expressed with the following probabilistic format (Eqs. 5.7 and 5.8):

$$\Pr(\mathbf{x}_{t_k+1}|\mathbf{x}_{t_k}) = \mathrm{Normal}(\mathbf{x}_{t_k+1}|\mathbf{A}_{\mathrm{d}}\mathbf{x}_{t_k} + \mathbf{B}_{\mathrm{d}}\mathbf{u}_{t_k}, \mathbf{\Sigma}_{\mathrm{d},x}), \tag{5-7}$$

$$\Pr(y_{x_s,t_k}|\mathbf{x}_{t_k}) = \mathrm{Normal}(y_{x_s,t_k}|\mathbf{C}_d\mathbf{x}_{t_k}, \sigma^2_{\mathrm{d},y}), \tag{5-8}$$

where $\mathbf{x}_{t_k} = \left[x_{\mathrm{e},t_k}, x_{\mathrm{i},t_k}, x_{\mathrm{m},t_k}, x_{\mathrm{s},t_k}, x_{\mathrm{n},t_k}\right]^{\mathsf{T}}$ are states; y_{x_s,t_k} is measurement; $\mathbf{u}_{t_k} = \left[x_{\mathrm{a},t_k}, \dot{q}_{\mathrm{sol},t_k}, \dot{Q}_{\mathrm{ig},t_k}, \dot{Q}_{\mathrm{cal,hc},t_k}\right]^{\mathsf{T}}$ are external inputs; $\mathbf{A}_{\mathrm{d}}$ and $\mathbf{B}_{\mathrm{d}}$ are discretized system matrix from $\mathbf{A}$ and $\mathbf{B}$ (Eq. 5.9 and (Rouchier et al., 2019)). $\mathbf{C}_{\mathrm{d}} = [0 \quad 0 \quad 0 \quad 1 \quad 0]$.

$$\mathbf{A} = \begin{bmatrix} \frac{-1}{R_{\mathrm{ea}}C_{\mathrm{e}}} + \frac{-1}{R_{\mathrm{ie}}C_{\mathrm{e}}} & \frac{1}{R_{\mathrm{ie}}C_{\mathrm{e}}} & 0 & 0 & 0 \\ \frac{1}{R_{\mathrm{ie}}C_{\mathrm{i}}} & \frac{-1}{R_{\mathrm{ie}}C_{\mathrm{i}}} + \frac{-1}{R_{\mathrm{im}}C_{\mathrm{i}}} + \frac{-1}{R_{\mathrm{is}}C_{\mathrm{i}}} & \frac{1}{R_{\mathrm{im}}C_{\mathrm{i}}} & \frac{1}{R_{\mathrm{is}}C_{\mathrm{i}}} & 0 \\ 0 & \frac{1}{R_{\mathrm{im}}C_{\mathrm{m}}} & \frac{-1}{R_{\mathrm{im}}C_{\mathrm{m}}} + \frac{-1}{R_{\mathrm{nm}}C_{\mathrm{m}}} & 0 & \frac{1}{R_{\mathrm{nm}}C_{\mathrm{m}}} \\ 0 & \frac{1}{R_{\mathrm{is}}C_{\mathrm{s}}} & 0 & \frac{-1}{R_{\mathrm{is}}C_{\mathrm{s}}} & 0 \\ 0 & 0 & 0 & 0 & 0 \end{bmatrix}, \quad \text{(5-9)}$$

$$\mathbf{B} = \begin{bmatrix} \frac{1}{R_{\mathrm{ea}}C_{\mathrm{e}}} & 0 & 0 & 0 \\ 0 & \frac{\zeta_{\mathrm{sol}}}{C_{\mathrm{i}}} & \frac{\zeta_{\mathrm{ig}}}{C_{\mathrm{i}}} & \frac{\eta_{\mathrm{hc}}}{C_{\mathrm{i}}} \\ 0 & 0 & 0 & 0 \\ 0 & 0 & 0 & 0 \\ 0 & 0 & 0 & 0 \end{bmatrix}.$$

The solar heat gain to the unit is modeled with a lumped parameter (ζ_{sol}) that includes the effective window area, orientation of window, and window thermal properties, multiplied by the global horizontal irradiance ($\dot{q}_{\mathrm{rad},t_k}$). Although this is a simplification, we believe that it adequately captures the effect of solar radiation, and our model structure allows the parameter value to be updated with new data. We assume that internal heat gains are governed by large appliances such as oven range while the occupant heat gains are correlated with the plug loads. Therefore, the total internal heat gains due to appliances (e.g., plug loads, oven, etc.) and occupants (e.g., body heat gain) is calculated with a constant (η_{ig}) multiplied by power consumption ($\dot{Q}_{\mathrm{ig},t_k}$). We assume that other disturbances such as infiltration, ventilation, etc. are included in the disturbance state ($x_{\mathrm{n},t}$) as mentioned earlier.

The HC system in our testbed has four modes of operation (Eqs. 5.10 and 5.11): (1) heat pump heating (htg), (2) auxiliary heating (aux), (3) heat pump heating with defrost cycle (df), and (4) heat pump cooling (clg). The operation mode $\left(i_{\mathrm{hc},t_k} \in \{\mathrm{htg}, \mathrm{aux}, \mathrm{df}, \mathrm{clg}\}\right)$ is determined based on the thermostat setting, current sensor temperature and outdoor air temperature. The actual heat flow rate ($\dot{Q}_{\mathrm{hc},t_k}$) from the heating and cooling system is obtained using a constant efficiency coefficient (η_{hc}) times the calculated heat flow rate ($\dot{Q}_{\mathrm{cal,hc},t_k}$) determined using information from the equipment manufacturer.

$$\eta_{\mathrm{hc},t_k} = \begin{cases} \eta_{\mathrm{htg}} & \text{if } i_{\mathrm{hc},t_k} = \mathrm{htg} \\ \eta_{\mathrm{aux}} & \text{if } i_{\mathrm{hc},t_k} = \mathrm{aux} \\ \eta_{\mathrm{df}} & \text{if } i_{\mathrm{hc},t_k} = \mathrm{df}\text{'} \\ \eta_{\mathrm{clg}} & \text{if } i_{\mathrm{hc},t_k} = \mathrm{clg} \end{cases} \tag{5-10}$$

where η_{hc,t_k} is an efficiency coefficient of each operation mode ($i_{\mathrm{hc},t_k} \in \{\mathrm{htg}, \mathrm{aux}, \mathrm{df}, \mathrm{clg}\}$).

The calculated heat flow rate ($\dot{Q}_{\mathrm{cal,hc},t_k}$) is estimated from the measured power consumption ($P_{\mathrm{mes,hc}}$) times the coefficient of performance (COP). Then, the actual heating or cooling rate ($\dot{Q}_{\mathrm{hc},t_k}$) is determined as the product of the efficiency coefficient and calculated heat flow according to binary control signal (i_{hc,t_k}) as:

$$\dot{Q}_{\mathrm{hc},t_k} = \begin{cases} \dot{Q}_{\mathrm{htg},t_k} = \eta_{\mathrm{htg}}\dot{Q}_{\mathrm{cal,htg},t_k} = \eta_{\mathrm{htg}}\mathrm{COP}_{\mathrm{htg},t_k}P_{\mathrm{mes,htg},t_k} & \text{if } i_{\mathrm{hc},t_k} = \mathrm{htg} \\ \dot{Q}_{\mathrm{aux},t_k} = \eta_{\mathrm{aux}}\dot{Q}_{\mathrm{cal,aux},t_k} = \eta_{\mathrm{aux}}\mathrm{COP}_{\mathrm{aux},t_k}P_{\mathrm{mes,aux},t_k} & \text{if } i_{\mathrm{hc},t_k} = \mathrm{aux} \\ \dot{Q}_{\mathrm{df},t_k} = \eta_{\mathrm{df}}\dot{Q}_{\mathrm{cal,df},t_k} = \eta_{\mathrm{df}}\left(\mathrm{COP}_{\mathrm{aux},t_k}P_{\mathrm{mes,aux},t_k} + \mathrm{COP}_{\mathrm{htg},t_k}P_{\mathrm{mes,htg},t_k}\right) & \text{if } i_{\mathrm{hc},t_k} = \mathrm{df}\text{'} \\ \dot{Q}_{\mathrm{clg},t_k} = \eta_{\mathrm{clg}}\dot{Q}_{\mathrm{cal,clg},t_k} = \eta_{\mathrm{clg}}\mathrm{COP}_{\mathrm{clg},t_k}P_{\mathrm{mes,clg},t_k} & \text{if } i_{\mathrm{hc},t_k} = \mathrm{clg} \end{cases} \tag{5-11}$$

where $\mathrm{COP}_{\mathrm{htg},t_k}$ and $\mathrm{COP}_{\mathrm{clg},t_k}$ are the coefficient of performance values of the heat pump for heating and cooling, respectively.

The COP curves were acquired from manufacturer's catalogue data and modelled as a linear function of the outdoor air temperature (x_{a,t_k}). The coefficient of performance of the electric auxiliary heating ($\mathrm{COP}_{\mathrm{aux},t_k}$) is set to 1.

5.2.2 State filter with real-time parameter learning

There are several approaches to estimate posterior distributions of states and parameters for Eq. 5.7. A naive approach is to estimate the full joint probability of states and parameters ($P\left(\mathbf{x}_{0:t_K}, \boldsymbol{\theta} | \mathbf{y}_{1:t_K}\right)$), but this is inefficient because the state dimension is proportional to the time dimension ($1{:}\, t_K$). In addition, estimation could fail because of the large sampling space of states especially when not all **x** are observed in **y**.

A typical approach to solve this problem is to use a state filter. Given the posterior distribution of parameters with data measured so far ($P\left(\boldsymbol{\theta} | \mathbf{y}_{1:t_K}\right)$), the posterior of states ($P\left(\mathbf{x}_{1:t_K}, | \mathbf{y}_{1:t_K}\right)$) can be easily obtained by solving a filtering problem. Kalman filter is used for a linear Gaussian model (Rouchier et al., 2019), and particle filter (i.e., Sequential Monte Carlo (SMC)) (Eq. 16) is used for a non-Gaussian model (Doucet, 2006). Since these filters provide the

state-marginalized likelihood ($P(\mathbf{y}_{1:t_K}|\boldsymbol{\theta}) = \int P(\mathbf{y}_{1:t_K}|\mathbf{x}_{1:t_K}, \boldsymbol{\theta})\, P(\mathbf{x}_{1:t_K}|\boldsymbol{\theta}) d\mathbf{x}_{1:t_K}$), it is possible to get the posterior distribution of parameters by sampling through a Markov Chain Monte Carlo (MCMC) technique on the marginal-likelihood (i.e., $P(\boldsymbol{\theta}|\mathbf{y}_{1:t_K}) \propto P(\mathbf{y}_{1:t_K}|\boldsymbol{\theta})\, P(\boldsymbol{\theta})$) (Andrieu et al., 2010).

However, these parameter estimation methods are not designed to estimate parameters with real-time streaming data. In this case, when new data become available, the posterior of parameters and states need to be updated together. With the new data ($\mathbf{y}_{t_k+1}$), the posterior distribution of updated states and parameters can be written as Eq. 5.12:

$$\begin{aligned}\Pr(\mathbf{x}_{t_k+1}, \mathbf{x}_{0:t_k}, \boldsymbol{\theta}|\mathbf{y}_{1:t_k}, \mathbf{y}_{t_k+1}) &\propto \Pr(\mathbf{y}_{t_k+1}|\mathbf{x}_{t_k+1}, \mathbf{x}_{0:t_k}, \boldsymbol{\theta}, \mathbf{y}_{1:t_k}) \Pr(\mathbf{x}_{t_k+1}, \mathbf{x}_{0:t_k}, \boldsymbol{\theta}|\mathbf{y}_{1:t_k}) \\ &\propto \Pr(\mathbf{y}_{t_k+1}|\mathbf{x}_{t_k+1}, \boldsymbol{\theta}) \Pr(\mathbf{x}_{t_k+1}|\mathbf{x}_{t_k}, \boldsymbol{\theta}) \underbrace{\Pr(\mathbf{x}_{0:t_k}|\boldsymbol{\theta}, \mathbf{y}_{1:t_k}) \Pr(\boldsymbol{\theta}|\mathbf{y}_{1:t_k})}_{\text{Posterior without new data}}. \end{aligned} \quad (5\text{-}12)$$

In Bayesian inference, when drawing a new parameter set, it is necessary to calculate the probability density of $P(\mathbf{x}_{0:t_k}|\boldsymbol{\theta}, \mathbf{y}_{1:t_k})\, P(\boldsymbol{\theta}|\mathbf{y}_{1:t_k})$ in Eq. 5.12. Although $P(\mathbf{x}_{0:t_k}|\boldsymbol{\theta}, \mathbf{y}_{1:t_k})$ can be marginalized through the particle filter, all the historic data is used for density of $P(\boldsymbol{\theta}|\mathbf{y}_{1:t_k})$ unless this posterior is approximated by a certain distribution. For this reason, the real-time version of state and parameter sampler called SMC^2 needs to use all historic data (Chopin et al., 2013; Rouchier et al., 2019).

Real-time methods that do not require all historic data have been proposed (Lopes & Tsay, 2011). In these methods, while the posterior distribution of states is updated through a particle filter, the posterior distribution of parameters is also updated at the same time. Storvik-filter (Storvik, 2002) or particle learning methods (Carvalho et al., 2010) use sufficient statistics to generate new parameter samples during the update step. In this method, by putting conjugate priors, the posterior distribution with previous data can be expressed in a closed form of sufficient statistics. However, when the model structure is complex, having the closed form of parameter posterior distribution is challenging.

Liu-West filter (LW filter) (Liu & West, 2001) takes a slightly different approach. The posterior distributions of parameters are approximated by a mixture of multivariate normal distribution (i.e., kernel mixture smoothing) (West, 1993). The posterior distributions of the next time step are updated when new data are available by adding small noise to the current posterior distributions for generating new parameters while the posterior distributions of states are obtained through auxiliary particle filter (Pitt & Shephard, 1999). This is similar to the augmented state-

space approach for parameter learning (Radecki & Hencey, 2017; Simon, 2006). However, adding small noise in each time step results in diffusion in posterior distributions. LW filter overcomes this diffusion problem using location shrinkage of posterior samples to their mean to regulate the dispersion of variance of posterior distributions.

Although the tuning process of this model (e.g., prior selection) is difficult (Kantas et al., 2015), we adopt LW filter because it handles streaming data and learns the parameters in real-time without analytical derivation of sufficient statistics of parameters by using kernel smoothing technique. How to create prior distributions is discussed in the next section. The mathematical details of LW filter are shown in the original paper (Liu & West, 2001). The steps of the algorithm used in our model are presented in Appendix D. To demonstrate the applicability of LW filter to a building gray-box model, we created a synthetic dataset with realistic building parameters and then applied the filter to see the proposed prior generation and filtering method will find the correct posterior distribution. The source code is available in author's Github repository (Ham, 2021).

5.2.3 Model initialization (prior generation)

Using the LW filter, the model needs to initiate all state and parameter particle samples to sequentially filter and learn states and parameters, respectively. Theoretically, when the filtering step proceeds, the posterior distribution of parameters converges to a certain distribution from any initial points (i.e., non-informative or flat priors). However, we observed several training divergences with these broad prior distributions because of the way the filter updates. Specifically, unlike batch learning (such as MCMC), LW filter holds posterior samples that have high likelihood in each time step. In this case, when there is unexpectedly large unmodeled disturbances (e.g., window/door opening, infiltration, etc.) or an unstable measurement, the filter can hold wrong parameter samples to account for the disturbances in the modeled parameters. In addition, it is also possible that the model could be a null model in which the adjacent spaces temperature state governs the whole dynamical process. For example, if the adjacent spaces temperature state is connected to the sensor temperature state with a very small thermal resistance value, the adjacent spaces temperature state could follow almost the same trajectory with the sensor temperature state. In this case, the model does not capture the thermal dynamics of the building. From this analysis,

we conclude that some parameters that related to the building thermal dynamics need to start with good prior distributions.

Two approaches are considered to create the prior distributions in this research. With one-week of training data, we create a prior distribution by using (1) MCMC or (2) system identification. With a Kalman filter and state-marginalized likelihood, it is possible to sample the posterior of parameters via MCMC. The final posterior distribution can be used for prior particles of the LW filter for the new data. However, we found that MCMC is unstable and slow for our application. In our model, the adjacent spaces state (x_{n}) acts as a disturbance governed by the noise parameters, so the MCMC results are strongly affected by how we normalize the numerical scale of the state noise variance ($\boldsymbol{\sigma}_x^2$), which requires trial-and-error tuning.

Therefore, we adopt the second approach (system identification). The parameters are estimated by solving an optimization problem in Eq. 5.13 (Joe et al., 2018; S. Wang & Xu, 2006):

$$\mathbf{x}_1^{\mathrm{opt}}, \boldsymbol{\zeta}^{\mathrm{opt}} = \arg\min_{\mathbf{x}_1, \boldsymbol{\zeta}} \sum \left(\mathbf{y}_{1:t_K} - \hat{\mathbf{y}}_{1:t_K}\right)^2 / t_K \,, \tag{5-13}$$

where $\hat{\mathbf{y}}_{t_k} = \mathbf{C}_{\mathrm{d}}\left(\mathbf{A}_{\mathrm{d}}\mathbf{x}_{t_k-1} + \mathbf{B}_{\mathrm{d}}\mathbf{u}_{t_k-1}\right)$ for $t_k = 1, \ldots, t_K$, and

$$\boldsymbol{\zeta} = \left\{C_{\mathrm{e}}, C_{\mathrm{m}}, C_{\mathrm{i}}, C_{\mathrm{s}}, R_{\mathrm{ea}}, R_{\mathrm{ie}}, R_{\mathrm{in}}, R_{\mathrm{nm}}, R_{\mathrm{is}}, \zeta_{\mathrm{solg}}, \zeta_{\mathrm{ig}}, \eta_{\mathrm{htg}}, \eta_{\mathrm{aux}}, \eta_{\mathrm{df}}, \eta_{\mathrm{clg}}\right\}.$$

Since we neglect the state noise ($\boldsymbol{\sigma}_x^2$) and use fixed adjacent spaces temperature ($x_{\mathrm{n},t_k+1} = x_{\mathrm{n},t_k}$), various local optimum solutions can be obtained by having random initial values within the wide ranges of parameters (Table 5.2). These ranges are roughly determined based on the scale of each material's physical property (ASHRAE, 2013a). Due to the wide ranges and different scales of parameters, n-step prediction could diverge due to numerically instable system matrix after the discretization (i.e., $\mathbf{A}_{\mathrm{d}}$ and $\mathbf{B}_{\mathrm{d}}$ in Eq. 5.13). When there is divergence, we revised the cost function to return large cost instead of error so that the optimizer would not fail. Each parameter set has the dynamics of the building thermal process because it is obtained from the n-step (or t_K-step) ahead prediction in Eq. 13 with various $x_{\mathrm{n},1}$. With this approach, when the parameter particles are slightly updated to correct the posterior with new data, the parameter particles do not easily lose the dynamic characteristics of the building thermal process from temporal disturbances. For the optimization, we use a differential evolutionary global optimization method (Mullen et al., 2011). Also, we use a multivariate kernel density estimator (Nagler, 2017) to generate prior particles instead of directly using the optimum solutions as particles. From 500 optimization solutions, 10000 particles are generated to create kernel density estimators.

Table 5.2. Optimization bounds

Optimization variable	Lower bound	Upper bound
$x_{\mathrm{a},1}[℃]$	-1	21.1
$x_{\mathrm{i},1}, x_{\mathrm{m},1}, x_{\mathrm{s},1}, x_{\mathrm{n},1}$ [℃]	15.5	26.7
C_{e} [kJ/K]	190	57000
C_{i} [kJ/K]	9.49	9495
C_{m} [kJ/K]	19000	123441
C_{s} [kJ/K]	9.5	1900
$R_{\mathrm{ea}}, R_{\mathrm{ie}}$ [K/kW]	2.6	52.6
$R_{\mathrm{is}}, R_{\mathrm{im}}, R_{\mathrm{n}}$ [K/kW]	5.2·1e-5	5.26
$\zeta_{\mathrm{sol}}[-]$	0	0.01
$\zeta_{\mathrm{ig}}, \eta_{\mathrm{htg}}, \eta_{\mathrm{aux}}, \eta_{\mathrm{df}}, \eta_{\mathrm{clg}}[-]$	0	1

5.2.4 Prediction of counterfactual scenario

Two types of prediction scenarios are typically considered in terms of message framing in eco-feedback design: counterfactual and hypothetical. In a counterfactual scenario, we pose the following question: '*how much energy would I have consumed if I had a different setpoint schedule for last week?*'. On the other hand, in a hypothetical scenario, we ask '*how much energy will I consume if I have a different setpoint schedule for this coming week?*'.

In this study, we use the model to make predictions in a counterfactual scenario as shown in Figure 5.2. Specifically, we use all measured inputs, $\mathbf{u}$: $x_{\mathrm{a}}, \dot{q}_{\mathrm{sol}}, \dot{Q}_{\mathrm{ig}}$, except for the calculated HC rate and the filtered temperature of adjacent spaces (x_{n}). In the unit-level model (Figure 5.1), x_{n} is modeled as a randomly moving temperature source, and its posterior profile is obtained during the filtering process. If we put this temperature into the prediction process, we can simulate the thermal dynamics of a specific unit with consideration of the effect of adjacent spaces by assuming the bi-directional effect of the unit's temperature change from adjacent spaces. This assumption is discussed in Section 5.2.5.

During the filtering and learning process, we use the calculated HC flow rate ($\dot{Q}_{\mathrm{cal,hc}}$) from the observed HC binary signal and the measured power. However, in a prediction scenario, the HC binary signal for the next time step ($\hat{\imath}_{\mathrm{hc},t_k} = \{\mathrm{htg}, \mathrm{clg}, \mathrm{aux}, \mathrm{df}\}$) is determined from the thermostat based on the setpoint (x_{sp}) and the predicted sensor temperature ($\hat{x}_{\mathrm{s}}$). Therefore, we implemented

a rule-based thermostat model using the thermostat specifications and settings (Table 5.3) to determine the heat/cool binary signal every time step. We use a 5-minute time step because many of the settings in the thermostat have a 5-minute resolution.

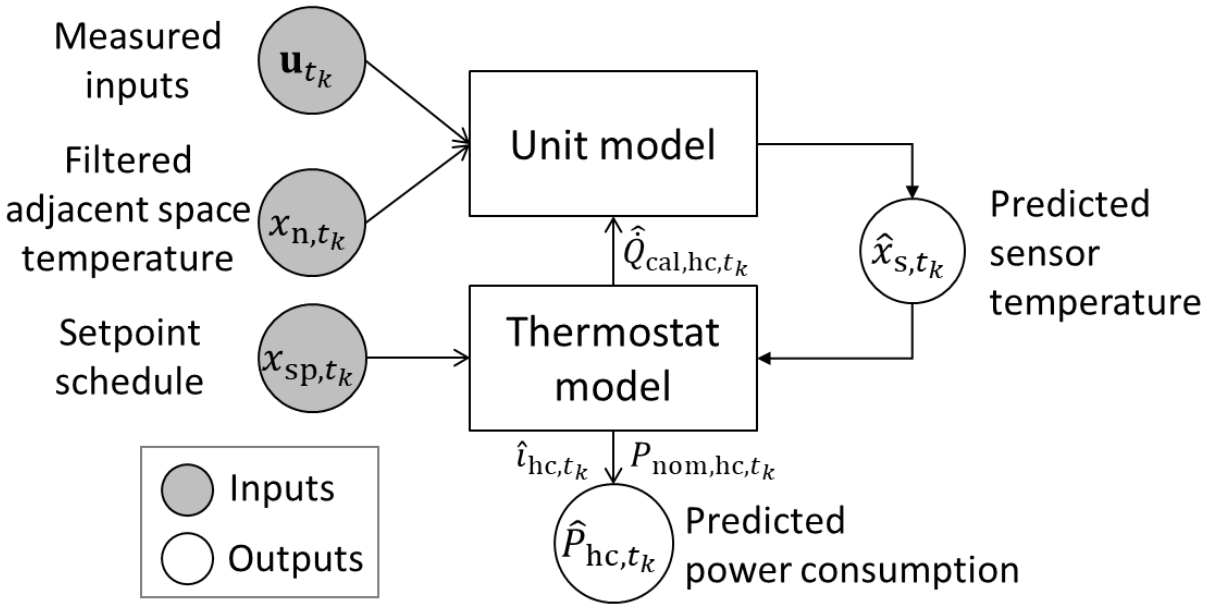

Figure 5.2. Counterfactual prediction process.

The HC supply heat rate ($\dot{Q}_{\mathrm{cal,hc}}$) is estimated from measurements of the power consumption ($P_{\mathrm{mes,hc}}$) for the predicted HC signal ($\hat{\imath}_{\mathrm{hc},t_k}$). In an ideal scenario, the power consumption is the same under the same $\hat{\imath}_{\mathrm{hc},t_k}$. However, the measured power is affected by various factors such as on/off cycling frequency, start-up operation, outdoor air temperature, status of refrigerant, etc. Therefore, the relationship between $\hat{\imath}_{\mathrm{hc}}$ and predicted power measurement ($\hat{P}_{\mathrm{mes,hc}}$) is modeled using the real to nominal power ratio (k_{hc}) times the nominal power ($P_{\mathrm{nom,hc}}$) (Eq. 5.14), and it used to calculate $\hat{\dot{Q}}_{\mathrm{cal,hc}}$ as shown in Eq. 5.11. The nominal power can be obtained from manufacturer's catalog data.

$$P_{\mathrm{mes,hc},t_k}: \begin{cases} P_{\mathrm{mes,htg},t_k} = k_{\mathrm{htg}} P_{\mathrm{nom,htg},t_k} & \text{when } i_{\mathrm{hc},t_k} = \text{htg or df} \\ P_{\mathrm{mes,aux},t_k} = k_{\mathrm{aux}} P_{\mathrm{nom,aux},t_k} & \text{when } i_{\mathrm{hc},t_k} = \text{aux or df.} \\ P_{\mathrm{mes,clg},t_k} = k_{\mathrm{clg}} P_{\mathrm{nom,clg}} & \text{when } i_{\mathrm{hc},t_k} = \text{clg} \end{cases} \tag{5-14}$$

The real to nominal power ratio k_{hc} is obtained by calculating $P_{\mathrm{mes,htg},t_k}/P_{\mathrm{nom,htg}}$ in each time step, and these values are expressed as a distribution instead of a single number. However, this requires a large amount of data to calculate all k_{hc} values for all combinations of the heat pump operation. Therefore, we approximate the distribution of k_{hc} as a normal distribution, and then the distribution is automatically updated with incoming data by using a Normal-Gamma distribution and its conjugate priors (Appendix E). Since the current posterior of k_{hc} is parameterized as a Normal-Gamma distribution, we can update the posterior of k_{hc} with new data without all the historic data.

Table 5.3. Thermostat rules

The minimum heat pump cycling time is 5 minutes (on/off and HC).
The minimum auxiliary heating ON time is 5 minutes.
When outdoor temperature is lower than $0℃$, the defrost cycle is activated. The cycling interval is determined by the sensor in outdoor unit.
Heating or cooling is enabled when the current temperature is lower or higher than $0.28℃$.
Heat pump heating is disabled when the outdoor temperature is lower than $-15℃$.
Auxiliary electric heating is disabled when the outdoor air temperature is higher than $12.8℃$.
When the setpoint is not met for 30 minutes with heat pump heating, the auxiliary heating is used together with the heat pump heating.

5.2.5 Model validation and performance evaluation

We consider two cases for seasonal and counterfactual scenario validation. Our model is designed to handle streaming data, so it is important to validate if the updated model prediction is accurate after a few months of continuous update, i.e., in a different season. This can be achieved by comparing the actual summer energy consumption with the summer energy prediction using the updated model from the winter season. The result is also compared with the non-updated model.

For the counterfactual scenario, the power consumption from a new setpoint scenario cannot be verified unless there is a dataset from parallel experiments. Since this is a physics-informed state-space model, it guarantees extrapolation of prediction (i.e., a new setpoint scenario) to some extent. However, in a multifamily residential building, counterfactual validation poses a challenge due to the heat transfer between units. As shown in Figure 5.2, the filtered value of the overall

temperature of adjacent spaces from the past data is used as an input for counterfactual prediction. But, when the target unit has a new setpoint scenario, the temperatures of adjacent spaces could change. We assume that this change is negligible as the adjacent units still have the same setpoint schedules. For example, when the target unit has a new heating setpoint schedule with high temperature, it could provide free heat to its adjacent units. While this would reduce the number of heating operation time of the adjacent units, the temperature of adjacent units would be similar during the heating season because they still have same heating setpoint schedules. To validate this assumption, we develop a multizone model that can capture the thermal dynamics of adjacent units for a target unit and compare the prediction results with the proposed approach. For the multizone model, we select one target unit and include its adjacent spaces. The details of the multizone model are presented in Appendix F.

5.3 Results

The results consist of three parts. First, we generate a synthetic dataset with known true parameters and test the proposed model. Due to space limitations, details are presented in Github repository (Ham, 2021). The second part is the process of model training with real data. This includes the prior generation (Section 5.3.1), state filtering and parameter learning (Section 5.3.2), and seasonal validation (Section 5.3.3). In the final part, the counterfactual validation is presented (Section 5.3.4). We use one non-corner unit on the 2nd floor for the second part as it is the most common type in this building. For the third part, one non-corner unit on the 4th floor is used.

5.3.1 Prior generation

To generate prior particles, 500 optimizations (Eq. 5.13) were conducted. One week of heating season data (January 2018) was used for the optimization to learn the heating efficiency coefficient. 10000 initial prior particles were generated through a kernel approximation. Figure 5.3 shows the comparison between generated prior particles and optimization results for a few parameters ($C_{\mathrm{e}}, C_{\mathrm{m}}, R_{\mathrm{ea}}, R_{\mathrm{ie}}, R_{\mathrm{im}}$). We observe two distinctive characteristics. First, the generated prior particles cover a wider range compared to the optimization results. The other characteristic is that the correlation between parameters in optimization results are preserved in the generated prior particles. For example, R_{ie} and R_{ea} show inverse correlation. This approach helps to explore

a broad parameter space as well as preserve characteristics of the building thermal dynamics in the parameters.

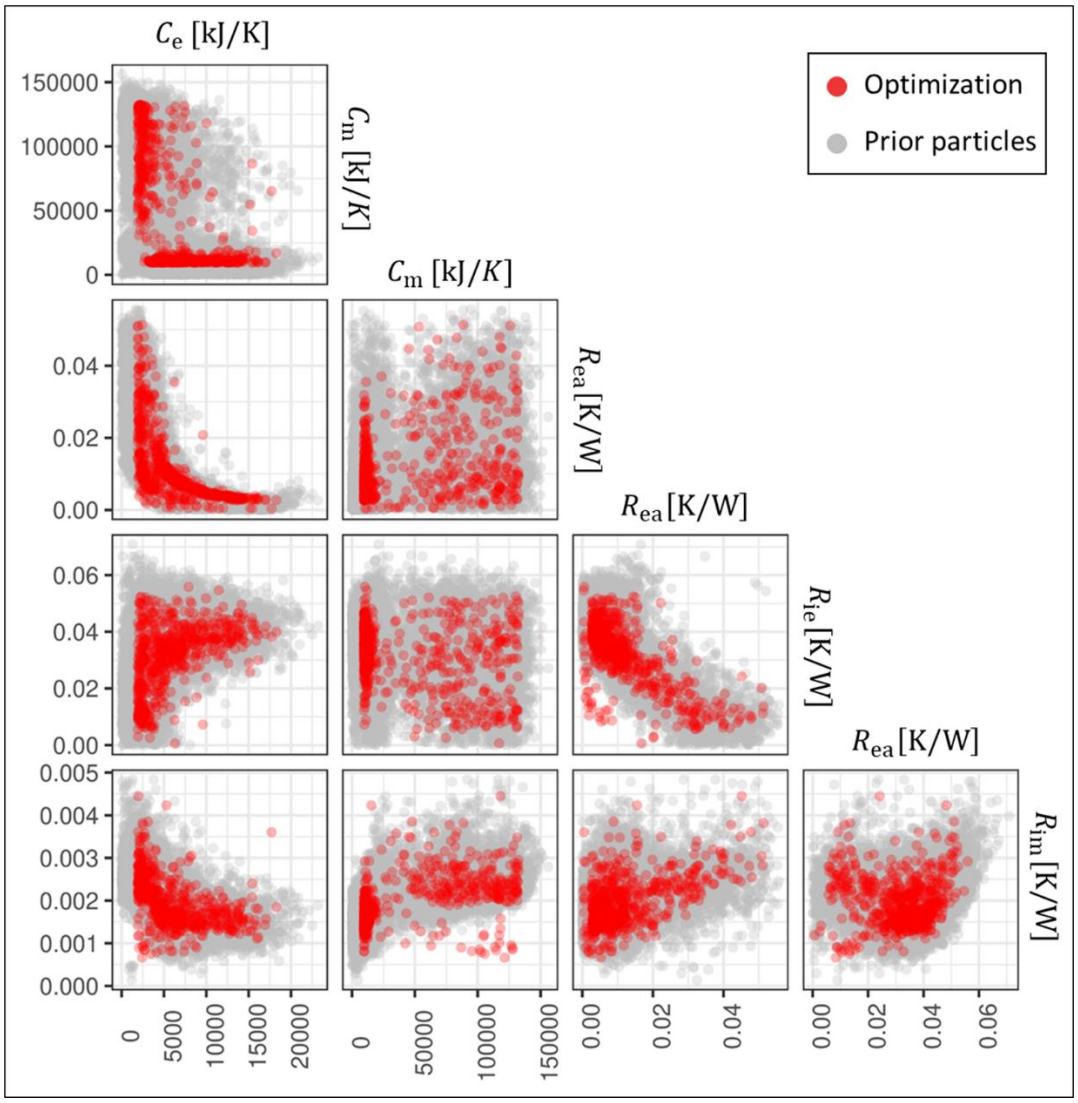

Figure 5.3. Correlation matrix of generated prior particles from optimization results.

5.3.2 State filtering and parameter learning

Figure 5.4 shows the filtered states for a specific unit through the particle filtering process and heating power data for a week in Sep 2018. The computation time of weekly update is approximately 10 minutes for one unit based on 10000 particles of each state and parameter by using 7 processors for parallel computation on a desktop machine (Intel® CPU i7-6700@3.4GHz,

4 Cores with 8 Logical processors and 16 GB memory). The For the thermostat sensor temperature state (x_s), 2.5, 50, and 97.5 percentiles of the filtered distribution are visualized. In this period, the measured sensor temperature (y_{x_s}) is mostly in the filtered distribution of sensor temperature state despite of the measurement noise. There are two possible explanations. The raw measured data is smoothed by the thermostat cloud server every 5-minute, and therefore, there is no significant measurement oscillation due to measurement noise. In addition, since this analysis is conducted for the early Fall season, the parameters have been updated for 6 months of training period from January, and the measurement noise parameter is very small. The filtered states show a smoother profile because the field data include measurement noise and cycling due to heat pump on and off operation. In addition, we visualize the median profile of the state that represents the overall temperature of adjacent spaces (x_n). Before 2018-09-07, the filtered adjacent spaces temperature is notably higher than the indoor temperature. This can be interpreted by the fact that most neighboring spaces of this unit could have higher cooling setpoints. However, after 2018-09-07, the heat pump in this unit was turned off, and the adjacent spaces temperature profile is similar to the sensor temperature profile. As the adjacent spaces temperature node transfers heat through the indoor mass node (Figure 5.1), this can be viewed as a floating temperature profile resulting from the interaction among outdoor air, building mass, and adjacent spaces temperatures. Also, it should be noted that the adjacent spaces temperature includes unknown disturbances not incorporated in the unit-level model such as infiltration because it is modeled as floating state.

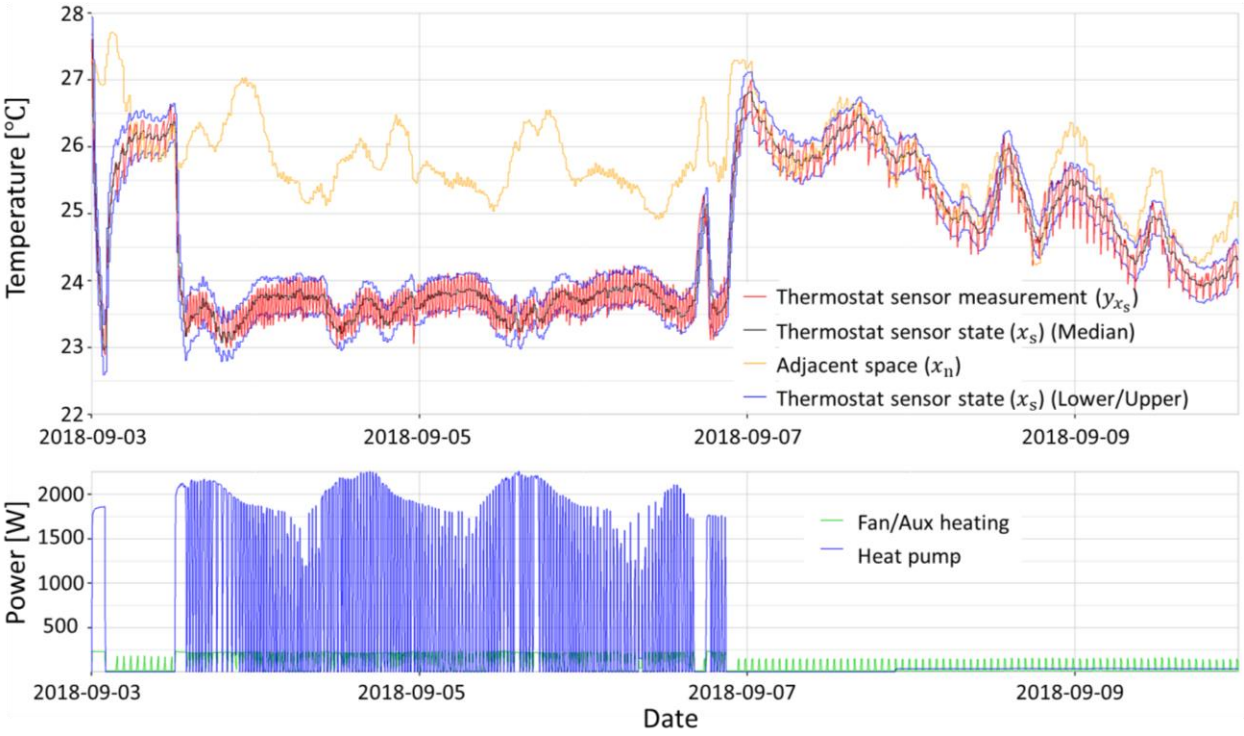

Figure 5.4. Particle filter for state filtering (c40).

One of the main advantages of this model is that it can efficiently learn seasonal parameters without re-training. Figure 5.5 shows a specific example for the heat pump cooling efficiency coefficient (η_{clg}). Period (A) is the first cooling operation period of the year in this unit. The filter starts from the winter period, and η_{clg} is updated once the cooling operation begins. After some drastic learning during period (A), the update stops and starts again during the second cooling period (B).

The changes of updated parameter distributions over different weeks are presented in Figure 5.6, The evolution of R_{ea} starts with a large distribution in the first week and quickly converges after 2 weeks of update. R_{ea} shows consistent distributions over different weeks because it represents building material characteristics. η_{htg} and η_{clg} are designed to be updated only if there are heat pump heating or cooling operations in a specific week. While η_{htg} updates during January and February, η_{clg} starts to update in April, which is visualized in Figure 5.5 in more detail.

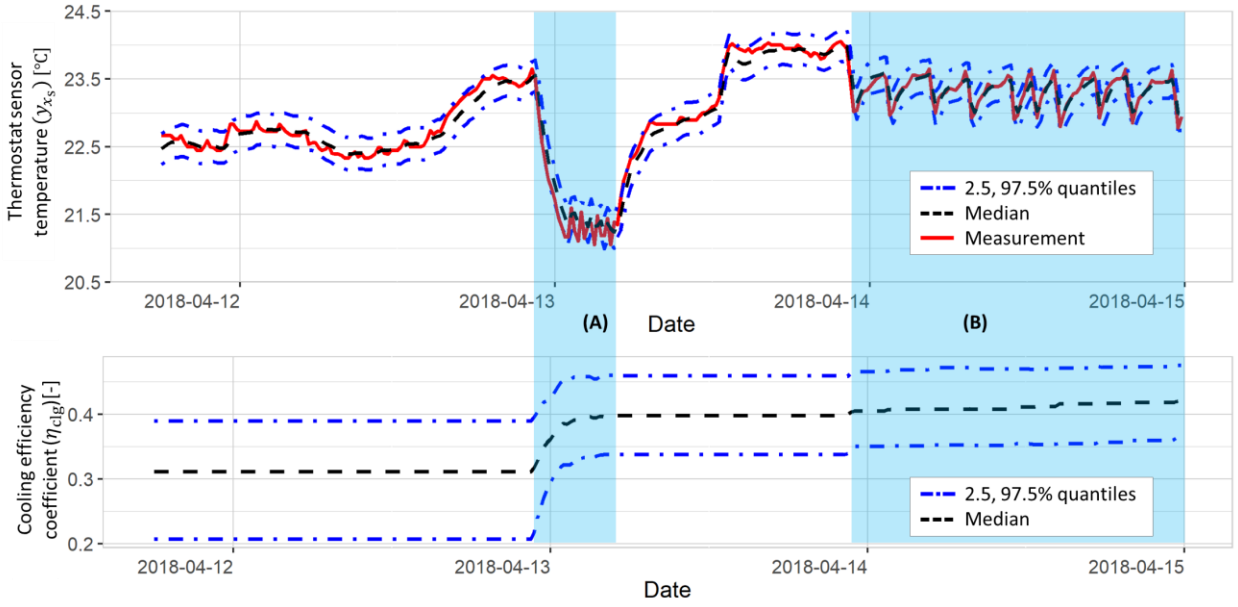

Figure 5.5. Learning of the heat pump cooling efficiency coefficient (η_{clg}, a10).

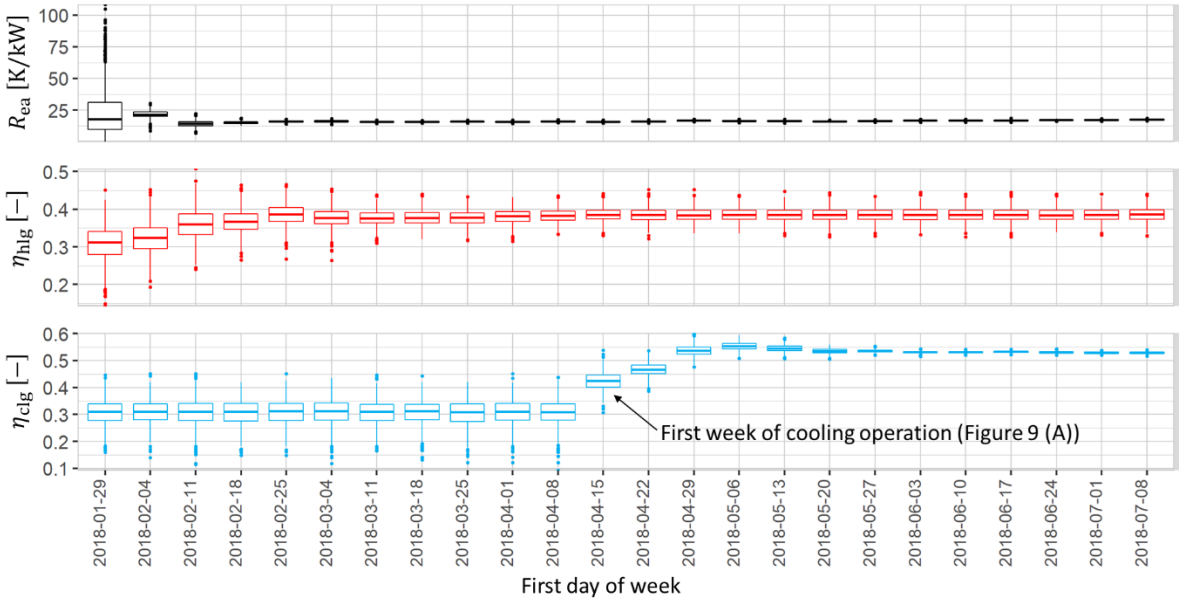

Figure 5.6. Changes of updated parameter distributions over different weeks (a10).

5.3.3 Seasonal validation and performance evaluation

For seasonal validation and performance evaluation, we conduct two comparisons for each unit (c40 and c37) in Figure 5.7 and Figure 5.8, respectively. First, the model is initialized in winter (January 2018) and then updated until the summer (July 2018) through the LW filter. The mean prediction of the thermostat sensor temperature from the updated model is compared to the measurement to validate the model updating process (i.e., seasonal validation). In addition, the updated model is compared with the non-updated model for the same summer data, which was obtained in the prior generation process with winter data. Specifically, the sets of initial parameters are obtained in the prior generation process via optimization, and a best set of parameters is selected based on the data for the subsequent week. For the prediction, the updated model uses the filtered adjacent spaces temperature, but a fixed value is used in the non-updated model.

However, to ensure a fair comparison, the initial values of all the temperature states from the updated model were used in both cases. For the seasonal validation, the mean prediction of the thermostat sensor temperature of updated models for c40 and c37 are in good agreement with the measurements with 0.74℃ and 0.41℃ of root mean squared errors (RMSE). However, the non-updated model for c40 has RMSE of 1.32℃ as it fails to capture the building thermal process especially during the non-cooling operation period (after 2018-06-23), and its prediction is flatter than the measurement. The non-updated model of unit c37 shows 3.32℃ of RMSE in Figure 5.8, and the prediction completely deviates from the measurement. This unit is located next to the unconditioned building electrical room, and its indoor temperature is significantly affected by the unconditioned space. The non-updated model uses a fixed adjacent spaces temperature, so the thermal resistances of exterior walls are under-estimated. In the summer season, this underestimation and the higher value of fixed adjacent spaces temperature result in higher cooling load.

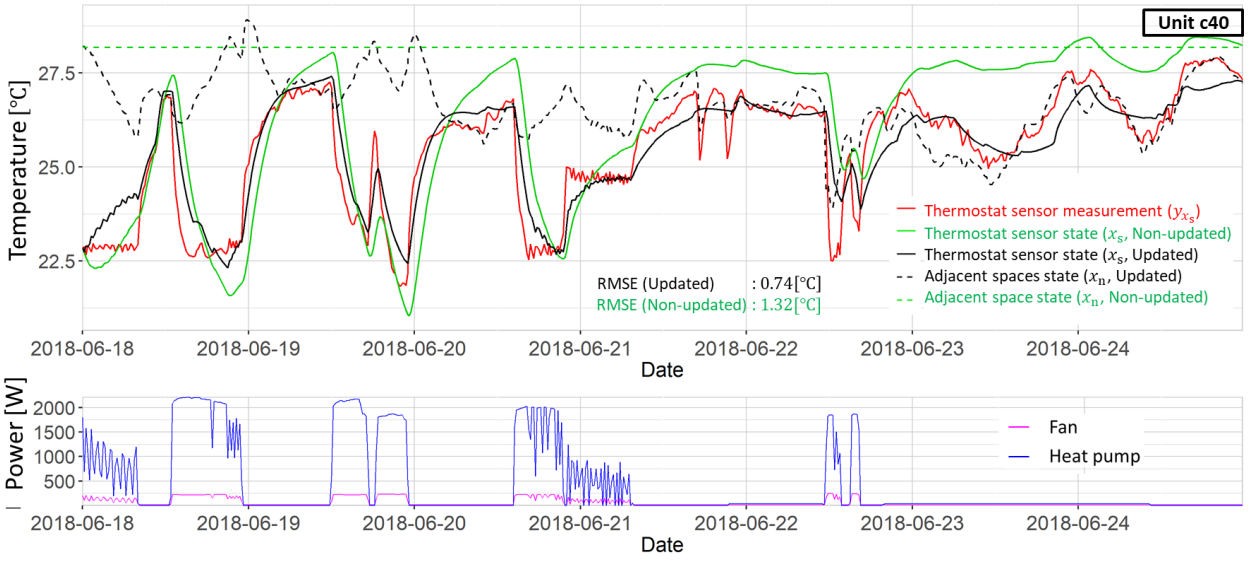

Figure 5.7. Comparison of mean prediction of thermostat sensor temperature for unit c40 using the updated and non-updated model for a week during the summer season.

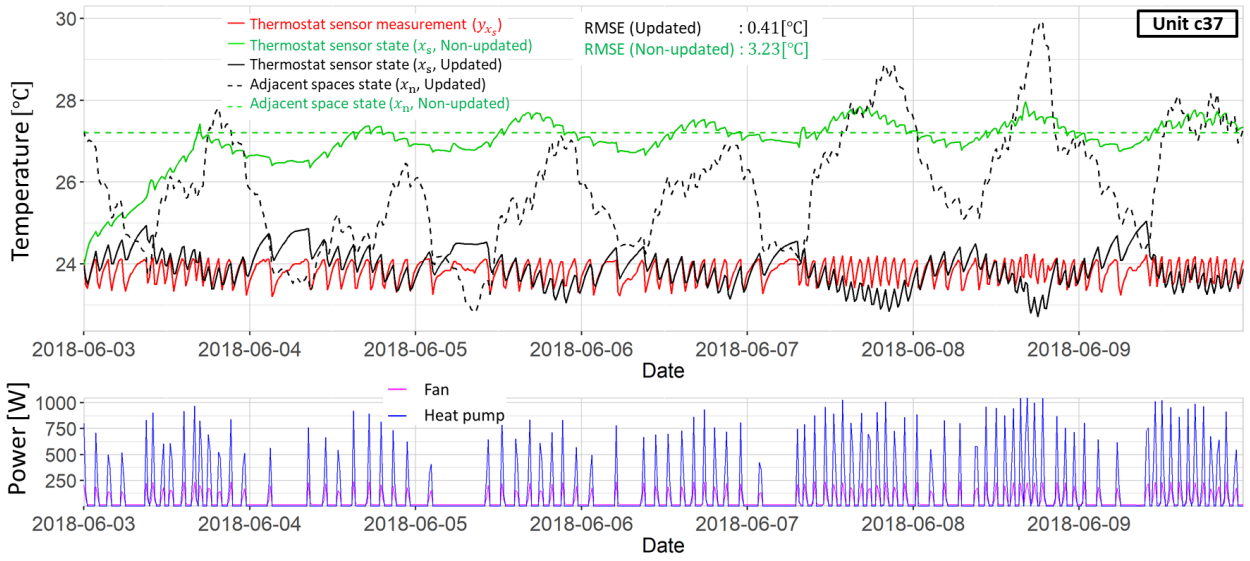

Figure 5.8. Comparison of mean prediction of thermostat sensor temperature for unit c37 using the updated and non-updated model for a week during the summer season.

In Figure 5.9, the power consumption prediction of the non-updated and updated models is compared with the measurements for the two units (c40 and c37). For both units, the updated model shows accurate results as the measured data is located near the median of the predictive

distribution (i.e., prediction uncertainty). The non-updated model for unit c40 shown in Figure 5.7 provides a satisfactory prediction of thermostat sensor temperature, and accordingly, the power prediction has 4.5% deviation while the mean of the updated model has 3.1% deviation from the measurements. On the contrary, the non-updated model for unit c37 shows poor prediction of thermostat sensor temperature as shown in Figure 5.8, and likewise the power prediction of the model completely deviates from the measurements with 190% error. In this case, one set of parameters for unit c37 obtained from the prior generation period through optimization is not only a local optimum but also fails to characterize the thermal dynamics of this unit. However, the updated model can successfully learn the model parameters as the filter holds numerous sets of parameters in the beginning, and local minima resulting in bad sets of parameters are dropped when the filter proceeds.

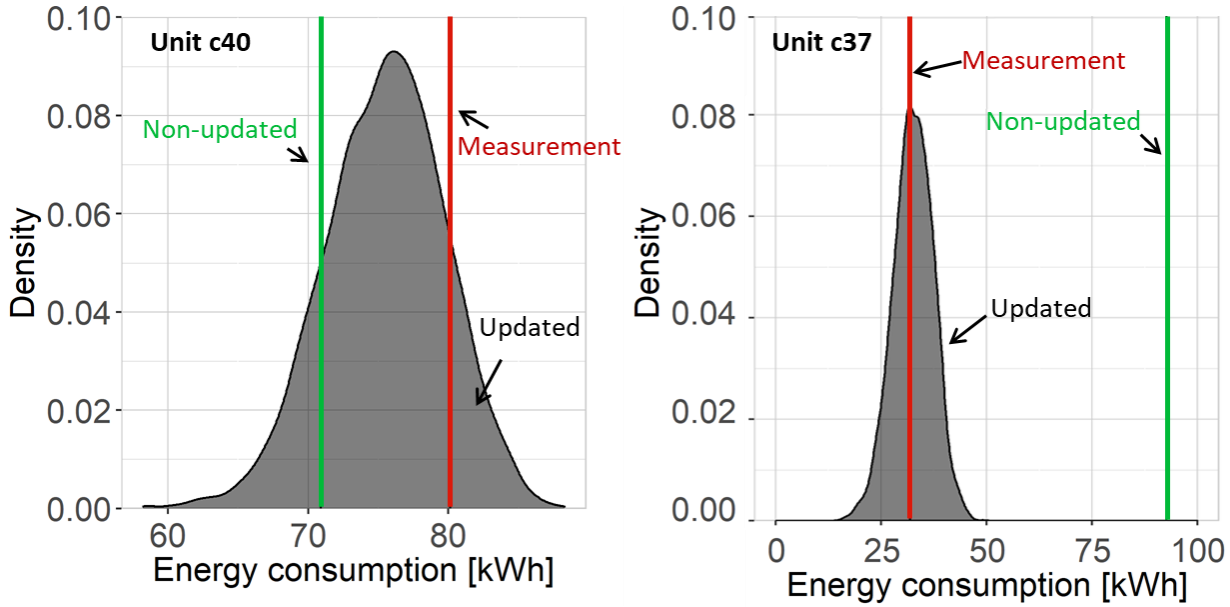

(a) Unit c40 (2018-06-18 ~2018-06-24) (b) Unit c37 (2018-06-03 ~2018-06-09)

Figure 5.9. Comparison of power prediction with the updated and non-updated model for a week during the summer season.

5.3.4 Counterfactual scenario

The predicted energy consumption of the unit-level model is compared with that of the multizone model for various setpoint schedules to validate whether the unit-level model can

accurately predict the counterfactual scenario without using a detailed model for the adjacent spaces. One residential unit on the top floor is selected for this analysis (Appendix F), and results are presented for the first week of September 2018. This period is selected due to the data availability for developing the multizone model. However, 5 days in this week show daily minimum and maximum temperatures around 23℃ and 35℃ respectively, and therefore, this week represents a typical summer period. Three setpoint schedule scenarios are tested: baseline, efficient, and inefficient. In the baseline scenario, the residents use a 24℃ cooling setpoint when they are home or away. For the efficient scenario, cooling setpoints of 25.5℃ and 29.5℃ are used for home or away mode. These setpoints are set to 20℃ and 21℃ in the inefficient scenario. To ensure a fair comparison with the measured data (i.e., baseline scenario), we assume that the thermostat for both the inefficient and efficient scenarios is set to "off" when the thermostat of the baseline scenario is set to "off". In other words, when the thermostat setting is "off", the cooling system is turned off regardless of home or away modes and their setpoints. The home and away states of residents were obtained from the proximity sensor of the thermostat. When no occupancy is observed from the proximity sensor for 30 minutes, it is considered as away state.

In Figure 5.10, the energy prediction of the unit-level model with full uncertainty is shown for the three scenarios. The multizone model prediction is shown with three vertical lines because it is a deterministic model. In the selected week, there were 80 hours and 45 minutes of cooling operation, and the total cooling energy consumption was 90 kWh. The 2.5, 50, and 97.5% percentiles of the predicted cooling energy consumption are 69.3, 80.7, and 92.2 kWh for the baseline setpoint scenario. There is a 10% deviation from the measured data from the mean prediction, but the predicted uncertainty includes the measured data at the high tail of the distribution. The 2.5, 50, and 97.5% percentiles of the predicted energy consumption of the energy efficient scenario are 28, 37.7, and 48.1 kWh. The prediction of the multizone model for the energy efficient scenario is 37.8 kWh and it is in a good agreement with the unit-level model prediction. For the inefficient scenario, the 2.5, 50, and 97.5% percentiles of the unit-level model's prediction is 153, 158.7, and 162.4 kWh). Likewise, the prediction of the multizone model for this scenario is 161.8 kWh, which is within the predicted distribution. From this comparison, we can confirm that the proposed model can accurately predict the counterfactual scenario without a detailed model of the adjacent spaces.

Furthermore, it should be noted that the energy consumption drastically increases in this case (inefficient scenario) because when the setpoint of the unit is lower than the temperature of adjacent spaces, the cooling system needs to operate more to offset the heat flux from the adjacent zones. Also, due to the low setpoint, there is less uncertainty from on/off cycling cooling operation, thus, the energy inefficient scenario has the narrowest distribution. Finally, the utility costs of baseline, energy efficient and energy inefficient scenarios are $30.2, $49.5, and $87.7, respectively. Therefore, the proposed model can be used to provide reliable information to residents in eco-feedback design.

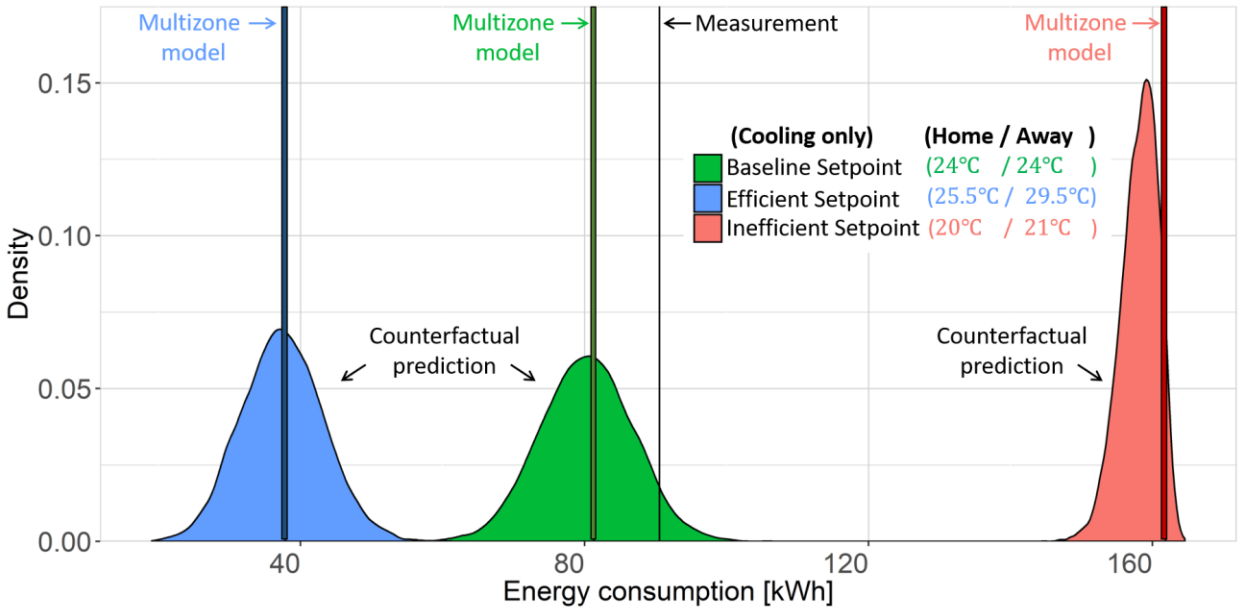

Figure 5.10. Predicted and measured power consumption for different setpoint scenarios.

5.4 Discussion

5.4.1 Modeling different heating and cooling systems

In the residential market, a thermostat is designed to be used with various types of heating and cooling systems. This means that the model would need to be modified to be applicable to buildings with other types of equipment. As shown in Figure 5.2, the sequence of heating and cooling system operation is determined by the current temperature, system operation status, and setpoint schedule based on the internal logic of the specific thermostat. The heating and cooling

system used in this research is a single-stage air-source heat pump with an auxiliary electric heater. The sequence of operation is modeled with an if-then-else rule-based controller model because the details of the logic are available for the thermostat implemented in our field study (Table 5.3). The outdoor air unit has its own defrost control logic, so the mapping between defrost operation, power consumption, outdoor air temperature, and heat flow rate is separately modeled based on insights developed from data as shown in Eq. 5.11 and 5.14. Therefore, our unit-level model is applicable to buildings with a thermostat and a heating and cooling system, but the approach can be easily extended to accommodate different configurations.

5.4.2 Model training

To generate the prior distribution (Section 5.2.3), the training period needs to be carefully selected. Our model is updated each week because a weekly setpoint schedule is typically used for the thermostat. One week of data is used for the prior generation, and this period preferably needs to include floating temperature conditions (i.e., no heating or cooling operation) and heating and cooling operation. The floating period is important for learning parameters representing the thermal dynamics of the building. In addition, a heating and cooling operation period is needed to identify the efficiency coefficients for the heating and cooling equipment. In our study, the heating system has various staging controls such as defrost control, auxiliary heating, and heat pump heating. Therefore, one week during the heating season with all three modes operating should be selected for generating the prior distribution. If our modeling approach is generalized, such rules can be embedded in the data management system and this process of prior generation can be automated.

5.4.3 Existence of unmodeled large disturbances

A distinct characteristic of our model is the ability to handle unmodeled disturbances. Small disturbances due to infiltration and internal heat gains were discussed in the previous section. In this section we focus on unmodeled large disturbances such as window opening during cold or hot weather. An example is illustrated in Figure 5.11 for unit c44 with open windows during the daytime in winter season. As there is no sensor to detect window opening behavior, we identify the behavior based on the temperature change, which is marked with a blue shadow in the Figure

5.11. This graph presents the outdoor air temperature, measured thermostat sensor temperature and setpoint and power consumption. The sensor temperature prediction and filtered adjacent spaces temperature are also shown.

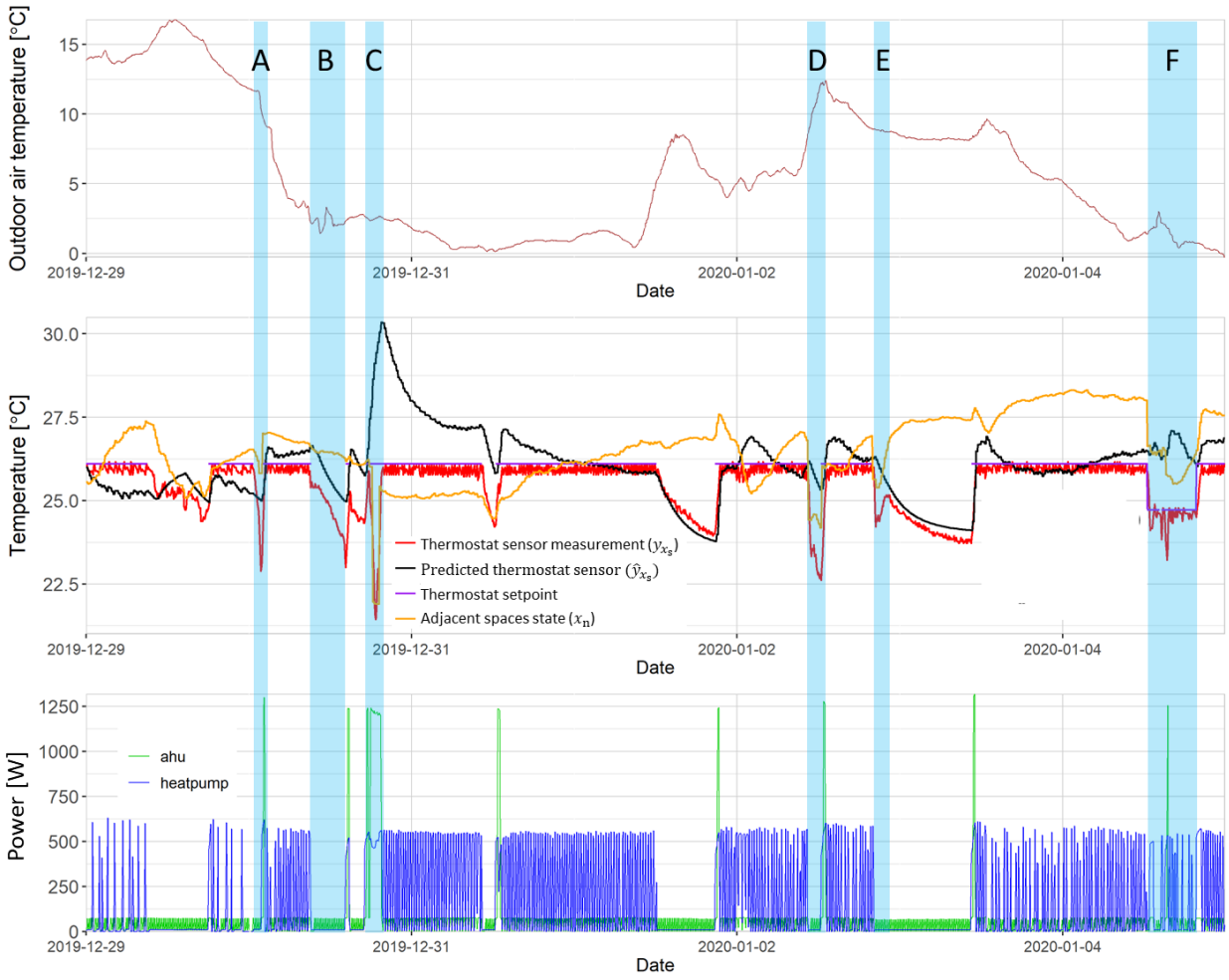

Figure 5.11 Window opening behavior for unit (c44).

To evaluate the model, we ask the following questions: (1) how do the large disturbances affect the filtered adjacent spaces temperature (x_n)? and (2) is coupling to the filtered neighbor temperature sufficient to characterize the large disturbances in the temperature and power prediction? We observe that when there is window opening behavior, the adjacent spaces temperature suddenly drops to account for this effect. However, the indoor air temperature change is not that responsive to capture the effect of this sudden disturbance. As a result, the predicted

temperature is higher than the measured temperature. This is more distinctive during period C and F as the resident opens the window while the heat pump heating is on. However, in general, the indoor air temperature follows the measured temperature, and the RMSE error is 1.15℃. The predicted energy consumption is shown in Figure 5.12. Despite the presence of large disturbances, the measured energy consumption is within the predicted distribution. This shows that the proposed model can handle the large unmeasured disturbances. But the model initialization and initial update sometimes fail when there are several unmeasured large disturbances during the prior generation and the beginning of the update period.

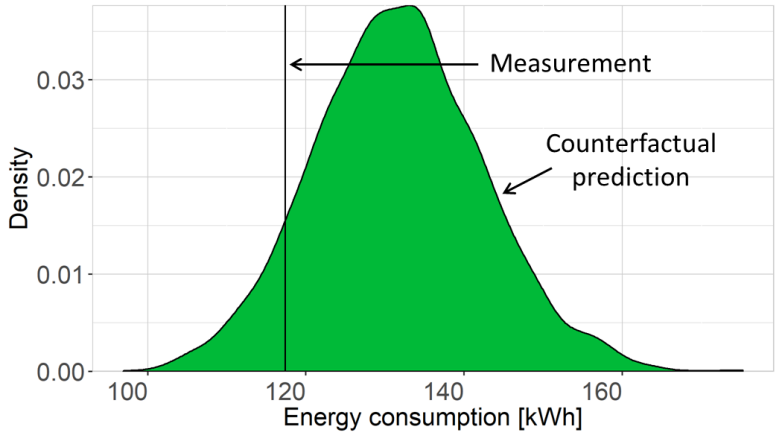

Figure 5.12. Energy consumption prediction under unmeasured large disturbances.

5.4.4 Hypothetical (future) prediction

In this paper, we focus on counterfactual prediction (Sections 5.2.4 and 5.3.4) for our model application. However, the hypothetical (future) prediction is useful in many applications such as demand control or predictive control. The main challenge in hypothetical prediction is how to handle the adjacent space temperature (x_{n}). In our model, the adjacent space temperature is modeled with an autoregressive approach (i.e., $x_{\mathrm{n},t_k+1} = x_{\mathrm{n},t_k} + \varepsilon_{\mathrm{n},t_k}$). While the filtered adjacent space temperature profile is used for counterfactual prediction, the hypothetical prediction uses the predicted adjacent space temperature according to the autoregressive process.

In Figure 5.13, counterfactual and hypothetical predictions for the same week are compared for unit c40. The mean values of counterfactual and hypothetical prediction are 80.3 and 106.4 kWh, respectively. While the counterfactual prediction shows 10% error, 17.5% error is observed

for the hypothetical prediction with very wide uncertainty. The main reason is uncertainty from the adjacent spaces temperature in the hypothetical prediction since it randomly moves according to the noise parameter. Therefore, the mean prediction can be possibly used for the hypothetical prediction, but more information is required for the adjacent spaces temperature to have higher confidence in the prediction. For example, various time series models such as autoregressive-moving-average (ARMA) can be developed based on the filtered overall temperature of adjacent spaces.

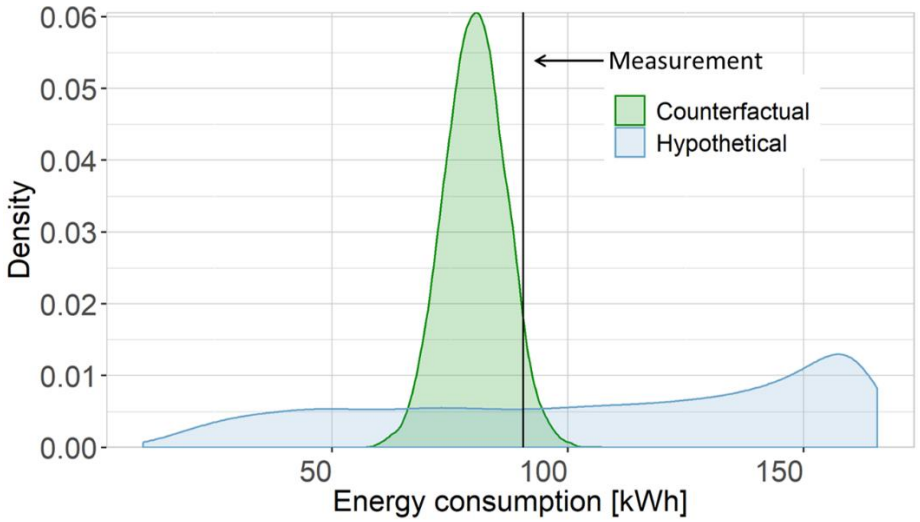

Figure 5.13. Comparison of counterfactual energy prediction for unit c40.

5.5 Chapter conclusions

In this chapter, we presented a real-time unit-level model to predict heating and cooling energy consumption in response to changes in thermostat behavior (i.e., setpoint schedule) in multifamily residential buildings. To develop and evaluate the proposed model, we collected thermostat usage and disaggregated power consumption data in a multi-family residential building located in Indiana, U.S. The model was designed to overcome four challenges in data-driven unit-level modelling of multifamily residential buildings: capturing the coupled dynamics of the building thermal processes and occupant behavior (i.e., setpoint schedules), accounting for unobserved boundary conditions (i.e., inter-unit heat transfer) and unobserved disturbances, inferring the operational characteristics of heating and cooling system based on limited data, and incorporating a real-time parameter learning to handle streaming data. The unit-level model was

formulated based on a Bayesian approach to analyze the effect of unobserved boundary conditions and disturbances on prediction uncertainty, and it was implemented in a real-time form using sequential Bayesian update.

The results show that the model is capable of learning seasonal parameters such as the cooling efficiency coefficient without new training. In a typical case, the median power prediction of the updated model deviates less than 3.1% from the measurements. In contrast, an optimization-based non-updated model provided predictions that deviate as much as 190% when the model was implemented using data from a different season than the training period, especially for units highly affected by adjacent spaces temperatures. To validate the proposed model, we considered two steps: seasonal and counterfactual scenario validation. In addition, three scenarios considering a baseline, energy efficient, and energy inefficient setpoint schedules were implemented for the counterfactual prediction as an example of actionable feedback along with its potential energy bill savings. Through a comparison with the prediction results from a multizone building model, we validated that the proposed unit-level model can be used in the presence of inter-unit heat transfer in a multi-family residential building. Typical efficient and inefficient setpoint scenarios were tested, and the median prediction shows 0.26% and 1.91% error in a typical unit, respectively. Although this model can be applied for a hypothetical prediction scenario, it is important to understand its wide predictive uncertainty. Future research could incorporate a stochastic model for the future temperature of adjacent spaces to reduce the predictive uncertainty.

The model presented in this chapter is implemented in a smart home energy management system installed in the multi-family residential building that was used as testbed and the results will be presented in future publications by the authors. Finally, this research methodology can be implemented in different multi-family residential buildings that have smart home energy systems with eco-feedback.

6. SCALABLE AND PRACTICAL HEATING AND COOLING ENERGY DISAGGREGATION BY USING SMART THERMOSTAT AND SMART METER DATA FOR ECO-FEEDBACK DESIGN

6.1 Overview

This chapter presents a scalable and practical heating and cooling (HC) disaggregation model for eco-feedback design by using smart thermostat and smart meter data for eco-feedback design. This includes the overall process of heating and cooling energy disaggregation model (section 6.2.1); the details of disaggregation model structure (section 6.2.1); a sequential Bayesian update approach to be used without long-term training data (section 6.2.2); the data processing rules for smart thermostat data (Section 6.2.3). The model results are presented in Section 6.4, and the limitations and recommendation of model application are discussed in Section 6.5.

6.2 Heating and cooling energy disaggregation model

6.2.1 Model structure

The overall process of HC energy disaggregation is shown in Figure 6.1. In the utility database, HC operation signal, outdoor air temperature, indoor air temperature, and indoor air humidity from smart thermostats and net electricity consumption from smart meters are being collected. With the sizing information (i.e., maximum values of net and HC power demand for data normalization), the data and prior distributions of parameters are sent to the disaggregation model for data processing. In the training module, posterior distributions of parameters are estimated from the processed data and prior distributions of parameters. HC energy consumption is obtained from the prediction module by using the posterior parameters. The estimated posterior distributions of parameters are used to predict HC energy consumption in the new data in the prediction module. When new data has a HC operation signal that has not been observed and trained (e.g., heat pump cooling signal for the model that is trained with winter data), the estimated posterior distributions of parameters are used as prior parameters and updated with the new data via sequential Bayesian update in the training module (see Section 6.2.2). Finally, the

disaggregation model is developed in Bayesian framework to consider skewed distribution of HC and non-HC consumption data (Section 3.7) and have sequential Bayesian update.

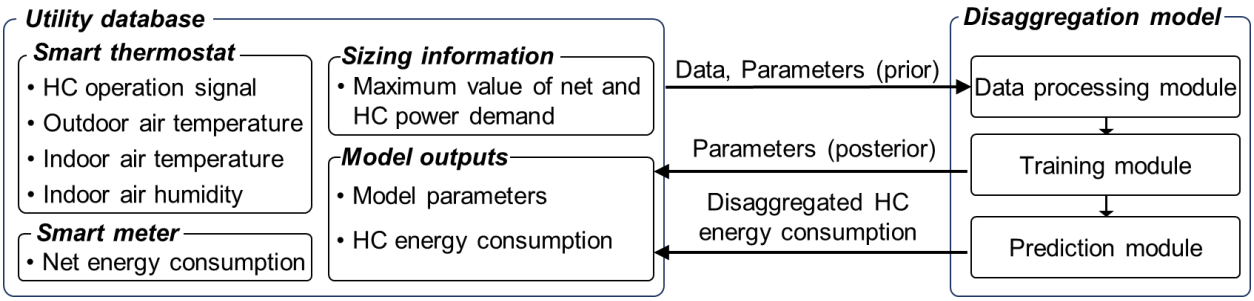

Figure 6.1. Heating and cooling energy disaggregation process.

The normalized net power (y^*_{net,t_k}) of a residential unit during discrete time (t_k) is modeled as a half-normal distribution because it is a left-skewed and positive distribution (Figure 3.10):

$$\Pr\left(y^*_{\mathrm{net},t_k}|\mu^*_{\mathrm{net},t_k},\sigma^*_{\mathrm{net}}\right)=\mathrm{HalfNormal}\left(y^*_{\mathrm{net},t_k}|\mu^*_{\mathrm{net},t_k},\sigma^*_{\mathrm{net}}\right), \tag{6-1}$$

where y_{net,t_k} is averaged net power [W] during t_k, and it is divided by its maximum value ($P_{\mathrm{net,max}}$) so that the normalized data (y^*_{net,t_k}) is in (0,1] range. μ^*_{net,t_k} and σ^*_{net} are the mean and standard deviation of the half-normal distribution. Normalized data and its parameters are marked with superscript *.

σ^*_{net} follows a normal distribution transformed by a softplus function (Murphy, 2021) for positive constraint, and the variable before the transformation is marked with superscript †:

$$\begin{aligned}&\Pr\left(\sigma^\dagger_{\mathrm{net}}|\mu^*_{\sigma_{\mathrm{net}}},\sigma^*_{\sigma_{\mathrm{net}}}\right)=\mathrm{Normal}\left(\sigma^\dagger_{\mathrm{net}}|\mu^*_{\sigma_{\mathrm{net}}},\sigma^*_{\sigma_{\mathrm{net}}}\right),\\&\sigma^*_{\mathrm{net}}=\mathrm{softplus}\left(\sigma^\dagger_{\mathrm{net}}\right),\end{aligned} \tag{6-2}$$

where $\mu^*_{\sigma_{\mathrm{net}}}$ and $\sigma^*_{\sigma_{\mathrm{net}}}$ are set to -0.5 and 0.5, respectively, for initial training so that 97.5% percentile of σ^*_{net} is near 1, which is large enough for noise parameter in normalized scale.

The mean of normalized net power (μ^*_{net,t_k}) during t_k is modeled as the summation of the normalized HC system power (i.e., a heat pump and an air handler, P^*_{hc,t_k}) and the normalized non-HC power (i.e., all power in a residential unit except for the HC system, $P^*_{\mathrm{non-hc},t_k}$):

$$\mu^*_{\mathrm{net},t_k}=P^*_{\mathrm{hc},t_k}+P^*_{\mathrm{non-hc},t_k}. \tag{6-3}$$

The normalized HC system power is the summation of each operation's normalized power times signal:

$$P^*_{\mathrm{hc},t_k} = \sum_s \big(i_{\mathrm{cool}_s,t_k} P^*_{\mathrm{cool}_s,t_k} + i_{\mathrm{heat}_s,t_k} P^*_{\mathrm{heat}_s,t_k} + i_{\mathrm{df}_s,t_k} P^*_{\mathrm{df}_s,t_k} + i_{\mathrm{aux},t_k} P^*_{\mathrm{aux},t_k} + i_{\mathrm{fan},t_k} P^*_{\mathrm{fan},t_k} \big), \tag{6-4}$$

where i is the signal of each operation (1 for under operation and 0 for idling), s is the staging control of each operation when applicable (e.g., heat_1 and heat_2 for 1st and 2nd staging control of heat pump heating, respectively), cool is heat pump cooling operation, heat is heat pump heating operation, df is heat pump heating operation with defrost control, aux is auxiliary heating operation, and fan is fan-only operation without any heating or cooling operation.

A residential heat pump is generally controlled by on/off signal from a thermostat, so heat pump HC operation is modeled as a separate distribution for each operation and staging control. However, it is noted that there is fraction of energy consumption during on/off period in discrete time scale, which results in a right-skewed shape. For example, when 5-minute interval of time is used for data sampling, about 40% of energy consumption is expected compared to the normal operation if the 'on' operation is being executed during 00:03:00-00:04:59. Therefore, $P^*_{\mathrm{heat}_s,t_k}$, $P^*_{\mathrm{df}_s,t_k}$, and $P^*_{\mathrm{cool}_s,t_k}$ are modeled as normal distributions transformed by a sigmoid function to have a right-skewed shape to model the operation during the on/off period:

$$\begin{aligned}
&\Pr\big(P^\dagger_{\mathrm{heat}_s,t_k} | \mu^*_{\mathrm{heat}_s,t_k}, \sigma^*_{\mathrm{heat}_s}\big) = \mathrm{Normal}\big(P^\dagger_{\mathrm{heat}_s,t_k} | \mu^*_{\mathrm{heat}_s,t_k}, \sigma^*_{\mathrm{heat}_s}\big), \\
&P^*_{\mathrm{heat}_s,t_k} = \mathrm{sigmoid}\big(P^\dagger_{\mathrm{heat}_s,t_k}\big) \frac{P_{\mathrm{heat}_s,\max}}{P_{\mathrm{net},\max}}, \\
&\Pr\Big(P^\dagger_{\mathrm{df}_s,t_k} | \mu^*_{\mathrm{df}_s,t_k}, \sigma^*_{\mathrm{df}_s}\Big) = \mathrm{Normal}\Big(P^\dagger_{\mathrm{df}_s,t_k} | \mu^*_{\mathrm{df}_s,t_k}, \sigma^*_{\mathrm{df}_s}\Big), \\
&P^*_{\mathrm{df}_s,t_k} = \mathrm{sigmoid}\Big(P^\dagger_{\mathrm{df}_s,t_k}\Big) \frac{P_{\mathrm{df}_s,\max}}{P_{\mathrm{net},\max}}, \\
&\Pr\big(P^\dagger_{\mathrm{cool}_s,t_k} | \mu^*_{\mathrm{cool}_s,t_k}, \sigma^*_{\mathrm{cool}_s}\big) = \mathrm{Normal}\big(P^\dagger_{\mathrm{cool}_s,t_k} | \mu^*_{\mathrm{cool}_s,t_k}, \sigma^*_{\mathrm{cool}_s}\big), \\
&P^*_{\mathrm{cool}_s,t_k} = \mathrm{sigmoid}\big(P^\dagger_{\mathrm{cool}_s,t_k}\big) \frac{P_{\mathrm{cool}_s,\max}}{P_{\mathrm{net},\max}},
\end{aligned} \tag{6-5}$$

where $\mu^*_{\mathrm{heat}_s,t_k}$, $\mu^*_{\mathrm{cool}_s,t_k}$ and $\mu^*_{\mathrm{df}_s,t_k}$ are mean and $\sigma^*_{\mathrm{heat}_s,t_k}$, $\sigma^*_{\mathrm{cool}_s,t_k}$ and $\sigma^*_{\mathrm{df}_s,t_k}$ are standard deviation of normal distribution for each operation (heat, cool, df) and staging control (s). $P_{\mathrm{heat}_s,\max}$, $P_{\mathrm{cool}_s,\max}$, and $P_{\mathrm{df}_s,\max}$ are maximum powers of heat pump heating, defrost heating,

and cooling for each staging control. The ratio of maximum value of each operation power to net power is multiplied to the sigmoid-transformed distribution because the value of each operation is in (0,1] after sigmoid transformation, and the summation of all operations need to be corrected to have the same scale with the normalized net power.

In a whole-building energy simulation software such as EnergyPlus, a heat pump energy consumption is characterized by several empirical performance curves calibrated with measured or catalogue data (U.S. Department of Energy, 2021a). Specifically, when the part-load operation is neglected, supply heating or cooling flow rate is the rated flow rate times a performance curve as a function of indoor and outdoor air temperature (or humidity). Energy consumption is also obtained by multiplying another performance curve to the supply heating or cooling flow rate. EnergyPlus recommends using bivariate quadratic function for both curves (U.S. Department of Energy, 2021a). Therefore, the power of each operation of heat pump is characterized by the combination of all terms of the two performance functions. Since the performance curves are functions of indoor air and outdoor air temperatures for the air source heat pump heating, the mean of heat pump heating ($\mu^*_{\mathrm{heat}_s,t_k}$) can be written as:

$$\begin{aligned}\mu^*_{\mathrm{heat}_s,t_k} = {} & \beta^*_{0,\mathrm{heat}_s} + \beta^*_{1,\mathrm{heat}_s} T^*_{\mathrm{in},t_k} + \beta^*_{2,\mathrm{heat}_s} {T^*_{\mathrm{in},t_k}}^2 + \beta^*_{3,\mathrm{heat}_s} {T^*_{\mathrm{in},t_k}}^3 + \beta^*_{4,\mathrm{heat}_s} T^*_{\mathrm{out},t_k} \\ & + \beta^*_{5,\mathrm{heat}_s} {T^*_{\mathrm{out},t_k}}^2 + \beta^*_{6,\mathrm{heat}_s} {T^*_{\mathrm{out},t_k}}^3 + \beta^*_{7,\mathrm{heat}_s} T^*_{\mathrm{in},u,t_k} T^*_{\mathrm{out},u,t_k} \\ & + \beta^*_{8,\mathrm{heat}_s} {T^*_{\mathrm{in},t_k}}^2 T^*_{\mathrm{out},t_k} + \beta^*_{9,\mathrm{heat}_s} T^*_{\mathrm{in},t_k} {T^*_{\mathrm{out},t_k}}^2 + \beta^*_{10,\mathrm{heat}_s} {T^*_{\mathrm{in},t_k}}^2 {T^*_{\mathrm{out},t_k}}^2,\end{aligned} \tag{6-6}$$

where T^*_{in,t_k} is scaled average indoor air temperature during t_k [℃], and T^*_{out,t_k} is scaled average outdoor air temperature during t_k [℃]. Min-max normalization (Han et al., 2012) is used for both temperatures. Outdoor air temperature in the range of [-20,40] is normalized to [-1,1] range, and indoor air temperature in the range of [10,30] is normalized to [-1,1] range.

The cooling operation is modeled in the same way with the heating operation except for indoor air temperature. Wet-bulb temperature is used instead of indoor air temperature to capture the effect of dehumidification (U.S. Department of Energy, 2021a):

$$\begin{aligned}\mu^*_{\mathrm{cool}_s,t_k} = {} & \beta^*_{0,\mathrm{cool}_s} + \beta^*_{1,\mathrm{cool}_s} WB^*_{\mathrm{in},t_k} + \beta^*_{2,\mathrm{cool}_s} {WB^*_{\mathrm{in},t_k}}^2 + \beta^*_{3,\mathrm{cool}_s} {WB^*_{\mathrm{in},t_k}}^3 \\ & + \beta^*_{4,\mathrm{cool}_s} T^*_{\mathrm{out},t_k} + \beta^*_{5,\mathrm{cool}_s} {T^*_{\mathrm{out},t_k}}^2 + \beta^*_{6,\mathrm{cool}_s} {T^*_{\mathrm{out},t_k}}^3 \\ & + \beta^*_{7,\mathrm{cool}_s} WB^*_{\mathrm{in},t_k} T^*_{\mathrm{out},t_k} + \beta^*_{8,\mathrm{cool}_s} {WB^*_{\mathrm{in},t_k}}^2 T^*_{\mathrm{out},t_k} \\ & + \beta^*_{9,\mathrm{cool}_s} WB^*_{\mathrm{in},t_k} {T^*_{\mathrm{out},t_k}}^2 + \beta^*_{10,\mathrm{cool}_s} {WB^*_{\mathrm{in},t_k}}^2 {T^*_{\mathrm{out},t_k}}^2,\end{aligned} \tag{6-7}$$

where WB^*_{in,t_k} is normalized average wet-bulb temperature of indoor air during t_k [℃]. For a heat pump system with evaporative outdoor air unit, wet-bulb temperature of outdoor air is used instead of T^*_{out,t_k}.

The defrost operation is modeled in the same way with the heating operation:

$$\begin{aligned}\mu^*_{\mathrm{df}_s,t_k} = {} & \beta^*_{0,\mathrm{df}_s} + \beta^*_{1,\mathrm{df}_s} T^*_{\mathrm{in},t_k} + \beta^*_{2,\mathrm{df}_s} {T^*_{\mathrm{in},t_k}}^2 + \beta^*_{3,\mathrm{df}_s} {T^*_{\mathrm{in},t_k}}^3 + \beta^*_{4,\mathrm{df}_s} T^*_{\mathrm{out},t_k} \\ & + \beta^*_{5,\mathrm{df}_s} {T^*_{\mathrm{out},t_k}}^2 + \beta^*_{6,\mathrm{df}_s} {T^*_{\mathrm{out},t_k}}^3 + \beta^*_{7,\mathrm{df}_s} T^*_{\mathrm{in},t_k} T^*_{\mathrm{out},t_k} \\ & + \beta^*_{8,\mathrm{df}_s} {T^*_{\mathrm{in},t_k}}^2 T^*_{\mathrm{out},t_k} + \beta^*_{9,\mathrm{df}_s} T^*_{\mathrm{in},t_k} {T^*_{\mathrm{out},t_k}}^2 + \beta^*_{10,\mathrm{df}_s} {T^*_{\mathrm{in},t_k}}^2 {T^*_{\mathrm{out},t_k}}^2.\end{aligned} \tag{6-8}$$

The prior distribution of each coefficient for each operation is set to a normal distribution for initial training:

$$\begin{aligned}&\Pr\left(\beta^*_{i,\mathrm{heat}_s} | \mu^*_{\beta_{i,\mathrm{heat}_s}}, \sigma^*_{\beta_{i,\mathrm{heat}_s}}\right) = \mathrm{Normal}\left(\beta^*_{i,\mathrm{heat}_s} | \mu^*_{\beta_{i,\mathrm{heat}_s}}, \sigma^*_{\beta_{i,\mathrm{heat}_s}}\right) \text{ for } i = 0,1,\dots,10, \\ &\Pr\left(\beta^*_{i,\mathrm{cool}_s} | \mu^*_{\beta_{i,\mathrm{cool}_s}}, \sigma^*_{\beta_{i,\mathrm{cool}_s}}\right) = \mathrm{Normal}\left(\beta^*_{i,\mathrm{cool}_s} | \mu^*_{\beta_{i,\mathrm{cool}_s}}, \sigma^*_{\beta_{i,\mathrm{cool}_s}}\right) \text{ for } i = 0,1,\dots,10, \\ &\Pr\left(\beta^*_{i,\mathrm{df}_s} | \mu^*_{\beta_{i,\mathrm{df}_s}}, \sigma^*_{\beta_{i,\mathrm{df}_s}}\right) = \mathrm{Normal}\left(\beta^*_{i,\mathrm{df}_s} | \mu^*_{\beta_{i,\mathrm{df}_s}}, \sigma^*_{\beta_{i,\mathrm{df}_s}}\right) \text{ for } i = 0,1,\dots,10,\end{aligned} \tag{6-9}$$

where $\mu^*_{\beta_{i,\mathrm{heat}_s}}$, $\mu^*_{\beta_{i,\mathrm{cool}}}$, and $\mu^*_{\beta_{i,\mathrm{df}_s}}$ are set to 0, and $\sigma^*_{\beta_{i,\mathrm{heat}_s}}$, $\sigma^*_{\beta_{i,\mathrm{cool}_s}}$, and $\sigma^*_{\beta_{i,\mathrm{df}_s}}$ are 0.25, respectively, for initial training to have [-1,1] range for 2.5-97.5% percentiles.

Noise variance parameters of heat pump heating, cooling and defrost operation ($\sigma^*_{\mathrm{heat}_s}$, $\sigma^*_{\mathrm{heat}_s}$, and $\sigma^*_{\mathrm{heat}_s}$, respectively) follow normal distributions transformed by softplus function (Murphy, 2021) for positive constraints:

$$\begin{aligned}&\Pr\left(\sigma^\dagger_{\mathrm{heat}_s} | \mu^*_{\sigma_{\mathrm{heat}_s}}, \sigma^*_{\sigma_{\mathrm{heat}_s}}\right) = \mathrm{Normal}\left(\sigma^\dagger_{\mathrm{heat}_s} | \mu^*_{\sigma_{\mathrm{heat}_s}}, \sigma^*_{\sigma_{\mathrm{heat}_s}}\right), \\ &\sigma^*_{\mathrm{heat}_s} = \mathrm{softplus}\left(\sigma^\dagger_{\mathrm{heat}_s}\right), \\ &\Pr\left(\sigma^\dagger_{\mathrm{cool}_s} | \mu^*_{\sigma_{\mathrm{cool}_s}}, \sigma^*_{\sigma_{\mathrm{cool}_s}}\right) = \mathrm{Normal}\left(\sigma^\dagger_{\mathrm{cool}_s} | \mu^*_{\sigma_{\mathrm{cool}_s}}, \sigma^*_{\sigma_{\mathrm{cool}_s}}\right), \\ &\sigma^*_{\mathrm{cool}_s} = \mathrm{softplus}\left(\sigma^\dagger_{\mathrm{cool}_s}\right), \\ &\Pr\left(\sigma^\dagger_{\mathrm{df}_s} | \mu^*_{\sigma_{\mathrm{df}_s}}, \sigma^*_{\sigma_{\mathrm{df}_s}}\right) = \mathrm{Normal}\left(\sigma^\dagger_{\mathrm{df}_s} | \mu^*_{\sigma_{\mathrm{df}_s}}, \sigma^*_{\sigma_{\mathrm{df}_s}}\right), \\ &\sigma^*_{\mathrm{df}_s} = \mathrm{softplus}\left(\sigma^\dagger_{\mathrm{df}_s}\right),\end{aligned} \tag{6-10}$$

where $\mu^*_{\sigma_{\mathrm{heat}_s}}$, $\mu^*_{\sigma_{\mathrm{cool}_s}}$, and $\mu^*_{\sigma_{\mathrm{df}_s}}$ are set to -0.5, and $\sigma^*_{\sigma_{\mathrm{heat}_s}}$, $\sigma^*_{\sigma_{\mathrm{cool}_s}}$, and $\sigma^*_{\sigma_{\mathrm{df}_s}}$ are set to - 0.5 for initial training so that 97.5% quantile of $\sigma^*_{\mathrm{heat}_s}$, $\sigma^*_{\mathrm{cool}_s}$, and $\sigma^*_{\mathrm{df}_s}$ are near 1, which is large enough for noise parameter in normalized scale.

Defrost operation is activated when there is frost in outdoor air coil during the heat pump heating operation by using resistive heating coil or defrost heat pump cycle (U.S. Department of Energy, 2021a). In general, it is controlled by heat pump's embedded internal logic and sensors (i.e., not observed). During this operation, there could be additional power due to the operation of resistive heating coil or auxiliary heating coil to compensate the reduced heating from the defrost cycle. We assume that defrost operation can be modeled as a separate operation of heat pump heating when the outdoor air temperature is below a certain number. Heat pump heating signal with staging control s ($i_{\text{heat,all}_s,t_k}$) can be split to heating operation without defrost control (i_{heat_s,t_k}) and with defrost control (i_{df_s,t_k}) based on outdoor air temperature and defrost cutoff variable (ϕ_{df}):

$$
\begin{aligned}
i_{\text{heat}_s,t_k} &= \begin{cases} 1 & \text{if } T_{\text{out},t_k} \geq \phi_{\text{df}} \text{ and } i_{\text{heat,all}_s,t_k} = 1 \\ 0 & \text{if } T_{\text{out},t_k} < \phi_{\text{df}} \text{ and } i_{\text{heat,all}_s,t_k} = 0 \end{cases}, \\
i_{\text{df}_s,t_k} &= \begin{cases} 1 & \text{if } T_{\text{out},t_k} < \phi_{\text{df}} \text{ and } i_{\text{heat,all}_s,t_k} = 1 \\ 0 & \text{if } T_{\text{out},t_k} \geq \phi_{\text{df}} \text{ and } i_{\text{heat,all}_s,t_k} = 0 \end{cases}, \\
\Pr\left(\phi_{\text{df}} | \mu_{\phi_{\text{df}}}, \sigma_{\phi_{\text{df}}}\right) &= \text{Normal}\left(\phi_{\text{df}} | \mu_{\phi_{\text{df}}}, \sigma_{\phi_{\text{df}}}\right),
\end{aligned}
\tag{6-11}
$$

where ϕ_{df} is cutoff value of outdoor temperature that splits heat pump heating and defrost operation, $\mu_{\phi_{\text{df}}}$ and $\sigma_{\phi_{\text{df}}}$ are mean and standard deviation of ϕ_{df}, and they are set to -1/3 and 0.2 for initial training to have $[-11℃, 11℃]$ in 2.5–97.5% percentiles with median of $0℃$ in unnormalized scale because defrost control is being activated near $0℃$.

Auxiliary heating is used during the cold weather (e.g., outdoor air temperature below $0℃$ or $-10℃$ according to thermostat setting) to compensate the performance degradation of heat pump heating or prevent the compressor from freezing (U.S. Department of Energy, 2021b). In general, resistive electric heating coil is used, and it is modeled as a normal distribution transformed by sigmoid function to have a right-skewed shape to model the operation during the on/off period:

$$
\begin{aligned}
\Pr\left(P^{\dagger}_{\text{aux},t_k} | \mu^{*}_{\text{aux}}, \sigma^{*}_{\text{aux}}\right) &= \text{Normal}\left(P^{\dagger}_{\text{aux},t_k} | \mu^{*}_{\text{aux}}, \sigma^{*}_{\text{aux}}\right), \\
P^{*}_{\text{aux},t_k} &= \text{sigmoid}\left(P^{\dagger}_{\text{aux},t_k}\right) \frac{P_{\text{aux,max}}}{P_{\text{net,max}}},
\end{aligned}
\tag{6-12}
$$

where μ^{*}_{aux} and σ^{*}_{aux} are mean and standard deviation of normal distribution. $P_{\text{aux,max}}$ is the maximum power of auxiliary heating.

μ^*_{aux} and σ^*_{net} follow a normal distribution, but σ^*_{net} is transformed by a softplus function (Murphy, 2021) for positive constraint:

$$\begin{aligned}
&\Pr\left(\mu^*_{\text{aux}}|\mu^*_{\mu_{\text{aux}}},\sigma^*_{\mu_{\text{aux}}}\right)=\text{Normal}\left(\mu^*_{\text{aux}}|\mu^*_{\mu_{\text{aux}}},\sigma^*_{\mu_{\text{aux}}}\right),\\
&\Pr\left(\sigma^\dagger_{\text{aux}}|\mu^*_{\sigma_{\text{aux}}},\sigma^*_{\sigma_{\text{aux}}}\right)=\text{Normal}\left(\sigma^\dagger_{\text{aux}}|\mu^*_{\sigma_{\text{aux}}},\sigma^*_{\sigma_{\text{aux}}}\right),\\
&\sigma^*_{\text{aux}}=\text{softplus}\left(\sigma^\dagger_{\text{aux}}\right),
\end{aligned} \tag{6-13}$$

where $\mu^*_{\mu_{\text{aux}}}$ and $\sigma^*_{\mu_{\text{aux}}}$ are set to 0.5 and 1.0, respectively, to have μ^*_{aux} in range of [0.2,0.9] for initial training. $\mu^*_{\sigma_{\text{aux}}}$ and $\sigma^*_{\sigma_{\text{aux}}}$ are set to -0.5 and 0.5, respectively, to have 97.5% percentile of σ^*_{aux} is near 1, which is large enough for noise parameter in normalized scale.

Typical thermostats provide fan-only operation without heating and cooling operation for air circulation or ventilation purpose. Since fan power during HC operation is included in HC, fan-only operation needs to be separately modeled. Single speed fan is modeled as a normal distribution transformed by softplus function (Murphy, 2021) to have a positive constraint:

$$\begin{aligned}
&\Pr\left(P^\dagger_{\text{fan},t_k}|\mu^*_{\text{fan}},\sigma^*_{\text{fan}}\right)=\text{Normal}\left(P^\dagger_{\text{fan},t_k}|\mu^*_{\text{fan}},\sigma^*_{\text{fan}}\right),\\
&P^*_{\text{fan},t_k}=\text{softplus}\left(P^\dagger_{\text{fan},t_k}\right),\\
&\Pr\left(\mu^*_{\text{fan}}|\mu^*_{\mu_{\text{fan}}},\sigma^*_{\mu_{\text{fan}}}\right)=\text{Normal}\left(\mu^*_{\text{fan}}|\mu^*_{\mu_{\text{fan}}},\sigma^*_{\mu_{\text{fan}}}\right),\\
&\Pr\left(\sigma^\dagger_{\text{fan}}|\mu^*_{\sigma_{\text{fan}}},\sigma^*_{\sigma_{\text{fan}}}\right)=\text{Normal}\left(\sigma^\dagger_{\text{fan}}|\mu^*_{\sigma_{\text{fan}}},\sigma^*_{\sigma_{\text{fan}}}\right),\\
&\sigma^*_{\text{fan}}=\text{softplus}\left(\sigma^\dagger_{\text{fan}}\right),
\end{aligned} \tag{6-14}$$

where $\mu^*_{\mu_{\text{fan}}}$ and $\sigma^*_{\mu_{\text{fan}}}$ are set to -3.0 and 0.5, respectively, because fan power is small number compared to net power. $\mu^*_{\sigma_{\text{fan}}}$ and $\sigma^*_{\sigma_{\text{fan}}}$ are set to -0.5 and 0.5, respectively, to have 97.5% percentile of σ^*_{fan} is near 1, which is large enough for noise parameter in normalized scale.

Finally, non-HC power is modeled as a normal distribution transformed by softplus function (Murphy, 2021) to have a positive constraint:

$$\begin{aligned}
&\Pr\left(P^\dagger_{\text{non-hc},t_k}|\mu^*_{\text{non-hc}},\sigma^*_{\text{non-hc}}\right)=\text{Normal}\left(P^\dagger_{\text{non-hc},t_k}|\mu^*_{\text{non-hc}},\sigma^*_{\text{non-hc}}\right),\\
&P^*_{\text{non-hc},t_k}=\text{softplus}\left(P^\dagger_{\text{non-hc},t_k}\right),\\
&\Pr\left(\mu^*_{\text{non-hc}}|\mu^*_{\mu_{\text{non-hc}}},\sigma^*_{\mu_{\text{non-hc}}}\right)=\text{Normal}\left(\mu^*_{\text{non-hc}}|\mu^*_{\mu_{\text{non-hc}}},\sigma^*_{\mu_{\text{non-hc}}}\right),\\
&\Pr\left(\sigma^\dagger_{\text{non-hc}}|\mu^*_{\sigma_{\text{non-hc}}},\sigma^*_{\sigma_{\text{non-hc}}}\right)=\text{Normal}\left(\sigma^\dagger_{\text{non-hc}}|\mu^*_{\sigma_{\text{non-hc}}},\sigma^*_{\sigma_{\text{non-hc}}}\right),\\
&\sigma^*_{\text{non-hc}}=\text{softplus}\left(\sigma^\dagger_{\text{non-hc}}\right),
\end{aligned} \tag{6-15}$$

where $\mu^*_{\mu_{\text{non-hc}}}$ and $\sigma^*_{\mu_{\text{non-hc}}}$ are set to -3.0 and 0.5, respectively, because non-HC power is highly left-skewed distribution (Figure 3.10). $\mu^*_{\sigma_{\text{non-hc}}}$ and $\sigma^*_{\sigma_{\text{non-hc}}}$ are set to -0.5 and 0.5, respectively, to have 97.5% percentile of $\sigma^*_{\text{non-hc}}$ is near 1, which is large enough for noise parameter in normalized scale.

6.2.2 Training, prediction, and sequential Bayesian update

Automatic differentiation variation inference (ADVI) (Kucukelbir et al., 2017) is used to estimate the posterior distribution of parameters in the model (i.e., training). ADVI approximates the posterior distribution of parameters by using several variational distributions through automatic differentiation and stochastic optimization. PyMC3 (Salvatier et al., 2016) is used for ADVI, and mean-field ADVI (a factorized Gaussian variational approximation (Kucukelbir et al., 2017)), which assumes each parameter is independent, is used for this model because each HC operation is independent.

Once the posterior distributions of parameters are obtained, HC power of each operation is predicted by calculating the posterior predictive distributions. They are approximated via samples obtained from the posterior predictive simulation (Gelman et al., 2013):

$$\Pr\left(\tilde{P}^*_{t_k}|y^*_{\text{net},1:t_{\text{train}}}\right) = \int \Pr\left(\tilde{P}^*_{t_k}|\theta\right)\Pr\left(\theta|y^*_{\text{net},1:t_{\text{train}}}\right)d\theta \approx \frac{1}{n_{\text{sample}}}\sum_{i_s=1}^{n_{\text{sample}}} \Pr\left(\tilde{P}^*_{t_k}|\theta^{[i_s]}\right), \tag{6-16}$$

where $\tilde{P}^*_{t_k}$ is the posterior predicted normalized power of each operation (i.e., $\tilde{P}^*_{\text{heat}_s,t_k}$, $\tilde{P}^*_{\text{df}_s,t_k}$, $\tilde{P}^*_{\text{cool}_s,t_k}$, $\tilde{P}^*_{\text{aux},t_k}$, and $\tilde{P}^*_{\text{fan},t_k}$, presented in Eqs. 6-5, 6-12, and 6-14) at time t_k. $y^*_{\text{net},1:t_{\text{train}}}$ is normalized power observation during the training period $(1,2,\dots,t_{\text{train}})$. θ is all parameters used in this model. n_{sample} is number of samples that approximates posterior predictive distribution (e.g., 10000). i_s is index of samples.

The energy consumption of each operation during the prediction period can be estimated from the posterior predictive distribution:

$$\tilde{E}_{1:t_{\text{pred}}} = P_{\text{net,max}}\Delta t \sum_{t_k=1}^{t_{\text{pred}}} i_{t_k}\tilde{P}^*_{t_k}, \tag{6-17}$$

where $\tilde{E}_{t_{\text{pred}}}$ is the posterior predicted energy consumption of each operation (i.e., $\tilde{E}_{\text{heat}_s,1:t_{\text{pred}}}$, $\tilde{E}_{\text{df}_s,1:t_{\text{pred}}}$, $\tilde{E}_{\text{cool}_s,1:t_{\text{pred}}}$, $\tilde{E}_{\text{aux},1:t_{\text{pred}}}$, and $\tilde{E}_{\text{fan},1:t_{\text{pred}}}$) during the prediction period $(1,2,\dots,t_{\text{pred}})$.

$P_{\text{net,max}}$ is normalization constant (Eq. 6-1). Δt is time interval in second for discrete data sampling (e.g., 900 seconds in this study, see Section 6.1.3). i_{t_k} is observed signal of each operation (i.e., i_{heat_s,t_k}, i_{df_s,t_k}, i_{cool_s,t_k}, i_{aux,t_k}, and i_{fan,t_k}).

Not only ADVI gives fast but accurate approximation, but it also allows to have sequential Bayesian update when new data is observed (Broderick et al., 2013). Specifically, the approximated posterior distributions are used as prior distributions, and the model is trained with the new data to estimate updated posterior distributions. It is beneficial for this model because the model does not need to be trained again with all historic data. For example, when the initial training period is winter season, parameters related to cooling operation are not trained. Instead of training the model again with cooling operation data by using all historic data, the cooling-related parameters can be updated with new summer data via sequential Bayesian update.

6.2.3 Smart thermostat data

In Figure 6.1, the HC operation signal needs to be collected from a smart thermostat. Ecobee smart thermostat (Ecobee, 2021) provides HC operation signal via its cloud-based API service (Ecobee developers, 2021) or web interface (Ecobee, 2021). Figure 6.2 shows how to process raw thermostat data to HC operation signal. For explanation purpose, we only present a single stage heat pump heating and cooling with electric auxiliary heater system. From csv format data obtained in the web interface or json format data through API service, we can obtain how long each operation is being activated in each discrete sampling time. Case 1 is 300 seconds of operation for heat pump cooling, and it is converted as 1/3 for i_{cool_1}. As described in Section 3.7, 15-minute interval data is used for this model, so 300 seconds of operation is 1/3 in 15-minute interval. Case 2 is heat pump heating operation, and i_{heat_1} is 1/3. Case 3 is simultaneous operation of heat pump heating and auxiliary heating, so both i_{heat_1} and i_{aux} are 1/3. When there is fan-only operation, i_{fan} is 1/3. When each operation is being activated for the part of each sampling time, its fraction is also used for input data format.

Raw data format

Case	Cool Stage 1	Heat Stage 1	Aux Heat 1	Fan
1	300	0	0	300
2	0	300	0	300
3	0	300	300	300
4	0	0	300	300
5	0	0	0	300
6	0	150	0	150

Input data format

Case	i_{cool_1}	i_{heat_1}	i_{aux}	i_{fan}
1	1/3	0	0	0
2	0	1/3	0	0
3	0	1/3	1/3	0
4	0	0	1/3	0
5	0	0	0	1/3
6	0	1/6	0	0

Figure 6.2. Raw data preprocessing for HC operation signal.

6.3 Results

The result of disaggregation model for a unit in a winter week (2018/01/28 - 2018/02/03) is shown in Figure 6.3. The model parameters are trained with this week's data, and the disaggregated HC power is predicted for the same week. Predicted HC power (95% uncertainty with median) and measured HC power in every 15-minute interval are shown in Figure 6.3 (a). Also, the first two days of prediction results are visualized in Figure 6.3 (c) for better readability. The measurement shows a good agreement with median prediction, and the 95% of predictive uncertainty shows the model can successfully replicate the observation. In addition, energy (electricity) consumption of each operation during this week is summarized in Figure 6.3 (b). During this week, there are 128 hours of HC operations (hc). Specifically, there are 36 hours of heat pump heating (heat), 88 hours of heat pump heating with defrost control (df), and 4 hours of auxiliary heating (aux)). While the measurement of each operation is in the 95% of predictive uncertainty of each operation, heat pump heating with defrost control shows large variance with slight over-prediction. This could be attributed to the stochastic behavior of auxiliary heating during the defrost control (Figure 3.11). As a result, the median of weekly HC energy prediction is 140.8 kWh, and this shows 11.5% of deviation compared to the measurement (126.3 kWh).

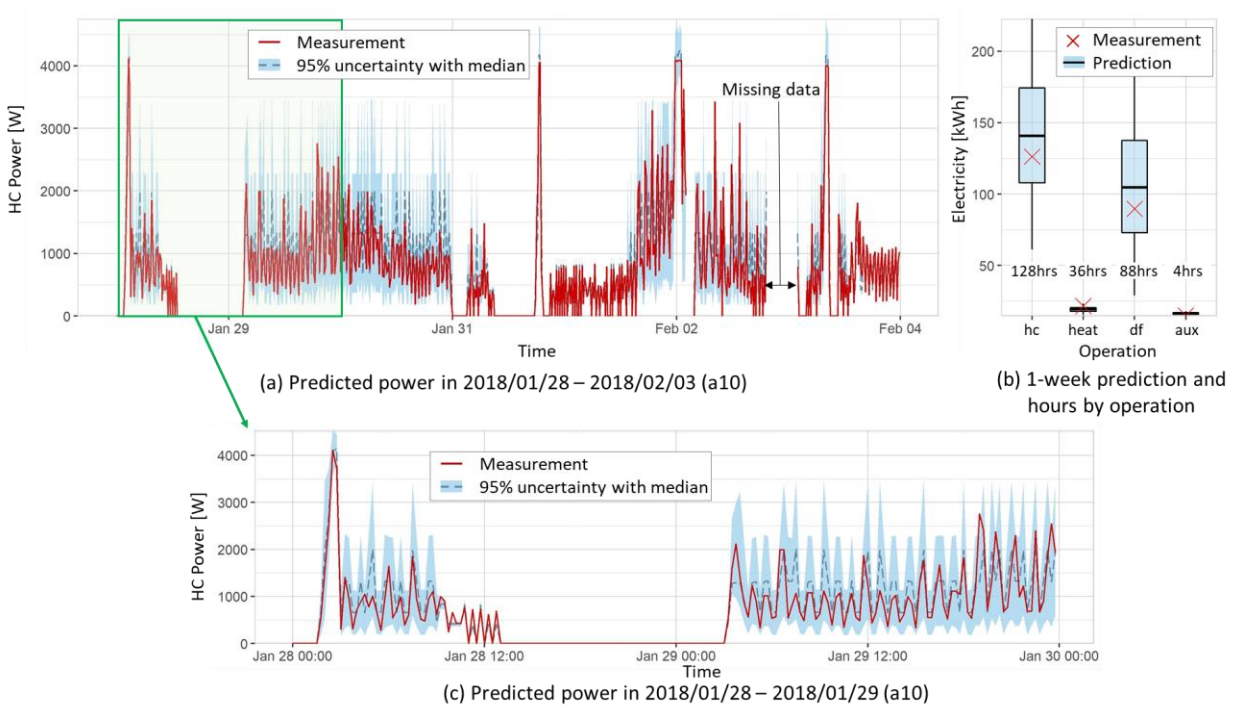

Figure 6.3. HC power and weekly electricity energy prediction in a winter week.

The model parameters estimated in Figure 6.3 is used to predict the disaggregated HC power from the net power for the following consecutive three weeks without model update (Figure 6.4). The results show that the predicted HC power is in good agreement of the measurement, and the model successfully disaggregates the HC power from 15-min interval data even for the future prediction. Similar to Figure 6.3, high uncertainty is observed during the defrost control (df), while heat pump heating (heat) and auxiliary heating (aux) show good predictions with small uncertainties. As a result, the median prediction of weekly energy consumption in each week is 164.8, 93.5, 18.4 kWh, respectively, and this gives 7.3, 7.7, and 1% of errors compared to the measurement (153.6, 86.8, and 18.6 kWh), respectively.

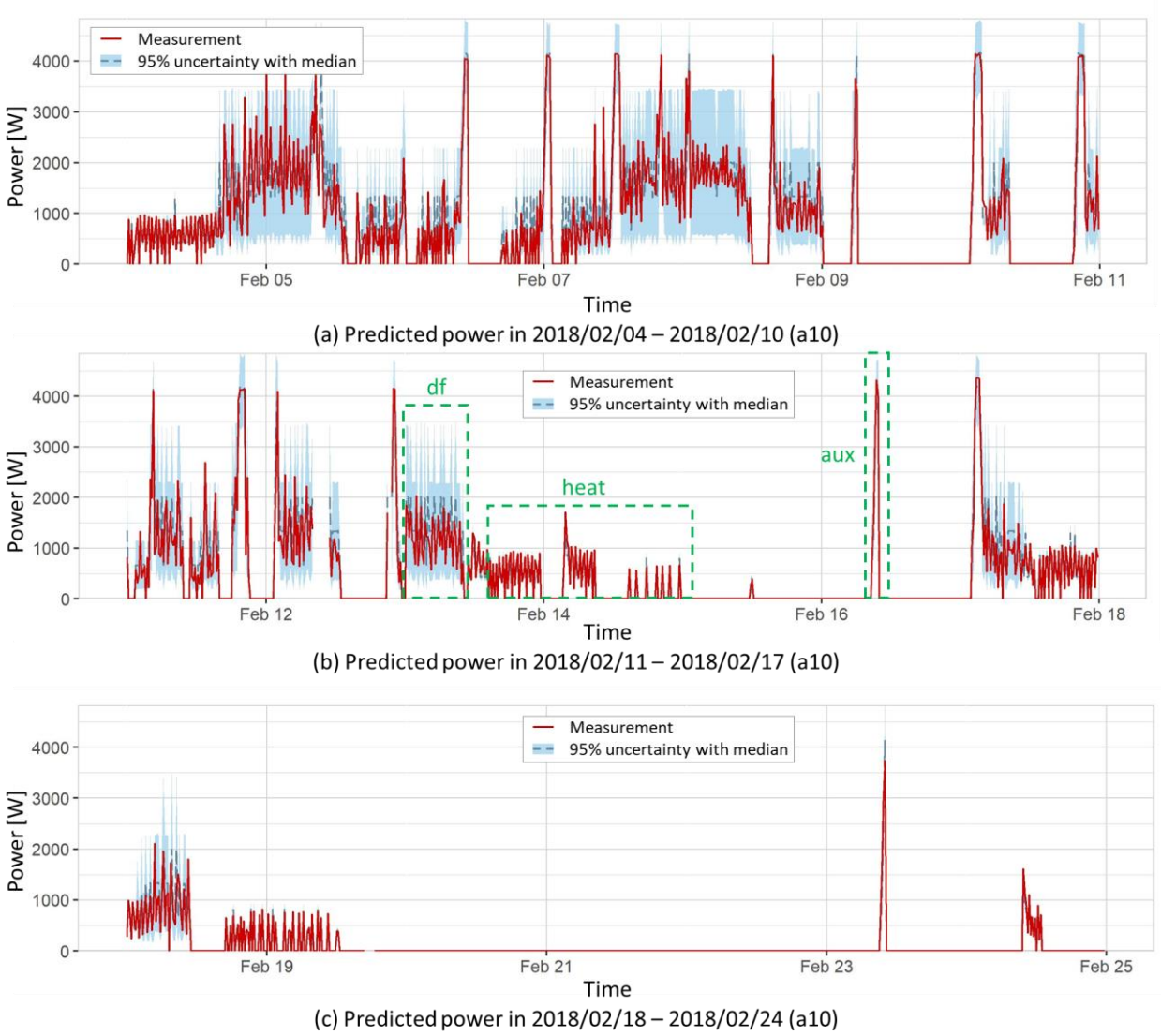

Figure 6.4. Prediction of disaggregated HC power on future data.

In Figure 6.5, the prediction of disaggregated weekly HC energy consumption for different units are visualized. Units that have different building characteristics (i.e., locations, number of bedrooms, floor) are selected. In this prediction, all units are trained with the first week of data, and the trained model is used to predict the disaggregated HC energy consumption for the following 5 consecutive weeks. The prediction results show good performance for all units.

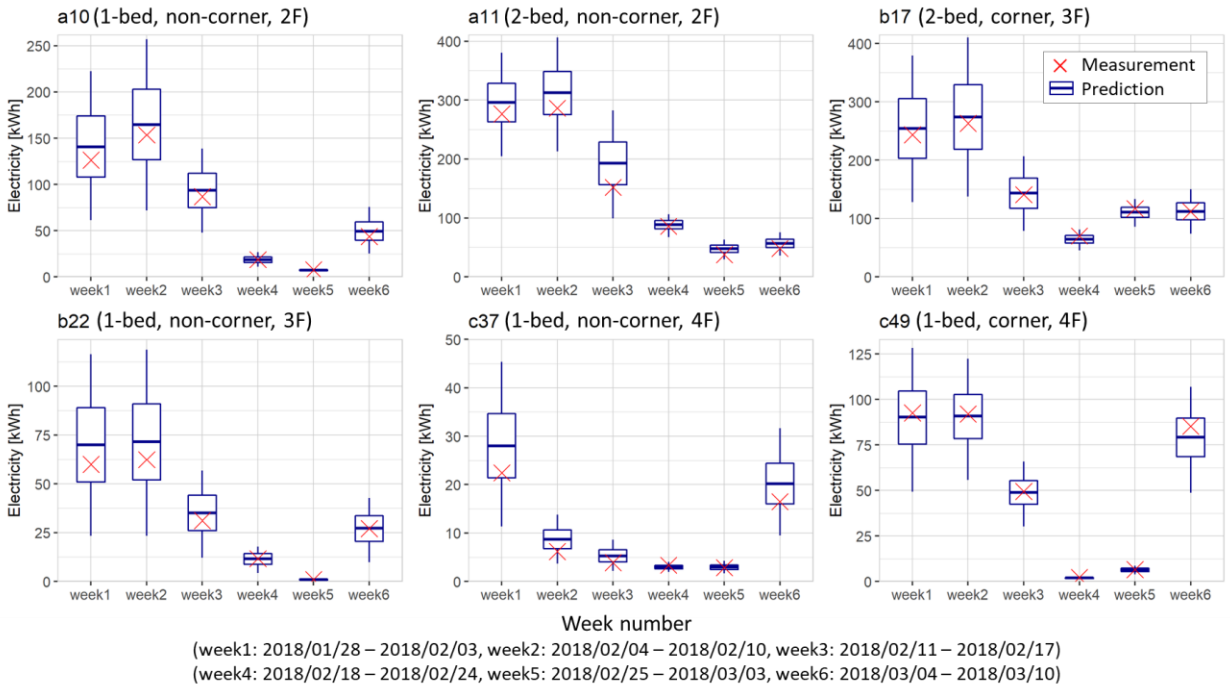

Figure 6.5. Prediction of disaggregated HC energy consumption on future data for different units.

In Figure 6.6, the prediction of disaggregated weekly HC energy consumption of unit a10 for different seasons is visualized. The model parameters are trained with the first week of data and then used to predict the following weeks. In the week of 2018/04/08, the heat pump cooling operation is detected, so the model parameters related to heat pump cooling are updated. While large uncertainty is observed in the winter season due to defrost control, the model prediction shows good agreement with measured data in the following weeks. It is noted that the predicted cooling energy consumption shows good agreement with measured data after the model update.

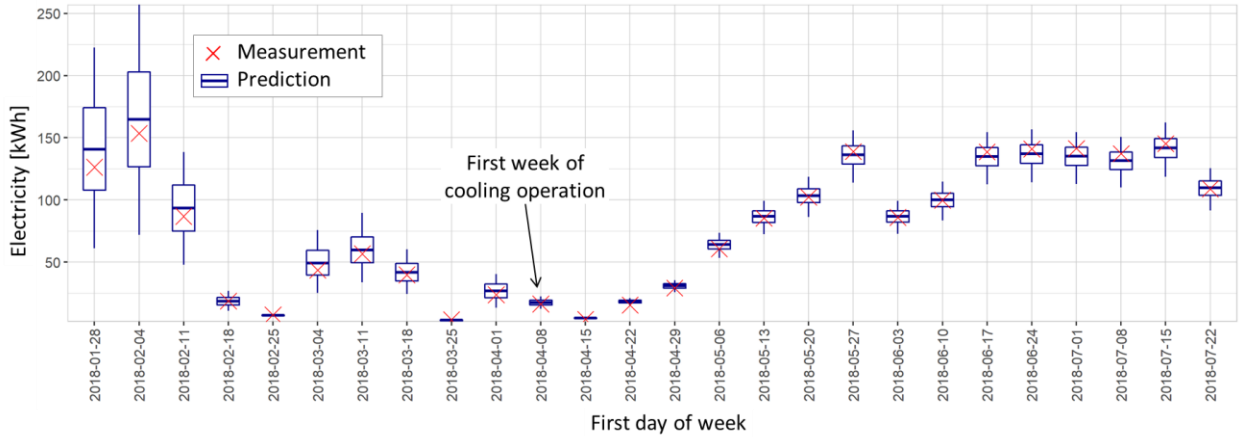

Figure 6.6. Prediction of disaggregated weekly HC energy consumption for different seasons with model update (a10).

In Figure 6.7, the prediction performances of models trained with different amount of training data are compared. While all models show good prediction results, the prediction uncertainty does not decrease when the amount of training data increases. It is noted that the model trained with a one day shows good prediction results. In this day, there are 5, 16, and 3 hours of heat pump heating, heat pump heating with defrost control, and auxiliary heating operations, respectively. This indicates when there are enough variations in HC operation, the model can be successfully trained with small amount of data.

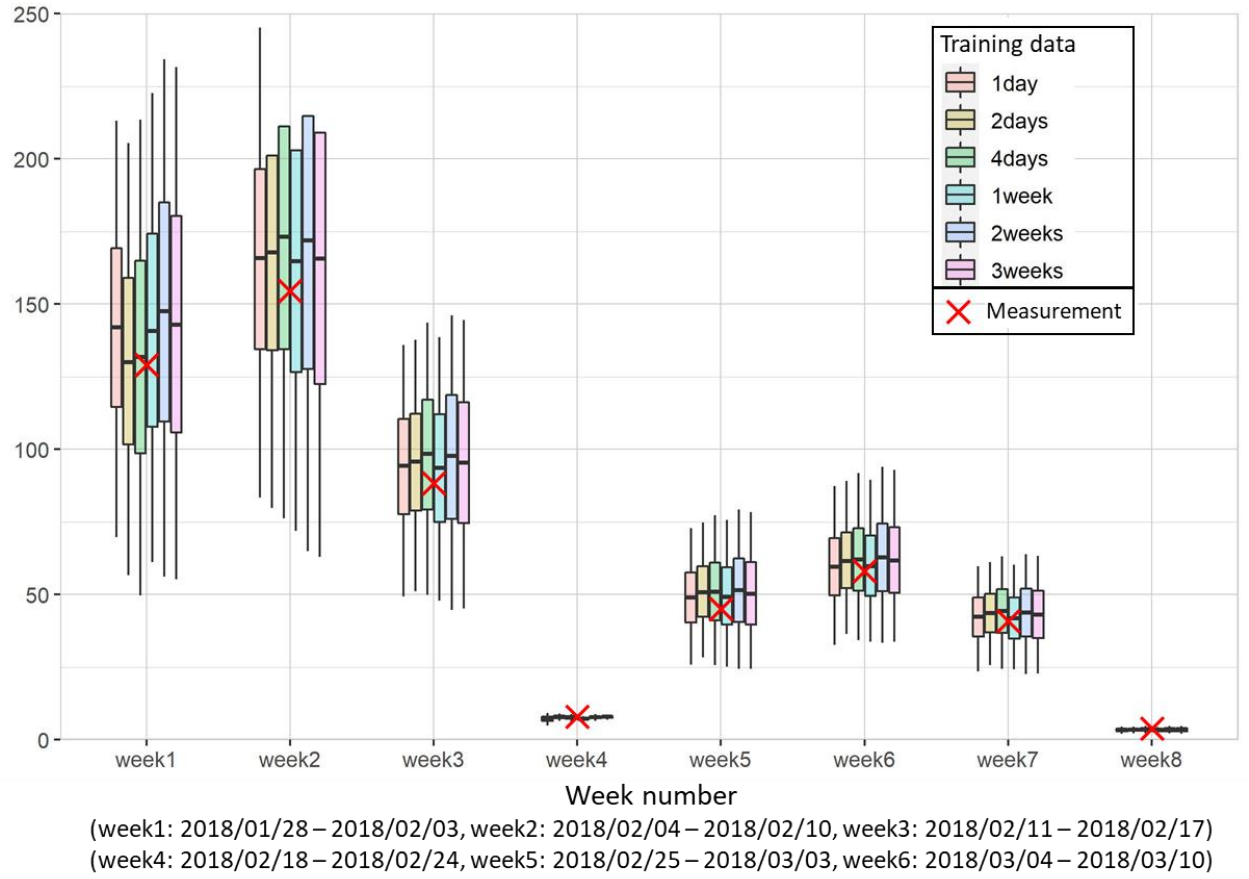

Figure 6.7. Effect of amount of training data (a10).

6.4 Discussions

The proposed approach is designed to be applicable for an any residential house that have a heat pump HC system, but there could be a limitation of the applicability according to the availability of the thermostat data. The model requires HC operation signal data, which is currently available from one thermostat company (Ecobee, 2021). Some thermostat companies such as Carrier or Bryant can provide the operation signal data because they use Ecobee's API server (Ecobee developers, 2021). Other smart thermostat companies such as Nest (Google, 2021) do not provide the HC operation signal data, so therefore, the proposed model is not.

A single stage heat pump with electric auxiliary heater is used to validate the proposed model in this research. However, the model can be applicable for other systems with minor modification. For example, as shown in Eq. 6.4, multi-staging heat pump system can be also modeled by including parameters for each stage of heating and cooling. However, it is necessary to add or

subtract model parameters for specific operations when different types of heating system are used such as an electric heater without heat pump, a ventilator, a heat pump with gas-fired auxiliary heater, etc. For example, if the gas-fired auxiliary heater is used, then the parameter and thermostat signal related to electric auxiliary heating should be removed as the model disaggregates only electric consumption data.

Although the median prediction of the proposed approach shows errors less than 12% in weekly HC energy consumption, it gives large predictive uncertainty. And the uncertainty does not decrease with increased training data. This could be attributed to the model structure and data. As discussed in Section 3.7 and Figure 6.3, the stochastic operation of auxiliary heating during defrost control is approximated as a discrete on/off operation after 15-minute interval data smoothing. In addition, there are sometimes a time-lags between thermostat signal and energy consumption data because HC system may be turned on or off with some delay to protect a HC system from malfunctions. In other words, the model is able to predict the median characteristics, but large predictive uncertainty can be happened due to the model structure and data.

Finally, the appropriate amount of data for the model training needs to be decided by the modeler. As shown in Figure 6.7, when there are enough variations of HC system operation in the training period, one-day of data is enough to train the model. However, in a practical viewpoint, we recommend using one-week of data for the initial training that has enough variations in cooling or heating season. Also, it could be useful to regularly update model (e.g., every month) to ensure the model accounts for various heating and cooling operation data.

6.5 Chapter conclusions

In this chapter, a scalable and practical HC energy disaggregation model by using smart thermostat and smart meter data is presented. The model is meant to be scalable and practical for use in eco-feedback design e.g., actionable feedback via energy model or demand response targeting via HC consumption analysis. Unlike a complex NILM model developed with high resolution data, the proposed approach only uses smart thermostat and smart meter data that are available in current AMI is meant to be used for typical residential houses without additional sensors. While previous methods require large amount of training data (e.g., 6 months) to learn seasonal parameters of a HC system, this method can be established with small amount of data

(e.g., one week) by learning seasonal parameters through sequential Bayesian update whenever new operation is observed. Finally, the Bayesian modeling approach allows to capture skewed characteristics of HC and non-HC power data. To develop and evaluate the proposed model, we collected thermostat usage and disaggregated power consumption data through WiFi-enabled smart thermostats and power meters in a multi-family residential building located in Indiana, U.S. The results show that the model successfully predict disaggregated HC power from 15-min interval data, and it shows less than 12% of error in weekly HC energy consumption. Finally, the model is able to learn seasonal parameters via sequential Bayesian update and gives good prediction results in different seasons.

7. CONCLUSIONS AND FUTURE WORKS

7.1 Main achievements

The main contributions of this doctoral thesis are three new approaches for energy analytics in multi-family residential buildings: 1) a unit-level HC energy prediction model for actionable eco-feedback, 2) a building energy normalization approach for normative comparison, and 3) a HC energy disaggregation model from smart thermostat and smart meter data. All the analytics are scalable and practical based on typical metering infrastructure in multi-family residential buildings and are developed with focus on modeling the inter-unit heat transfer and unobserved disturbances and incorporating sequential Bayesian update without long-term training data. More specifically, key achievements of this doctoral thesis are:

- A unit-level data-driven modeling approach to normalize heating and cooling (HC) energy usage in multi-family residential buildings. The developed modeling approach identifies normalized groups of units that have similar building characteristics to provide the relative evaluation of energy-related behaviors. The physics-informed approach starts from a heat balance equation to derive a linear regression model and uses a Bayesian mixture model to identify groups of units that have similar regression coefficients. The model captures the effect of behavior on HC energy consumption by normalizing the effect of building characteristics and accounting for the inter-unit heat transfer and unobserved variables. The probabilistic approach incorporates unit- and season-specific prior information and sequential Bayesian updating of model parameters when new data become available. The model identifies distinct normalized HC energy use groups in different seasons and provides more accurate rankings compared to the case without normalization.
- A real-time modeling approach to predict the heating and cooling energy consumption of each unit in a multi-family residential building. The model has a state-space structure to capture the building thermal dynamics, includes the setpoint schedule as an input, and incorporates real-time state filtering and parameter learning to consider uncertainties from unobserved boundary conditions (e.g., temperatures of adjacent spaces) and unobserved disturbances (i.e., window opening, infiltration, etc.). Through this real-time form, the model does not need to be re-trained for different seasons. The results show that the

median power prediction of the model deviates less than 3.1% from measurements while the model learns seasonal parameters such as the cooling efficiency coefficient through sequential Bayesian update.

- A scalable and practical HC energy disaggregation model by using smart thermostat and smart meter data for eco-feedback design. The model is designed to be applicable for smart meters and smart thermostats data that is available in current AMI to be used for typical residential houses. In addition, the model is developed based on Bayesian modeling approach to be trained without long-term data (e.g., 6-month data) by learning seasonal parameters through sequential Bayesian update whenever new operation is observed and to capture skewed characteristics of HC and non-HC power data. The results show that the model successfully predict disaggregated HC power from 15-min interval data with less than 12% of prediction error in weekly HC energy consumption. Finally, the model is able to learn seasonal parameters via sequential Bayesian update and gives good prediction results in different seasons.

7.2 Future work

7.2.1 Data-driven building normalization for various buildings

The building energy normalization model developed in Chapter 4 is a promising approach combining data-driven unsupervised learning with physics-based heat balance equations and does not require detailed model calibration. This is especially beneficial because it leverages a large amount of data from smart devices which are not organized.

However, the proposed normalization approach is only applicable for units in multi-family residential buildings located in a single location (i.e., same weather condition). The proposed approach can be extended to various buildings by changing the parameterization level (Eq. 4.7) when developing the Bayesian mixture model from the heat balance equation. For example, including the outdoor air temperature term in the regression model enables identification of normalized groups of buildings in different locations.

7.2.2 Scalable heating and cooling energy prediction model for future prediction

The HC energy prediction model presented in this thesis is limited to the counterfactual prediction in a unit with a heat pump system with electric auxiliary heater. In addition, when applying this approach into a new multi-family residential building, it is required to collect data and calibrate the energy model which entails some engineering effort.

There are two main topics of improvement: the development of model for unobserved disturbances and inter-unit heat transfer for future prediction and the generalized HC energy model based on deep neural networks. For the hypothetical (future) prediction, it is necessary to predict future unobserved disturbances and inter-unit heat transfer. Since the proposed approach provides the filtered unobserved disturbances and inter-unit heat transfer, am interesting future research topic would be how to use the filtered information to develop the prediction model. Typical timeseries model such as autoregressive-moving-average model (ARMA) or data-driven model such as Gaussian process can be used.

In addition, the proposed approach is based on a gray-box model, so trial-and-error for model design is inevitable. Deep neural networks show powerful performance to model complex data, and it can be used for this application by including the unobserved disturbances and inter-unit heat transfer in the model. The main difficulty in the deep neural network is that is susceptible to over-fitting. Fusing physical knowledge into the prior distributions of the deep neural network parameters, it enables developing a deep neural network model that does not over-fit with small number of observations for real-world application via sequential Bayesian update.

7.2.3 Scalable and practical heating and cooling energy disaggregation for various HC systems

The proposed HC energy disaggregation model is currently applicable for a heat pump system with electric auxiliary heater. Since this model is based on the discrete HC operational signal of thermostat, the model can be easily extended to other HC systems. However, the types of various HC systems are not categorized, so the model needs to be manually modified when different types of HC system are used. The development of classification of various HC systems with their operational signals can make the proposed approach be applicable for any residential application. In addition, the proposed work is not limited to the HC system. It can be also applicable for any other appliances with discrete operational signal such as a water heater. With

the development of smart technology, there are many opportunities to get the discrete operation signal from smart switches, smart water heaters, etc. By having all these components in a single model, it is possible to develop a scalable and practical non-intrusive load monitoring model for all individual appliances.

APPENDIX A. MARGINALIZED MIXTURE MODEL

The posterior distributions of parameters and latent variables ($z_{h,w}$, s_w) of the model for unit h at week w can be written as Eq. A.1:

$$\begin{aligned} &P\left(\beta_{0,1:K,w}, \beta_{1,1:K,1:C,w}, \mu_{\beta_1,1:K,1:C}, \sigma_h, z_{h,w}, s_w, \pi_{1:C}, \phi \middle| y_{h,w}, x_{h,w}\right) \\ &\quad \propto P\left(y_{h,w} \middle| \beta_{0,1:K,w}, \beta_{1,1:K,1:C,w}, \sigma_h, z_{h,w}, s_w, x_{h,w}\right) P\left(\beta_{0,1:K,w}\right) \\ &\qquad P\left(\beta_{1,1:K,1:C,w} \middle| \mu_{\beta_1,1:K,1:C}\right) P\left(\mu_{\beta_1,1:K,1:C}\right) P(\sigma_h) P\left(z_{h,w} \middle| \pi_{1:C}, s_w\right) P(\pi_{1:C}) \\ &\qquad P(s_w|\boldsymbol{\phi}) P(\boldsymbol{\phi}). \end{aligned} \tag{A.1}$$

To be used in a gradient based Bayesian approach (e.g., Hamiltonian Monte Carlo (HMC) or automatic differentiation variational inference (ADVI)), Eq. A.1 can be marginalized over latent categorical variables ($z_{h,w}$, s_w) (Stan Development Team, 2020b). The right-hand side equation (i.e., unnormalized posterior) of Eq. A.1 can be written as Eq. A.2:

$$\sum_{k=1}^{K} \sum_{c=1}^{C} \begin{bmatrix} P\left(y_{h,w} \middle| \beta_{0,k,w}, \beta_{1,k,c,w}, \mu_{\beta_1,k,c}, \sigma_h, x_{h,w}, z_{h,w} = k, s_w = c\right) P\left(\beta_{0,k,w}\right) P\left(\beta_{1,k,c,w} \middle| \mu_{\beta_1,k,c}\right) \\ P\left(\mu_{\beta_1,k,c}\right) P(\sigma_h) P\left(z_{h,w} = k \middle| \pi_{1:C}, s_w = c\right) P(\pi_c) P(s_w = c|\boldsymbol{\phi}) P(\boldsymbol{\phi}) \end{bmatrix}. \tag{A.2}$$

Eq. A.2 can be written as Eq. A.3 by using mixture weights (π_c and $\lambda_{c,w}$):

$$\sum_{k=1}^{K} \begin{bmatrix} P\left(y_{h,w} \middle| \beta_{0,k,w}, \left(\sum_{c=1}^{C} P\left(\beta_{1,k,c,w} \middle| \mu_{\beta_1,k,c}\right) P\left(\mu_{\beta_1,k,c}\right) P\left(\lambda_{c,w} \middle| \boldsymbol{\phi}\right)\right), \sigma_h, x_{h,w}\right) \\ \left(\sum_{c=1}^{C} P(\pi_c) P\left(\lambda_{c,w} \middle| \boldsymbol{\phi}\right)\right) P\left(\beta_{0,k,w}\right) P(\sigma_h) P(\boldsymbol{\phi}) \end{bmatrix}, \tag{A.3}$$

$$\boldsymbol{\lambda}_w: \begin{cases} \lambda_{1,w} = 1 - \text{softmax}\left(T_{\text{out},w} - \phi_{\text{winter}}\right) \\ \lambda_{2,w} = \text{softmax}\left(T_{\text{out},w} - \phi_{\text{winter}}\right) - \text{softmax}\left(T_{\text{out},w} - \phi_{\text{summer}}\right), \\ \lambda_{3,w} = \text{softmax}\left(T_{\text{out},w} - \phi_{\text{summer}}\right) \end{cases} \tag{A.4}$$

where $\lambda_{c,w}$ is ordered logit classifier from $\boldsymbol{\phi}$ (Eq. A.4).

HMC or ADVI would find posterior distributions of parameters by using unnormalized posterior (i.e., Eq. A.3).

APPENDIX B. ANALYSIS ON TIME DEPEDENCY OF NON-HEATING AND COOLING (NON-HC) ENERGY CONSUMPTION

Non-HC energy consumption such as plug loads, lighting, water heater, range cooking, etc., is closely related to human daily activities. Therefore, analysis on non-heating and cooling energy consumption can be used to understand if the human behavior and the resulting heat generation have any time dependencies, because it is difficult to directly monitor individual human activities in residential houses.

In this study, it is assumed that human behavior and the resulting heat generation has a time dependency in Eq.8 and 9. In other words, residents have daily or weekly routines in general, and heat generation from their behavior has time dependencies. To demonstrate this dependency, we plot the raw non-HC electricity data for different timescales. In Figure B.1, three typical temporal patterns are shown from yearly data (2018). Unit a5 (Figure B.1. (a)) has a weekday/weekend pattern. On Sun and Sat (i.e., weekend), there is energy consumption during the daytime (10:00-20:00), but weekdays show high energy consumption during nighttime (near 20:00). Unit 49 (Figure B.1. (b)) shows a more consistent pattern for all days regardless of weekday/weekend. On the other hand, it seems that there is no pattern for unit a9 (Figure B.1. (c)) over time.

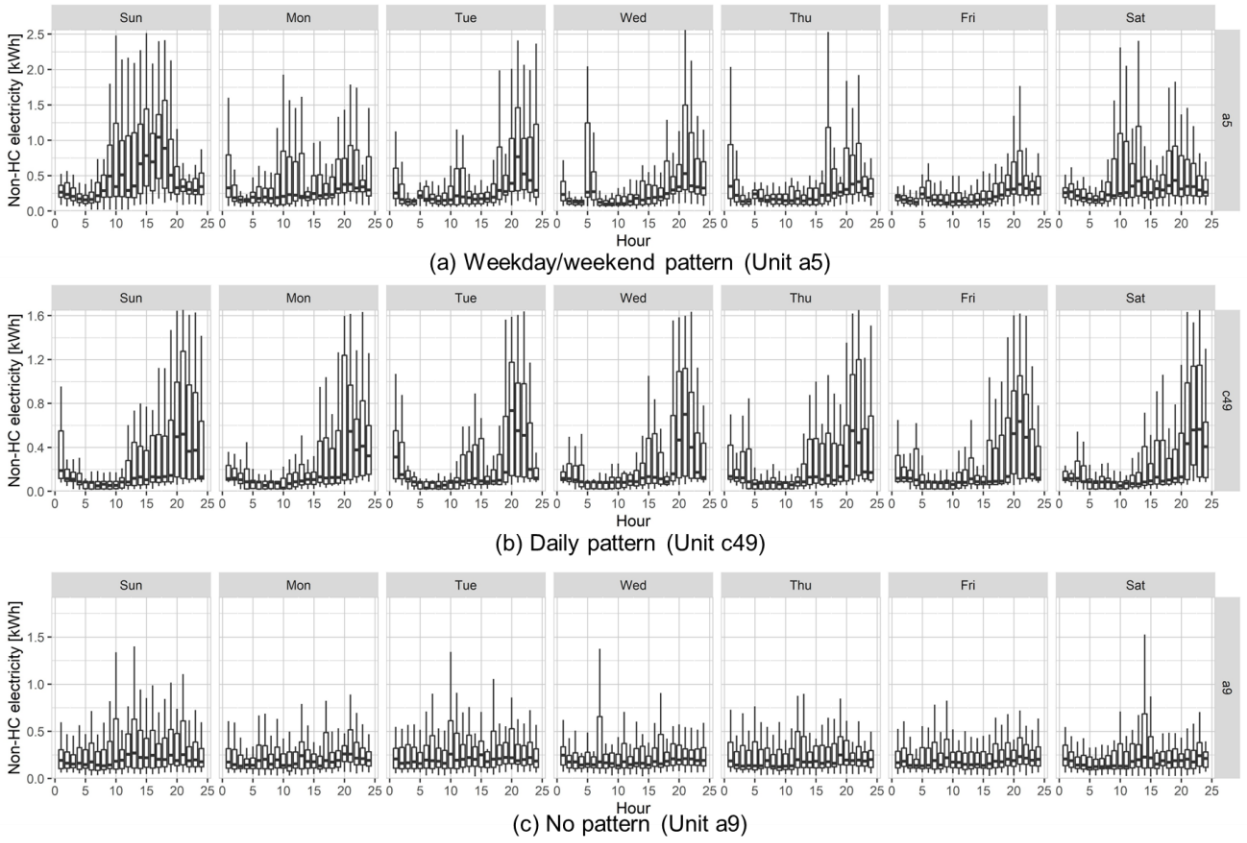

Figure B.1. non-HC energy consumption for each hour in a week by temporal patterns based on one-year of data (2018).

Recognition of time dependency through visual inspection is subjective due to the randomness in the data. Having a complete model to explain the data is challenging, but it is possible to test if the data have a certain time dependency by making a comparison between various model hypotheses with different time dependencies. In this study, we proposed the following three model hypotheses:

$\mathcal{M}_{\text{hour}}$: non-HC energy consumption of each unit follows a complete random process regardless of time (i.e., $E_{\text{non-HC},h,j} \sim \Pr\left(E_{\text{non-HC},h,j} | \mu_{\text{non-HC},h}, \sigma^2_{\text{non-HC},h}\right)$),

$\mathcal{M}_{\text{day}}$: non-HC energy consumption of each unit follows hour-specific random process (i.e., daily pattern) (i.e., $E_{\text{non-HC},h,j} \sim \Pr\left(E_{\text{non-HC},h,j} | \mu_{\text{non-HC,day},hr[j]}, \sigma^2_{\text{non-HC,day},hr[j]}\right)$),

$\mathcal{M}_{\text{week}}$: non-HC energy consumption of each unit follows week specific random process (i.e., weekly pattern) (i.e., $E_{\text{non-HC},h,j} \sim \Pr\left(E_{\text{non-HC},h,j} | \mu_{\text{non-HC,week},whr[j]}, \sigma^2_{\text{non-HC,week},whr[j]}\right)$),

where $\mathcal{M}$ is model hypothesis, $E_{\text{non-hc}}$ is non-HC energy consumption for an hour [kWh], h is household unit index, j is data index ($1 \dots J$), $\mu_{\text{non-hc}}$ and $\sigma^2_{\text{non-hc}}$ are mean and variance parameters of a normal distribution (N), hr is hour index (1 to 24) for data $j = 1 \dots J$, whr is weekly hour index (1 to 168) for data $j = 1 \dots J$.

All models are constructed through Bayesian inference by using Stan software (Carpenter et al., 2017). Once the posterior of each model is obtained, the model hypotheses can be compared through Bayes Factor (BF) (Murphy, 2012). BF is a relative evidence of one model over another, and therefore one model hypothesis prefers than the other. Given the data ($\mathcal{D}$), the posterior of model ($P(\mathcal{M}|\mathcal{D})$) is proportional to $P(\mathcal{D}|\mathcal{M})P(\mathcal{M})$. The posterior odds of different models can be written as Eq. B.1. Once the prior probabilities of each model are assumed to be equal (i.e., $P(\mathcal{M}_1) = P(\mathcal{M}_2)$), the likelihood odds can be used for model comparison, which is called Bayes Factor. BF (i.e., model evidence) from Stan output can be calculated through bridgesampling package (Gronau et al., 2020) via bridge sampling. After conducting z-score normalization (Han et al., 2012) over all data for each household unit (i.e., all data for each unit with zero mean and one standard deviation), we assign $N(0,1)$ for all μs and $\log N(0,1)$ for all σs for priors.

$$\underbrace{\frac{\Pr(\mathcal{M}_1|\mathcal{D})}{\Pr(\mathcal{M}_2|\mathcal{D})}}_{\text{Posterior odds}} = \underbrace{\frac{\Pr(\mathcal{D}|\mathcal{M}_1)}{\Pr(\mathcal{D}|\mathcal{M}_2)}}_{\text{Likelihood odds}} \underbrace{\frac{\Pr(\mathcal{M}_1)}{\Pr(\mathcal{M}_2)}}_{\text{Prior odds}}. \tag{B.1}$$

In Figure B.2, we visualized log-BF of two model hypotheses for each household unit, and higher numbers are expressed with darker blue color. In a typical model comparison, log-BF more than 4.6 (i.e., BF>100) is considered as decisive evidence. Our study uses a large amount of data (i.e., 1 year), so log scale of BFs is shown because the original BFs are too large. In the second row, all the numbers of $\log\text{BF}(\mathcal{M}_{\text{day}}/\mathcal{M}_{\text{hour}})$ are positive, indicating the data is more likely to have a daily dependency instead of complete random. In addition, $\log\text{BF}(\mathcal{M}_{\text{week}}/\mathcal{M}_{\text{day}})$ show mostly positive values except for 7 units. This can be interpreted as those units have clear daily dependencies, but the weekly dependency is a simply 7 repeated daily patterns. Therefore, in this case, the daily dependency model ($\mathcal{M}_{\text{day}}$) is good enough, and more parameters in $\mathcal{M}_{\text{week}}$ are redundant to explain the data (i.e., over-parameterization). There are two units showing that the weekly dependency model is worse than the hourly dependency model, but it can be also considered as redundant parameter case, because the daily dependency model already shows

higher evidence than the hourly dependency model for all cases. This does not mean there are clear periodic weekly behavior patterns, but the behavior terms are better explained when it is modeled as a random process with weekly interval.

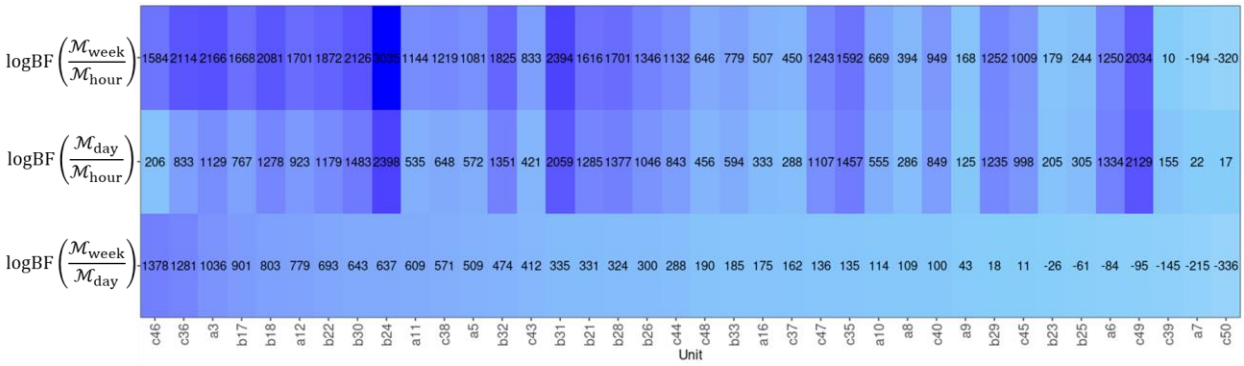

Figure B.2 Bayes Factors of model hypothesis.

APPENDIX C. INVESTIGATION ON MODEL STRUCTURE

For the selection of model structure, we adopt an iterative process to determine the simplest structure that can capture the building thermal dynamics based on our metrics (e.g., mean squared error of n-step ahead prediction, likelihood test (Bacher & Madsen, 2011), prediction error method (Ljung, 1999), etc.).From a practical viewpoint, the purpose of this process is to determine if the RC model is complex enough to explain the data based on the building thermal dynamics. In this study, the overall temperature of adjacent spaces (x_{n}) is modeled as a stochastic random process (i.e., a disturbance as an augmented state), so it is possible that the data is explained by the disturbance instead of the RC model. For this reason, we use a deterministic system identification without stochastic random process to decide the structure of RC model (Rouchier et al., 2018). Specifically, several RC model structures are developed, and then the model parameters are estimated to minimize the mean squared error of thermostat sensor temperature prediction (Eq. 5.13). In this case, x_{n} is assumed as a fixed temperature source. In reality, it randomly varies within a certain range (e.g., $20-30℃$), and the fixed temperature source can be considered as an average effect during the training period. Through this assumption, it is possible to evaluate the model structure s while preventing the disturbance from explaining the data.

The housing units in our field study have a small floor area ($65-111\mathrm{m}^2$), so three single zone model structures shown in Figure C.1 are developed (see Table 5.1 for notations). The 3R2C model (Figure C.1 (a)) is the simplest one, and it consists of the minimum necessary temperature nodes (outdoor air temperature: T_{a}, indoor air temperature: x_{i}, thermostat temperature sensor: x_{s}, overall temperature of adjacent spaces: x_{n}). $\dot{Q}$ represents the summation of heat flows to the zone (i.e., heating and cooling system ($\dot{Q}_{\mathrm{hc}}$), internal gains ($\zeta_{\mathrm{sol}}\dot{q}_{\mathrm{sol}}$), and solar gains ($\zeta_{\mathrm{ig}}\dot{Q}_{\mathrm{ig}}$), see Table 5.1). Since the building consists of concrete walls and slabs, thermal lags are expected, so the exterior wall temperature (x_{e}) and floor slab temperature (x_{m}) are added in the 5R4C model (Figure C.1 (b)). Finally, in the 7R5C model the exterior wall is modeled in more detail with two temperature nodes representing the wall layers (x_{e1} and x_{e2}) and a temperature node for the interior surface (x_{es}) (Figure C.1 (c)).

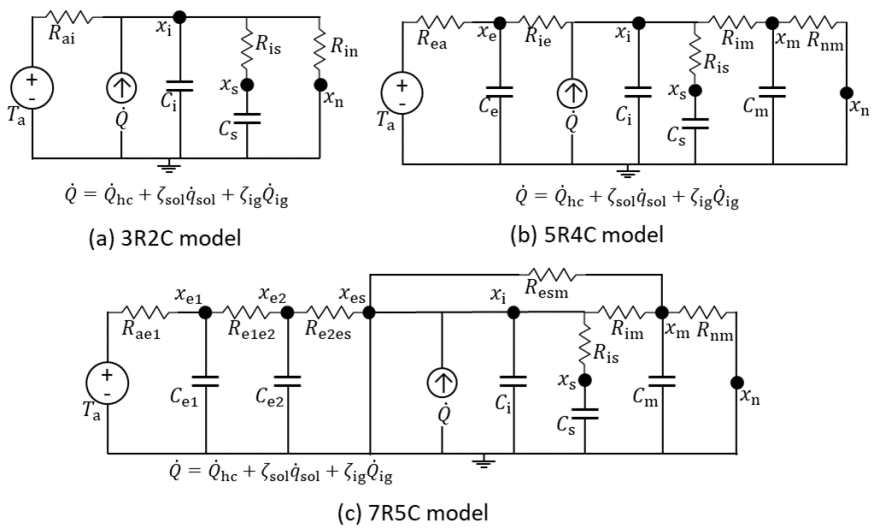

Figure C.1. Model structures of unit-level model.

In Figure C.2. Temperature predictions of various structures of unit-level model., presents the temperature predictions for the different model structures. The first four days of data is for training, and the three days are used for the prediction. Identified x_n is used as an input for both periods to account for the average effect. The simplest model (3R2C) shows the largest root mean squared error (RMSE) of 0.63℃ while the other two models have lower RMSE about 0.11℃. In other words, the 3R2C model is not adequate to explain the building thermal dynamics, but there is no distinctive advantage of using the 7R5C model (which is more complex. For this reason, the 5R4C model was selected.

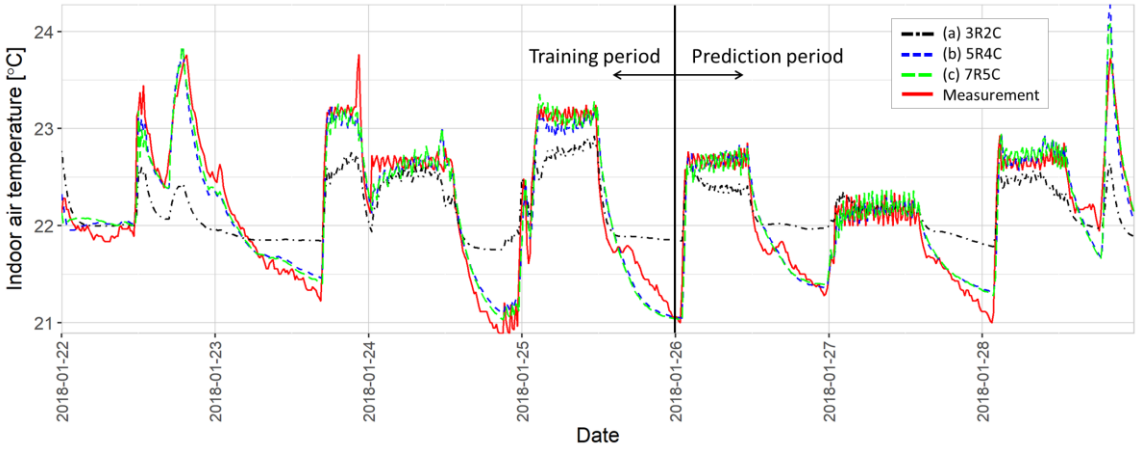

Figure C.2. Temperature predictions of various structures of unit-level model.

APPENDIX D. LIU-WEST FILTER ALGORITHM FOR THE UNIT-LEVEL MODEL

Nomenclature

$\mathbf{x}_{t_k} = \{x_{\mathrm{e},t_k}, x_{\mathrm{i},t_k}, x_{\mathrm{m},t_k}, x_{\mathrm{s},t_k}, x_{\mathrm{n},t_k}\}$ are states. $\mathbf{u}_{t_k} = \{x_{\mathrm{a},t_k}, \dot{q}_{\mathrm{sol},t_k}, \dot{Q}_{\mathrm{ig},t_k}, \dot{Q}_{\mathrm{cal,hc},t_k}\}$ are inputs.

$\boldsymbol{\theta}^* = \{C_{\mathrm{e}}^*, C_{\mathrm{m}}^*, C_{\mathrm{i}}^*, C_{\mathrm{s}}^*, R_{\mathrm{ea}}^*, R_{\mathrm{ie}}^*, R_{\mathrm{in}}^*, R_{\mathrm{nm}}^* R_{\mathrm{is}}^*, \zeta_{\mathrm{sol}}^*, \zeta_{\mathrm{ig}}^*, \eta_{\mathrm{htg}}^*, \eta_{\mathrm{aux}}^*, \eta_{\mathrm{df}}^*, \eta_{\mathrm{clg}}^*, \sigma_{\mathrm{e}}^*, \sigma_{\mathrm{i}}^*, \sigma_{\mathrm{m}}^*, \sigma_{\mathrm{s}}^*, \sigma_{\mathrm{n}}^*\}$ normalized parameters[(1)].

a is shrinkage coefficient. $a = (3\delta - 1)/2\delta$ where δ is discount factor (0,1]. $\delta = 0.9$ is used in this study.

$t_k = \{1, \dots, t_K\}$ is discrete time, $i = \{1{:}\,N_p\}$ is particle, $t_k|t_k - 1$ is predicted information at time (t_k) from time $(t_k - 1)$.

$\boldsymbol{\theta}_{t_k}^{*(i)}$ Monte Carlo approximation of $P(\boldsymbol{\theta}^*|y_{1:t_k})$

$w_{t_k}^{(i)}$ and $\pi_{t_k}^{(i)}$ are normalized and unnormalized weight of particle (i) at time (t_k).

$\mu_{\boldsymbol{\theta}^*}^{(i)}$ is location of smoothed kernel of each particle (i). COV is covariance.

$\sigma_{\mathrm{d},y}$ is set to 0.28 based on sensor accuracy (± 0.56℃).

$\mathcal{K}(\mathrm{x}_0)$ is kernel density approximation to generate prior (see 3.4 Model initialization). $\mathcal{N}$ is multivariate normal distribution.

Algorithm

1: Generate initial particles $\mathbf{x}_0^{(1:N_p)} \sim \mathcal{K}(\mathbf{x}_0)$ and set $\mathbf{x}_1^{(1:N_p)} = \mathbf{x}_0^{(1:N_p)}$

2: Generate initial particles $\boldsymbol{\theta}_1^{(1:N_p)} \sim \mathcal{K}(\boldsymbol{\theta})$ and normalize/set it $\boldsymbol{\theta}_1^{*(1:N_p)} = \boldsymbol{\theta}_1^{(1:N_p)}$

3: Set initial weight of each particles as $w_1^{(1:N_p)} = 1/N_p$

4: **for** t_k in $2{:}\,t_K$ **do**

5: Compute $\bar{\boldsymbol{\theta}}_{t_k-1}^* = \sum_{i=1}^{N_P} \boldsymbol{\theta}_{t-1}^{*(i)} / N_p$

6: Compute $\mathbf{V}_{\boldsymbol{\theta}_{t_k-1}^*} = \mathrm{COV}\left(\boldsymbol{\theta}_{t_k-1}^{*(1:N_p)}\right) = \sum_{i=1}^{N_p}\left[w_{t_k-1}^{(i)}\left(\boldsymbol{\theta}_{t_k}^{*(i)} - \bar{\boldsymbol{\theta}}_{t_k}^*\right)\left(\boldsymbol{\theta}_{t_k}^{*(i)} - \bar{\boldsymbol{\theta}}_{t_k}^*\right)^{\mathsf{T}}\right]$

7: Compute $\boldsymbol{\mu}_{\mathbf{x},t_k|t_k-1}^{(1:N_p)} = \mathbb{E}\left(\mathbf{x}_{t_k}|\mathbf{x}_{t_k-1}^{(1:N_p)}, \boldsymbol{\theta}_{t_k-1}^{(1:N)}, \mathbf{u}_{t_k-1}\right) = f_{\mathrm{d}}\left(\mathbf{x}_{t_k-1}^{(1:N)}, \boldsymbol{\theta}_{t_k-1}^{(1:N)}, \mathbf{u}_{t_k-1},\right)$ with unnormalized $\boldsymbol{\theta}_{t_k-1}^{(1:N)}$

8: Compute $\boldsymbol{\mu}_{\boldsymbol{\theta}^*,t_k|t_k-1}^{(1:N_p)} = a\boldsymbol{\theta}_{t_k-1}^{*(1:N_p)} + (\mathbf{1} - a)\bar{\boldsymbol{\theta}}_{t_k-1}^*$

9: Compute $\pi_{t_k|t_k-1}^{(1:N_p)} = w_{t_k-1}^{(1:N_p)}\, P\left(y_{t_k}|g_{\mathrm{d}}\left(\boldsymbol{\mu}_{\mathbf{x},t_k|t_k-1}^{(1:N_p)}, \boldsymbol{\mu}_{\boldsymbol{\theta},t_k|t_k-1}^{(1:N_p)}\right), \sigma_{\mathrm{d},y}\right)$ with unnormalized $\boldsymbol{\mu}_{\boldsymbol{\theta},t_k|t_k-1}^{(1:N_p)}$

10: Normalize $\pi_{t_k|t_k-1}^{(1:N_p)}$ as $w_{t_k|t_k-1}^{(1:N_p)} = \pi_{t_k|t_k-1}^{(1:N_p)} / \sum_{i=1}^{N_p} \pi_{t_k|t_k-1}^{(i)}$

11: Sample $m^{(1:N_p)} \sim \mathrm{Multinom}\left(1{:}\,N_p, w_{t_k|t_k-1}^{(1:N_p)}\right)$ and sort $m^{(1:N_p)}$ in increasing order.

12: Sample $\boldsymbol{\theta}_{t_k}^{*(1:N_p)} \sim \mathcal{N}\left(\boldsymbol{\mu}_{\boldsymbol{\theta}^*,t_k|t_k-1}^{\left(m^{(1:N_p)}\right)}, (1 - a^2)\mathbf{V}_{\theta^*,t_k-1}\right)$

13: Compute $\boldsymbol{\mu}_{\mathbf{x},t_k}^{(1:N_p)} = \mathbb{E}\left(\mathbf{x}_{t_k}|\mathbf{x}_{t_k-1}^{\left(m^{(1:N_p)}\right)}, \boldsymbol{\theta}_{t_k}^{(1:N_p)}\right) = f_{\mathrm{d}}\left(\mathbf{x}_{t_k-1}^{\left(m^{(1:N)}\right)}, \boldsymbol{\theta}_{t_k}^{(1:N)}, \mathbf{u}_{t_k-1}\right)$ with unnormalized $\boldsymbol{\theta}_{t_k}^{(1:N_p)}$

14: Sample $\mathbf{x}_{t_k}^{(1:N_p)} \sim \mathcal{N}\left(\boldsymbol{\mu}_{\mathbf{x},t_k}^{\left(m^{(1:N_p)}\right)}, \boldsymbol{\theta}_{t_k}^{(1:N_p)}\right)$

15: Compute $\pi_{t_k}^{(1:N_p)} = P\left(y_{t_k}|g_{\mathrm{d}}\left(\mathbf{x}_{t_k}^{(1:N_p)}, \boldsymbol{\theta}_{t_k}^{(1:N_p)}\right), \sigma_{\mathrm{d},y}\right) \Big/ \Pr\left(y_t|g_{\mathrm{d}}\left(\boldsymbol{\mu}_{\mathbf{x},t_k|t_k-1}^{\left(m^{(1:N_p)}\right)}, \boldsymbol{\mu}_{\boldsymbol{\theta},t_k|t_k-1}^{\left(m^{(1:N_p)}\right)}\right), \sigma_{\mathrm{d},y}\right)$ with unnormalized $\boldsymbol{\theta}_{t_k}^{(1:N_p)}, \boldsymbol{\mu}_{\boldsymbol{\theta},t_k|t_k-1}^{\left(m^{(1:N_p)}\right)}$

16: Normalize $\pi_{t_k}^{(1:N_p)}$ as $w_{t_k}^{(1:N_p)} = \pi_t^{(1:N_p)} / \sum_{i=1}^{N_p} \pi_{t_k}^{(i)}$

17: Sample $o^{(1:N_p)} \sim \mathrm{Multinom}\left(1{:}\,N_p, w_{t_k}^{(1:N_p)}\right)$ and sort $o^{(1:N_p)}$ in increasing order, and then $w_{t_k}^{(1:N_p)} = 1/N_p$

18: Set final $\mathbf{x}_{t_k}$ samples via permutation $\mathbf{x}_{t_k}^{(1:N)} \leftarrow \mathbf{x}_{t_k}^{\left(o^{(1:N)}\right)}$

19: Set final $\boldsymbol{\theta}_{t_k}^*$ samples via permutation $\boldsymbol{\theta}_{t_k}^{*(1:N_p)} \leftarrow \boldsymbol{\theta}_{t_k}^{*\left(o^{(1:N_p)}\right)}$

20: Set $\boldsymbol{\theta}_{u,t_k}^{*(1:N_p)} \leftarrow \boldsymbol{\theta}_{u,t_k-1}^{*(1:N_p)}$ if specific u_{t_k} of $\mathbf{u}_{t_k}$ is not involved in the time step t_k

21: **end for**

(1) All parameters are normalized in range of [-0.5, 0.5] by using the min-max normalization technique (Han et al., 2012) to have similar scales in multivariate normal sampling in line 12. The values are bounded in this range. Maximum values of parameters are selected by the maximum values of prior distribution (see section 5.2.3).

(2) Each of $\boldsymbol{\theta}_{\mathrm{u}}$ is updated when the parameter is involved in a building thermal process as shown in line 20. For example, during the heating process, cooling coefficient (k_{clg}) should not be updated.

(3) When there is missing data in y_{t} or $\mathbf{u}_t$, $\mathbf{x}_t$ and $\boldsymbol{\theta}_t$ particles are not updated until new data comes in.

APPENDIX E. NORMAL-GAMMA DISTRIBUTION

Our interest k value is positive, and we assume that $\log k$ follows a normal distribution:

$$\log k \sim \mathcal{N}(\mu_k, \tau_k^{-1}). \tag{E.1}$$

where μ_k and τ_k^{-1} are the mean and variance of the normal distribution (i.e., τ_k is precision).

When the prior of parameters of the normal distribution follows Eq. E.2 (α_0 is shape and β_0 is rate), the posterior of the parameters is given as a Normal-Gamma distribution in Eq. E.3. $\mu_{k,0}, \lambda_{k,0}, \alpha_{k,0}, \beta_{k,0}$ are constants for a prior distribution.

$$\begin{aligned} &\Pr(\tau_k|\alpha_{k,0}, \beta_{k,0}) \sim \Gamma(\alpha_{k,0}, \beta_{k,0}), \\ &\Pr(\mu_k|\tau_k) \sim \mathcal{N}(\mu_{k,0}, 1/(\lambda_{k,0}\tau_k)). \end{aligned} \tag{E.2}$$

$$\Pr(\mu_k, \tau_k|\mu_{k,0}, \lambda_{k,0}, \alpha_{k,0}, \beta_{k,0}) \sim \text{NormalGamma}(\mu_{k,0}, \lambda_{k,0}, \alpha_{k,0}, \beta_{k,0}). \tag{E.3}$$

When we have n observations $k_{1:n}$, the posterior of the Normal-Gamma distribution can be written as Eq. E.4

$$\begin{aligned} &\Pr(\mu_k, \tau_k|\log k_{1:n}) \sim \text{NormalGamma}(\mu_{k,n}, \lambda_{k,n}, \alpha_{k,n}, \beta_{k,n}), \\ &\text{where} \\ &\mu_{k,n} = \frac{\lambda_{k,0}\mu_{k,0} + n\,\overline{\log k}_{1:n}}{\lambda_{k,0} + n}, \\ &\lambda_{k,n} = \lambda_{k,0} + n, \\ &\alpha_{k,n} = \alpha_{k,0} + n/2\,, \\ &\beta_{k,n} = \beta_0 + \frac{1}{2}\sum_{i=1}^{n}\left(\log k_i - \overline{\log k}_{1:n}\right)^2 + \frac{\lambda_{k,0} n\left(\overline{\log k}_{1:n} - \mu_{k,0}\right)^2}{2\left(\lambda_{k,0} + n\right)}. \end{aligned} \tag{E.4}$$

In this research, $\mu_{k,0}, \lambda_{k,0}, \alpha_{k,0}, \beta_{k,0}$ are initially set to fixed numbers and updated based on the incoming data. For the heating/cooling/aux operation, $\mu_{k,0} = 0, \lambda_{k,0} = 1, \alpha_{k,0} = 500, \beta_{k,0} = 10$, which gives k values at the 95% quantile that are approximately in [0.5,1.5]. Similarly, $\mu_{k,0} = -0.7, \lambda_{k,0} = 1, \alpha_{k,0} = 600, \beta_{k,0} = 50$ are set for defrost operation of the auxiliary heater ($k_{\text{aux,df}}$), which results in 95% percentiles of values that are approximately in $[0 - 0.1]$.

APPENDIX F. MULTIZONE MODEL

To validate our counterfactual scenario, we developed a multizone model and we present an example for a specific unit located on the top floor of the building adjacent to unit A (left), B (right), and C (bottom) as shown in Figure F.1. The rear wall of the unit faces the hallway, and the ceiling is connected to the outside as the unit is located on the top floor. Figure F.2 shows the thermal network of the 4 units. All the notation is the same as presented in Table 5.1. Subscripts A, B, and C are used for the A, B, and C units, respectively. The adjacent spaces temperatures of units A, B, and C are modeled with fixed temperatures ($x_{\mathrm{nA},t}$, $x_{\mathrm{nB},t}$, and $x_{\mathrm{nC},t}$). The outdoor air temperature ($x_{\mathrm{a},t}$) and hallway temperature ($x_{\mathrm{hw},t}$) are obtained from the weather station and hallway thermostat. The sensor temperatures of units ($x_{\mathrm{sA},t}$, $x_{\mathrm{sB},t}$, $x_{\mathrm{sC},t}$, and $x_{\mathrm{s},t}$) are obtained from thermostats. The differential equations at each node are listed in Table F.1. The same approach of model initialization is used to learn the multizone model. The same optimizer is used to find best parameter sets for one week of training and test data in Sep 2018. The period is chosen based on data availability.

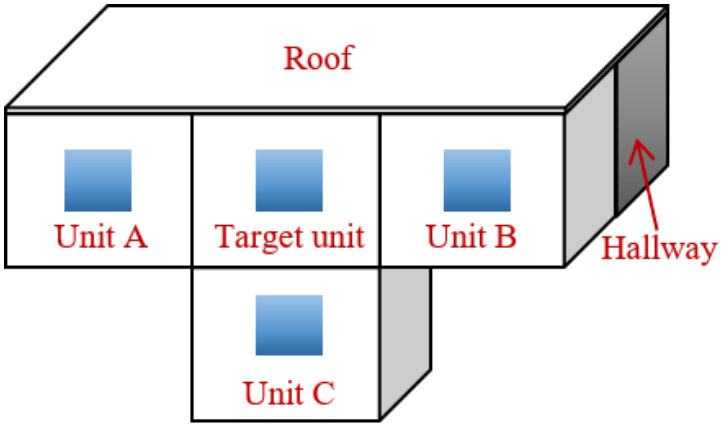

Figure F.1. Schematic building layout of multizone model.

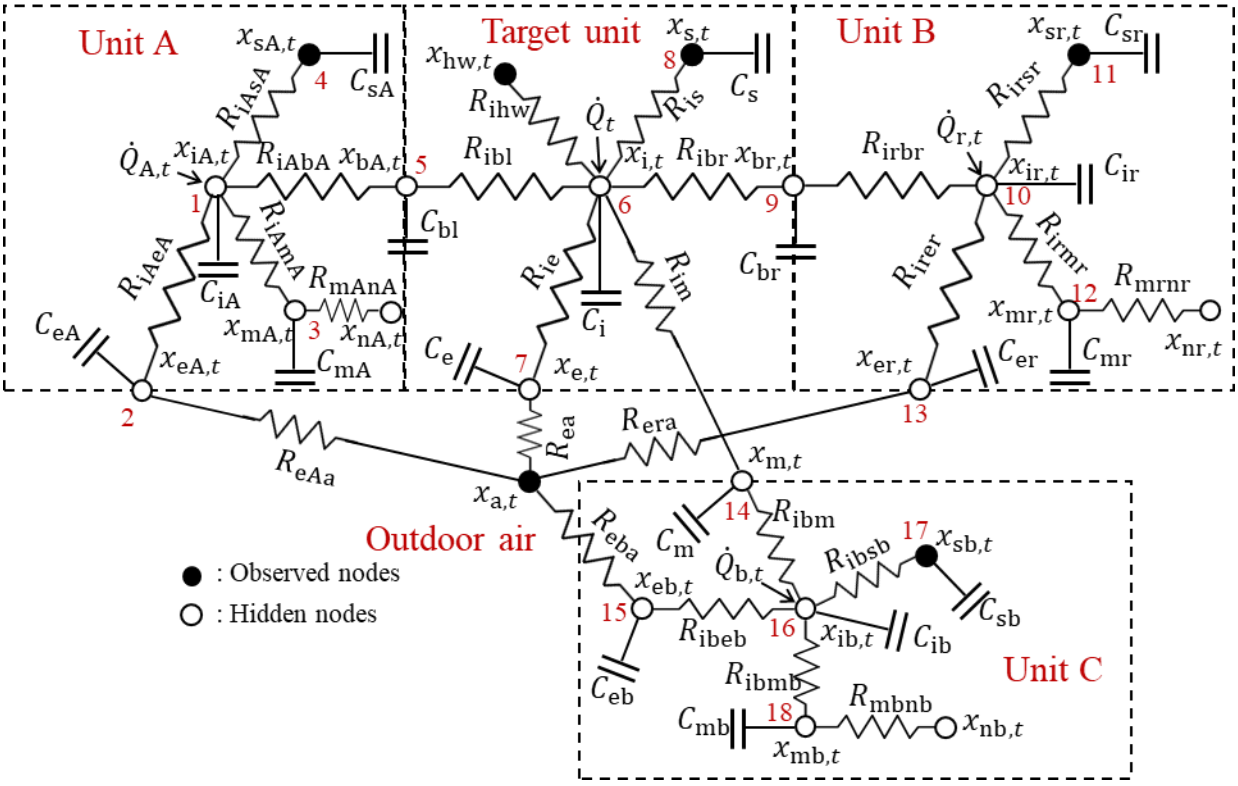

Figure F.2. Multizone model.

Table F.1. Multizone model equations.

1. $C_{\mathrm{iA}}\frac{dx_{\mathrm{iA},t}}{dt}=\frac{x_{\mathrm{eA},t}-x_{\mathrm{iA},t}}{R_{\mathrm{iAeA}}}+\frac{x_{\mathrm{sA},t}-x_{\mathrm{iA},t}}{R_{\mathrm{iAsA}}}+\frac{x_{\mathrm{bA},t}-x_{\mathrm{iA},t}}{R_{\mathrm{iAbA}}}+\frac{x_{\mathrm{mA},t}-x_{\mathrm{iA},t}}{R_{\mathrm{iAmA}}}+\dot{Q}_{A,t}$
2. $C_{\mathrm{eA}}\frac{dx_{\mathrm{eA},t}}{dt}=\frac{x_{\mathrm{iA},t}-x_{\mathrm{eA},t}}{R_{\mathrm{iAeA}}}+\frac{x_{\mathrm{a},t}-x_{\mathrm{eA},t}}{R_{\mathrm{eAa}}}$
3. $C_{\mathrm{mA}}\frac{dx_{\mathrm{mA},t}}{dt}=\frac{x_{\mathrm{iA},t}-x_{\mathrm{mA},t}}{R_{\mathrm{iAmA}}}+\frac{x_{\mathrm{nA},t}-x_{\mathrm{mA},t}}{R_{\mathrm{mAnA}}}$
4. $C_{\mathrm{sA}}\frac{dx_{\mathrm{sA},t}}{dt}=\frac{x_{\mathrm{iA},t}-x_{\mathrm{sA},t}}{R_{\mathrm{iAsA}}}$
5. $C_{\mathrm{bA}}\frac{dx_{\mathrm{bA},t}}{dt}=\frac{x_{\mathrm{iA},t}-x_{\mathrm{bA},t}}{R_{\mathrm{iAbA}}}+\frac{x_{\mathrm{i},t}-x_{\mathrm{bA},t}}{R_{\mathrm{ibA}}}$
6. $C_{\mathrm{i}}\frac{dx_{\mathrm{i},t}}{dt}=\frac{x_{\mathrm{bA},t}-x_{\mathrm{i},t}}{R_{\mathrm{ibA}}}+\frac{x_{\mathrm{hw},t}-x_{\mathrm{i},t}}{R_{\mathrm{ihw}}}+\frac{x_{\mathrm{s},t}-x_{\mathrm{i},t}}{R_{\mathrm{is}}}+\frac{x_{\mathrm{bB},t}-x_{\mathrm{i},t}}{R_{\mathrm{ibB}}}+\frac{x_{\mathrm{m},t}-x_{\mathrm{i},t}}{R_{\mathrm{im}}}+\frac{x_{\mathrm{e},t}-x_{\mathrm{i},t}}{R_{\mathrm{ie}}}+\dot{Q}_{t}$
7. $C_{\mathrm{e}}\frac{dx_{\mathrm{e},t}}{dt}=\frac{x_{\mathrm{i},t}-x_{\mathrm{e},t}}{R_{\mathrm{ie}}}+\frac{x_{\mathrm{a},t}-x_{\mathrm{e},t}}{R_{\mathrm{ea}}}$
8. $C_{\mathrm{s}}\frac{dx_{\mathrm{s},t}}{dt}=\frac{x_{\mathrm{i},t}-x_{\mathrm{s},t}}{R_{\mathrm{is}}}$
9. $C_{\mathrm{bB}}\frac{dx_{\mathrm{bB},t}}{dt}=\frac{x_{\mathrm{i},t}-x_{\mathrm{bB},t}}{R_{\mathrm{ibB}}}+\frac{x_{\mathrm{iB},t}-x_{\mathrm{bB},t}}{R_{\mathrm{iBbB}}}$
10. $C_{\mathrm{iB}}\frac{dx_{\mathrm{iB},t}}{dt}=\frac{x_{\mathrm{bB},t}-x_{\mathrm{iB},t}}{R_{\mathrm{iBbB}}}+\frac{x_{\mathrm{sB},t}-x_{\mathrm{iB},t}}{R_{\mathrm{iBsB}}}+\frac{x_{\mathrm{mB},t}-x_{\mathrm{iB},t}}{R_{\mathrm{iBmB}}}+\frac{x_{\mathrm{eB},t}-x_{\mathrm{iB},t}}{R_{\mathrm{iBeB}}}+\dot{Q}_{\mathrm{B},t}$
11. $C_{\mathrm{sB}}\frac{dx_{\mathrm{sB},t}}{dt}=\frac{x_{\mathrm{iB},t}-x_{\mathrm{sB},t}}{R_{\mathrm{iBsB}}}$
12. $C_{\mathrm{mB}}\frac{dx_{\mathrm{mB},t}}{dt}=\frac{x_{\mathrm{iB},t}-x_{\mathrm{mB},t}}{R_{\mathrm{iBmB}}}+\frac{x_{\mathrm{nB},t}-x_{\mathrm{mB},t}}{R_{\mathrm{mBnB}}}$
13. $C_{\mathrm{eB}}\frac{x_{\mathrm{eB},t}}{dt}=\frac{x_{\mathrm{iB},t}-x_{\mathrm{eB},t}}{R_{\mathrm{iBeB}}}+\frac{x_{\mathrm{a},t}-x_{\mathrm{eB},t}}{R_{\mathrm{eBa}}}$
14. $C_{\mathrm{m}}\frac{x_{\mathrm{m},t}}{dt}=\frac{x_{\mathrm{i},t}-x_{\mathrm{m},t}}{R_{\mathrm{im}}}+\frac{x_{\mathrm{iC},t}-x_{\mathrm{m},t}}{R_{\mathrm{iCm}}}$
15. $C_{\mathrm{eC}}\frac{dx_{\mathrm{eC},t}}{dt}=\frac{x_{\mathrm{iC},t}-x_{\mathrm{eC},t}}{R_{\mathrm{iCeC}}}+\frac{x_{\mathrm{a},t}-x_{\mathrm{eC},t}}{R_{\mathrm{eCa}}}$
16. $C_{\mathrm{iC}}\frac{x_{\mathrm{iC},t}}{dt}=\frac{x_{\mathrm{sC},t}-x_{\mathrm{iC},t}}{R_{\mathrm{iCsC}}}+\frac{x_{\mathrm{m},t}-x_{\mathrm{iC},t}}{R_{\mathrm{iCm}}}+\frac{x_{\mathrm{eC},t}-x_{\mathrm{iC},t}}{R_{\mathrm{iCeC}}}+\frac{x_{\mathrm{mC},t}-x_{\mathrm{iC},t}}{R_{\mathrm{iCmC}}}+\dot{Q}_{\mathrm{C},t}$
17. $C_{\mathrm{sC}}\frac{x_{\mathrm{sC},t}}{dt}=\frac{x_{\mathrm{iC},t}-x_{\mathrm{sC},t}}{R_{\mathrm{iCsC}}}$
18. $C_{\mathrm{mC}}\frac{x_{\mathrm{mC},t}}{dt}=\frac{x_{\mathrm{iC},t}-x_{\mathrm{mC},t}}{R_{\mathrm{iCmC}}}+\frac{x_{\mathrm{nC},t}-x_{\mathrm{mC},t}}{R_{\mathrm{mCnC}}}$

REFERENCES

Albert, A., & Rajagopal, R. (2015). Thermal Profiling of Residential Energy Use. In *IEEE Transactions on Power Systems* (Vol. 30, Issue 2, pp. 602–611). https://doi.org/10.1109/TPWRS.2014.2329485

Allcott, H. (2011). Social norms and energy conservation. *Journal of Public Economics*, *95*(9–10), 1082–1095. https://doi.org/10.1016/j.jpubeco.2011.03.003

American Council for an Energy-Efficient Economy. (2020). *Low-Income and Multifamily EE Programs*. https://database.aceee.org/city/low-income-multifamily

Amir, K., & Ram, R. (2014). Data-Driven Benchmarking of Building Energy Efficiency Utilizing Statistical Frontier Models. *Journal of Computing in Civil Engineering*, *28*(1), 79–88. https://doi.org/10.1061/(ASCE)CP.1943-5487.0000327

Anderson, K., Song, K., Lee, S. H., Krupka, E., Lee, H., & Park, M. (2017). Longitudinal analysis of normative energy use feedback on dormitory occupants. *Applied Energy*, *189*, 623–639. https://doi.org/10.1016/j.apenergy.2016.12.086

Andor, M. A., Gerster, A., Peters, J., & Schmidt, C. M. (2020). Social Norms and Energy Conservation Beyond the US. *Journal of Environmental Economics and Management*, *103*, 102351. https://doi.org/10.1016/j.jeem.2020.102351

Andrieu, C., Doucet, A., & Holenstein, R. (2010). Particle Markov chain Monte Carlo methods. *Journal of the Royal Statistical Society Series B-Statistical Methodology*, *72*(3), 269–342. https://doi.org/10.1111/j.1467-9868.2009.00736.x

Arambula Lara, R., Pernigotto, G., Cappelletti, F., Romagnoni, P., & Gasparella, A. (2015). Energy audit of schools by means of cluster analysis. *Energy and Buildings*, *95*, 160–171. https://doi.org/10.1016/j.enbuild.2015.03.036

Arjunan, P., Poolla, K., & Miller, C. (2020). EnergyStar++: Towards more accurate and explanatory building energy benchmarking. *Applied Energy*, *276*(15), 115413. https://doi.org/10.1016/j.apenergy.2020.115413

Asadinejad, A., Rahimpour, A., Tomsovic, K., Qi, H., & Chen, C. fei. (2018). Evaluation of residential customer elasticity for incentive based demand response programs. *Electric Power Systems Research*, *158*, 26–36. https://doi.org/10.1016/j.epsr.2017.12.017

Asensio, O. I., & Delmas, M. A. (2015). Nonprice incentives and energy conservation. *Proceedings of the National Academy of Sciences*, *112*(6), E510–E515. https://doi.org/10.1073/pnas.1401880112

ASHRAE. (2013a). *2013 ASHRAE Handbook: Fundamentals, Chapter 26 SI: Heat, Air, and Moisture Control in Building Assemblies - Material Properties*. Atlanta: American Society of Heating, Refrigerating and Air-Conditioning Engineers, Inc.

ASHRAE. (2013b). *ANSI/ASHRAE/IES Standard 169-2013 Climatic Data for Building Design Standards*. American Society of Heating, Refrigerating and Air-Conditioning Engineers.

Ayres, I., Raseman, S., & Shih, A. (2013). Evidence from Two Large Field Experiments that Peer Comparison Feedback Can Reduce Residential Energy Usage. *The Journal of Law, Economics, and Organization*, *29*(5), 992–1022. https://doi.org/10.1093/jleo/ews020

Bacher, P., & Madsen, H. (2011). Identifying suitable models for the heat dynamics of buildings. *Energy and Buildings*, *43*(7), 1511–1522. https://doi.org/10.1016/j.enbuild.2011.02.005

Baldi, S., Yuan, S., Endel, P., & Holub, O. (2016). Dual estimation: Constructing building energy models from data sampled at low rate. *Applied Energy*, *169*, 81–92. https://doi.org/10.1016/j.apenergy.2016.02.019

Batalla-Bejerano, J., Trujillo-Baute, E., & Villa-Arrieta, M. (2020). Smart meters and consumer behaviour: Insights from the empirical literature. *Energy Policy*, *144*(June), 111610. https://doi.org/10.1016/j.enpol.2020.111610

Batra, N., Singh, A., & Whitehouse, K. (2015). If You Measure It, Can You Improve It? Exploring The Value of Energy Disaggregation. *Proceedings of the 2nd ACM International Conference on Embedded Systems for Energy-Efficient Built Environments*, 191–200. https://doi.org/10.1145/2821650.2821660

Beckel, C. (2016). *Scalable and personalized energy efficiency services with smart meter data*. Ph.D. dissertation. ETH Zurich.

Better Buildings Initiative. (2019). *Working Toward a More Innovative, Affordable, and Energy Efficient Future, PROGRESS REPORT*. U.S. Department of Energy.

Bishop, C. M. (2006). *Pattern recognition and machine learning*. New York : Springer.

Bourassa, N. J., Rainer, L., Mills, E., & Glickman, J. (2012). The Home Energy Scoring Tool: A Simplified Asset Rating for Single Family Homes. *2012 ACEEE Summer Study on Energy Efficiency in Buildings*, *12*, 34–46.

Broderick, T., Boyd, N., Wibisono, A., Wilson, A. C., & Jordan, M. I. (2013). *Streaming Variational Bayes*. 1–9. http://arxiv.org/abs/1307.6769

Brultech. (2021). *GreenEye Monitor (Residential)*. https://www.brultech.com/greeneye/

Buchanan, K., Russo, R., & Anderson, B. (2015). The question of energy reduction: The problem(s) with feedback. *Energy Policy*, *77*, 89–96. https://doi.org/10.1016/j.enpol.2014.12.008

Carpenter, B., Gelman, A., Hoffman, M. D., Lee, D., Goodrich, B., Betancourt, M., Brubaker, M. A., Guo, J., Li, P., & Riddell, A. (2017). Stan: A Probabilistic Programming Language. *Journal of Statistical Software*, *76*(1), 1–32. https://doi.org/10.18637/jss.v076.i01

Carrie Armel, K., Gupta, A., Shrimali, G., & Albert, A. (2013). Is disaggregation the holy grail of energy efficiency? The case of electricity. *Energy Policy*, *52*, 213–234. https://doi.org/10.1016/j.enpol.2012.08.062

Carvalho, C. M., Johannes, M. S., Lopes, H. F., & Polson, N. G. (2010). Particle Learning and Smoothing. *Statistical Science*, *25*(1), 88–106. https://doi.org/10.1214/10-STS325

Chiang, T., Mevlevioglu, G., Natarajan, S., Padget, J., & Walker, I. (2014). Inducing [sub]conscious energy behaviour through visually displayed energy information: A case study in university accommodation. *Energy and Buildings*, *70*, 507–515. https://doi.org/10.1016/j.enbuild.2013.10.035

Chopin, N., Jacob, P. E., & Papaspiliopoulos, O. (2013). SMC 2 : an efficient algorithm for sequential analysis of state space models. *Journal of the Royal Statistical Society: Series B (Statistical Methodology)*, *75*(3), 397–426. https://doi.org/10.1111/j.1467-9868.2012.01046.x

CLEAResult. (2016). *Guide to Smart Thermostats*. CLEAResult. https://www.clearesult.com/insights/whitepapers/guide-to-smart-thermostats/

Corduneanu, A., & Bishop, C. M. (2001). Variational Bayesian model selection for mixture distributions. *Artificial Intelligence and Statistics*, *2001*, 27–34.

Culière, F., Leduc, L., & Belikov, A. (2020). Bayesian model of electrical heating disaggregation. *NILM 2020 - Proceedings of the 5th International Workshop on Non-Intrusive Load Monitoring*, 25–29. https://doi.org/10.1145/3427771.3427848

Cutler, D. S., Bernal Heredia, W. G., & Dean, J. D. (2019). *Case Study: Laboratory and Field Evaluation of Circuit-Level Electrical Submetering with Wireless Current Transformers*. National Renewable Energy Lab. https://doi.org/10.2172/1530174

Davis Instruments. (2021). *Vantage Pro2*. https://www.davisinstruments.com/pages/vantage-pro2

Doucet, A. (2006). Sequential Monte Carlo Methods. In *Encyclopedia of Statistical Sciences*. https://doi.org/doi:10.1002/0471667196.ess5089

Ecobee. (2021). *Ecobee - Smart thermostats*. https://www.ecobee.com/en-us/smart-thermostats/

Ecobee developers. (2021). *Getting Started with the ecobee API*. https://www.ecobee.com/home/developer/api/introduction/index.shtml

Ehrhardt-Martinez, K. (2015). Behaviour wedge profiles for cities. *ECEEE SUMMER STUDY PROCEEDINGS*, 691–702.

Ehrhardt-Martinez, K., Donnelly, K. A., & Latiner, J. A. "Skip." (2010). *Advanced Metering Initiatives and Residential Feedback Programs: A Meta-Review for Household Electricity-Saving Opportunities*. American Council for an energy-Efficient Economy, Washington, D.C.

EIA. (2015). *Residential Energy Consumption Survey (RECS)*. U.S. Energy Information Administration.

Ellis, M. J., & Alanqar, A. (2018). Formulation and Application of an Economic Model Predictive Control Scheme for Connected Thermostats. *5th International High Performance Buildings Conference at Purdue*, 3194. 1-10.

Energy Star. (2009). *A Guide to Energy-Efficient Heating and Cooling*. U.S. Environmental Protection Agency.

Energy Star. (2014a). *Technical Reference: ENERGY STAR Score*.

Energy Star. (2014b). *Technical Reference: ENERGY STAR Score for Multifamily Housing in the United States*. *November*, 1–13. http://www.energystar.gov/buildings/sites/default/uploads/tools/ENERGY STAR Score for K12 Schools_Canada.pdf?6422-e094

Energy Star. (2017). *Technical Reference: Climate and Weather*. https://www.energystar.gov/sites/default/files/tools/Climate_and_Weather_August_2017_EN_508.pdf

Fogg, B. J. (2009). A behavior model for persuasive design. *Proceedings of the 4th International Conference on Persuasive Technology*, 40.

Ford, R., Pritoni, M., Sanguinetti, A., & Karlin, B. (2017). Categories and functionality of smart home technology for energy management. *Building and Environment*, *123*, 543–554. https://doi.org/10.1016/j.buildenv.2017.07.020

Froehlich, J., Findlater, L., & Landay, J. (2010). The Design of Eco-feedback Technology. *Proceedings of the SIGCHI Conference on Human Factors in Computing Systems*, 1999–2008. https://doi.org/10.1145/1753326.1753629

Gao, G., & Whitehouse, K. (2009). The Self-programming Thermostat: Optimizing Setback Schedules Based on Home Occupancy Patterns. *Proceedings of the First ACM Workshop on Embedded Sensing Systems for Energy-Efficiency in Buildings*, 67–72. https://doi.org/10.1145/1810279.1810294

Gao, X., & Malkawi, A. (2014). A new methodology for building energy performance benchmarking: An approach based on intelligent clustering algorithm. *Energy and Buildings*, *84*, 607–616. https://doi.org/10.1016/j.enbuild.2014.08.030

Gelman, A., Carlin, J. B., Stern, H. S., & Rubin, D. B. (2013). *Bayesian Data Analysis* (3rd ed.). Chapman & Hall/CRC Boca Raton, FL, USA.

Ghajarkhosravi, M., Huang, Y., Fung, A. S., Kumar, R., & Straka, V. (2020). Energy benchmarking analysis of multi-unit residential buildings (MURBs) in Toronto, Canada. *Journal of Building Engineering*, *27*(July 2019), 100981. https://doi.org/10.1016/j.jobe.2019.100981

Giri, S., & Bergés, M. (2015). An energy estimation framework for event-based methods in Non-Intrusive Load Monitoring. *Energy Conversion and Management*, *90*, 488–498. https://doi.org/10.1016/j.enconman.2014.11.047

Gold, R., Waters, C., & York, D. (2020). *Leveraging Advanced Metering Infrastructure to Save Energy*. American Council for an Energy-Efficient Economy (ACEEE). https://aceee.org/research-report/u2001

Google. (2021). *Nest thermostat*. https://store.google.com/us/product/nest_thermostat

Gopinath, R., Kumar, M., Chandra Joshua, C. P., & Srinivas, K. (2020). Energy management using non-intrusive load monitoring techniques - State-of-the-art and future research directions. *Sustainable Cities and Society*, *62*(June), 102411. https://doi.org/10.1016/j.scs.2020.102411

Gronau, Q. F., Singmann, H., & Wagenmakers, E.-J. (2020). bridgesampling: An R Package for Estimating Normalizing Constants. *Journal of Statistical Software*, *92*(10). https://doi.org/10.18637/jss.v092.i10

Ham, S. woo. (2020). *Multifamily normalization toy example*. https://github.com/ecosang/multifamily_normalization_toy_example

Ham, S. woo. (2021). *Liu-West Filter for a building Gray-box model*. https://github.com/ecosang/building_lw_filter

Ham, S. woo, & Karava, P. (2020). Online model for unit-level heating and cooling energy use prediction in multi-family residential buildings for eco-feedback design. *Submitted to Journal of Building Performance Simulation*.

Ham, S. woo, Karava, P., Bilionis, I., & Braun, J. (2021). A data-driven model for building energy normalization to enable eco-feedback in multi-family residential buildings with smart and connected technology. *Journal of Building Performance Simulation*, *14*(4), 343–365. https://doi.org/10.1080/19401493.2021.1928755

Hammerstrom, D. J., Ambrosio, R., Carlon, T. A., DeSteese, J. G., Horst, G. R., Kajfasz, R., Kiesling, L. L., Michie, P., Pratt, R. G., Yao, M., Brous, J., Chassin, D. P., Guttromson, R. T., Jarvegren, O. M., Katipamula, S., Le, N. T., Oliver, T. V, & Thompson, S. E. (2007). *Pacific Northwest GridWise™ Testbed Demonstration Projects; Part I. Olympic Peninsula Project*. https://doi.org/10.2172/926113

Han, J., Kamber, M., & Pei, J. (2012). 3 - Data Preprocessing. In J. Han, M. Kamber, & J. B. T.-D. M. (Third E. Pei (Eds.), *The Morgan Kaufmann Series in Data Management Systems* (pp. 83–124). Morgan Kaufmann. https://doi.org/https://doi.org/10.1016/B978-0-12-381479-1.00003-4

Harding, M., & Lamarche, C. (2016). Empowering Consumers Through Data and Smart Technology: Experimental Evidence on the Consequences of Time-of-Use Electricity Pricing Policies. *Journal of Policy Analysis and Management*, *35*(4), 906–931. https://doi.org/https://doi.org/10.1002/pam.21928

Huchuk, B., O'Brien, W., & Sanner, S. (2018). A longitudinal study of thermostat behaviors based on climate, seasonal, and energy price considerations using connected thermostat data. *Building and Environment*, *139*(May), 199–210. https://doi.org/10.1016/j.buildenv.2018.05.003

Indianapolis Power & Light Company. (2018). *RATE RS RESIDENTIAL SERVICE*. https://www.aesindiana.com/sites/default/files/2021-02/Residential_Rates_ Rate RS_Effective 10-29-2020.pdf

Jain, R. K., Smith, K. M., Culligan, P. J., & Taylor, J. E. (2014). Forecasting energy consumption of multi-family residential buildings using support vector regression: Investigating the impact of temporal and spatial monitoring granularity on performance accuracy. *Applied Energy*, *123*, 168–178. https://doi.org/10.1016/j.apenergy.2014.02.057

Jain, R. K., Taylor, J. E., & Peschiera, G. (2012). Assessing eco-feedback interface usage and design to drive energy efficiency in buildings. *Energy and Buildings*, *48*, 8–17. https://doi.org/10.1016/j.enbuild.2011.12.033

Jang, H., & Kang, J. (2016). A stochastic model of integrating occupant behaviour into energy simulation with respect to actual energy consumption in high-rise apartment buildings. *Energy and Buildings*, *121*, 205–216. https://doi.org/10.1016/j.enbuild.2016.03.037

Jang, H., & Kang, J. (2018). An energy model of high-rise apartment buildings integrating variation in energy consumption between individual units. *Energy and Buildings*, *158*, 656–667. https://doi.org/10.1016/j.enbuild.2017.10.047

Joe, J., Karava, P., Hou, X., Xiao, Y., & Hu, J. (2018). A distributed approach to model-predictive control of radiant comfort delivery systems in office spaces with localized thermal environments. *Energy and Buildings*, *175*, 173–188. https://doi.org/10.1016/j.enbuild.2018.06.068

Jones, R. V., Fuertes, A., & Lomas, K. J. (2015). The socio-economic, dwelling and appliance related factors affecting electricity consumption in domestic buildings. *Renewable and Sustainable Energy Reviews*, *43*, 901–917. https://doi.org/10.1016/j.rser.2014.11.084

Kantas, N., Doucet, A., Singh, S. S., Maciejowski, J., & Chopin, N. (2015). On Particle Methods for Parameter Estimation in State-Space Models. *Statistical Science*, *30*(3), 328–351. https://doi.org/10.1214/14-STS511

Karlin, B., Zinger, J. F., & Ford, R. (2015). The effects of feedback on energy conservation: A meta-analysis. In *Psychological Bulletin* (Vol. 141, Issue 6, pp. 1205–1227). American Psychological Association. https://doi.org/10.1037/a0039650

Kelly, J., & Knottenbelt, W. (2016, May). Does disaggregated electricity feedback reduce domestic electricity consumption? A systematic review of the literature. *Conference: 3rd International NILM Workshop, At Vancouver, Canada*.

Khawaja, M. S., & Stewart, J. (2014). Long-Run Savings and Cost-Effectiveness of Home Energy Reports Programs. *Cadmus Group Inc. October*.

Khosrowpour, A., Xie, Y., Taylor, J. E., & Hong, Y. (2016). One size does not fit all: Establishing the need for targeted eco-feedback. *Applied Energy*, *184*, 523–530. https://doi.org/10.1016/j.apenergy.2016.10.036

Kimura, O., Komatsu, H., Nishio, K., & Mukai, T. (2018). A prototype tool for automatically generating energy-saving advice based on smart meter data. *Energy Efficiency*. https://doi.org/10.1007/s12053-018-9639-3

Kleiminger, W., Mattern, F., & Santini, S. (2014). Predicting household occupancy for smart heating control: A comparative performance analysis of state-of-the-art approaches. *Energy and Buildings*, *85*, 493–505. https://doi.org/10.1016/j.enbuild.2014.09.046

Kolter, J. Z., & Ferreira Jr., J. (2011). A Large-scale Study on Predicting and Contextualizing Building Energy Usage. *Proceedings of the Twenty-Fifth AAAI Conference on Artificial Intelligence*, 1349–1356. http://dl.acm.org/citation.cfm?id=2900423.2900637

Konstantakopoulos, I. C., Barkan, A. R., He, S., Veeravalli, T., Liu, H., & Spanos, C. (2019). A deep learning and gamification approach to improving human-building interaction and energy efficiency in smart infrastructure. *Applied Energy*, *237*(September 2018), 810–821. https://doi.org/10.1016/j.apenergy.2018.12.065

Kruschke, J. (2014). *Doing Bayesian data analysis: A tutorial with R, JAGS, and Stan*. Academic Press.

Kucukelbir, A., Tran, D., Ranganath, R., Gelman, A., & Blei, D. M. (2017). Automatic Differentiation Variational Inference. *J. Mach. Learn. Res.*, *18*(1), 430–474.

Kwac, J., & Rajagopal, R. (2016). Data-Driven Targeting of Customers for Demand Response. In *IEEE Transactions on Smart Grid* (Vol. 7, Issue 5, pp. 2199–2207). https://doi.org/10.1109/TSG.2015.2480841

Langevin, J., Gurian, P. L., & Wen, J. (2013). Reducing energy consumption in low income public housing: Interviewing residents about energy behaviors. *Applied Energy*, *102*, 1358–1370. https://doi.org/10.1016/j.apenergy.2012.07.003

Laskey, A., & Kavazovic, O. (2011). OPOWER Energy efficiency through behavioral science and technology. *XRDS*, *17*(4), 47–51. https://doi.org/10.1145/1961678.1961687

Lee, Z. E., & Zhang, K. M. (2021). Scalable identification and control of residential heat pumps: A minimal hardware approach. *Applied Energy*, *286*(July 2020), 116544. https://doi.org/10.1016/j.apenergy.2021.116544

Liang, M., Meng, Y., Lu, N., Lubkeman, D., & Kling, A. (2019). HVAC load Disaggregation using Low-resolution Smart Meter Data. *2019 IEEE Power & Energy Society Innovative Smart Grid Technologies Conference (ISGT)*, 1–5. https://doi.org/10.1109/ISGT.2019.8791578

Liu, J., & West, M. (2001). Combined Parameter and State Estimation in Simulation-Based Filtering. In A. Doucet, N. de Freitas, & N. Gordon (Eds.), *Sequential Monte Carlo Methods in Practice* (pp. 197–223). Springer New York. https://doi.org/10.1007/978-1-4757-3437-9_10

Ljung, L. (1999). *System Identification: Theory for User* (2nd ed.). Prentice Hall.

Lopes, H., & Tsay, R. S. (2011). Particle filters and Bayesian inference in financial econometrics. *Journal of Forecasting*, *30*(1), 168–209. https://doi.org/10.1002/for

Mäkivierikko, A. (2019). Designing Energy Feedback for a Local Social Network. *Energy and Buildings*. https://doi.org/https://doi.org/10.1016/j.enbuild.2019.06.038

Malhortra, M., Im, P., Accawi, G., Ternes, M., & MacDonald, M. (2018). *Multifamily Tool for Energy Audits (MulTEA) Engineering Manual (Version 1)*. Oak Ridge National Laboratory.

Malinick, T., Wilairat, N., Holmes, J., & Perry, L. (2012). Destined to Disappoint: Programmable Thermostat Savings are Only as Good as the Assumptions about Their Operating Characteristics. *ACEEE Summer Study on Energy Efficiency in Buildings*, *7*, 162–173.

Maruejols, L., & Young, D. (2011). Split incentives and energy efficiency in Canadian multi-family dwellings. *Energy Policy*, *39*(6), 3655–3668. https://doi.org/10.1016/j.enpol.2011.03.072

McElreath, R. (2020). *Statistical rethinking: A Bayesian course with examples in R and Stan*. CRC press.

McLoughlin, F., Duffy, A., & Conlon, M. (2015). A clustering approach to domestic electricity load profile characterisation using smart metering data. *Applied Energy*, *141*, 190–199. https://doi.org/10.1016/j.apenergy.2014.12.039

Meier, A., Aragon, C., Peffer, T., Perry, D., & Pritoni, M. (2011). Usability of residential thermostats: Preliminary investigations. *Building and Environment*, *46*(10), 1891–1898. https://doi.org/10.1016/j.buildenv.2011.03.009

Meier, A., Ueno, T., & Pritoni, M. (2019). Using data from connected thermostats to track large power outages in the United States. *Applied Energy*, *256*(September), 113940. https://doi.org/10.1016/j.apenergy.2019.113940

Mitchell, J. W., & Braun, J. E. (2012). *Principles of Heating, Ventilation, and Air Conditioning in Buildings* (1st ed.). Wiley.

Moeller, S., Weber, I., Schröder, F., Bauer, A., & Harter, H. (2020). Apartment related energy performance gap – how to address internal heat transfers in multi-apartment buildings. *Energy and Buildings*, *215*, 109887. https://doi.org/https://doi.org/10.1016/j.enbuild.2020.109887

Mullen, K. M., Ardia, D., Gil, D. L., Windover, D., & Cline, J. (2011). DEoptim: An R Package for Global Optimization by Differential Evolution. *Journal of Statistical Software; Vol 1, Issue 6 (2011)* . https://doi.org/10.18637/jss.v040.i06

Murphy, K. P. (2012). *Machine learning: a probabilistic perspective*. MIT press.

Murphy, K. P. (2021). *Probabilistic Machine Learning: An introduction*. MIT Press. probml.ai

Nagler, T. (2017). kdevine: Multivariate Kernel Density Estimation with Vine Copulas. *R Package Version 0.3. 0*.

Nest Labs. (2015). *Energy Savings from the Nest Learning Thermostat: Energy Bill Analysis Results*. Nest White Paper.

Northeast Energy Efficiency Partnerships. (2015). *Opportunities for Home Energy Management Systems (HEMS) in Advancing Residential Energy Efficiency Programs*. NEEP HEMS Research Report, Northeast Energy Efficiency Partnerships, Inc.

NREL. (2019). *Preparing for a City-Scale Building Energy Upgrade Analysis: A Case Study for New York City*. National Renewable Energy Laboratory.

Omar, F., Bushby, S. T., & Williams, R. D. (2017). A self-learning algorithm for estimating solar heat gain and temperature changes in a single-Family residence. *Energy and Buildings*, *150*, 100–110. https://doi.org/10.1016/j.enbuild.2017.06.001

Paiho, S., Hedman, Å., Abdurafikov, R., Hoang, H., Sepponen, M., Kouhia, I., & Meinander, M. (2013). Energy saving potentials of Moscow apartment buildings in residential districts. *Energy and Buildings*, *66*, 706–713. https://doi.org/10.1016/j.enbuild.2013.07.084

Pereira, L., & Nunes, N. (2020). An empirical exploration of performance metrics for event detection algorithms in Non-Intrusive Load Monitoring. *Sustainable Cities and Society*, *62*(January), 102399. https://doi.org/10.1016/j.scs.2020.102399

Pisharoty, D., Yang, R., Newman, M. W., & Whitehouse, K. (2015). ThermoCoach: Reducing Home Energy Consumption with Personalized Thermostat Recommendations. *Proceedings of the 2Nd ACM International Conference on Embedded Systems for Energy-Efficient Built Environments*, 201–210. https://doi.org/10.1145/2821650.2821671

Pitt, M. K., & Shephard, N. (1999). Filtering via Simulation: Auxiliary Particle Filters. *Journal of the American Statistical Association*, *94*(446), 590–599. https://doi.org/10.1080/01621459.1999.10474153

Pritoni, M., Woolley, J. M., & Modera, M. P. (2016). Do occupancy-responsive learning thermostats save energy ? A field study in university residence halls. *Energy & Buildings*, *127*, 469–478. https://doi.org/10.1016/j.enbuild.2016.05.024

Qi, N., Cheng, L., Xu, H., Wu, K., Li, X. L., Wang, Y., & Liu, R. (2020). Smart meter data-driven evaluation of operational demand response potential of residential air conditioning loads. *Applied Energy*, *279*(October), 115708. https://doi.org/10.1016/j.apenergy.2020.115708

Radecki, P., & Hencey, B. (2017). Online Model Estimation for Predictive Thermal Control of Buildings. *IEEE Transactions on Control Systems Technology*, *25*(4), 1414–1422. https://doi.org/10.1109/TCST.2016.2587737

Reina, V. J., & Kontokosta, C. (2017). Low hanging fruit? Regulations and energy efficiency in subsidized multifamily housing. *Energy Policy*, *106*(September 2016), 505–513. https://doi.org/10.1016/j.enpol.2017.04.002

Rogers, A., Ghosh, S., Wilcock, R., & Jennings, N. R. (2013). A Scalable Low-Cost Solution to Provide Personalised Home Heating Advice to Households. *Proceedings of the 5th ACM Workshop on Embedded Systems For Energy-Efficient Buildings*, 1:1--1:8. https://doi.org/10.1145/2528282.2528284

Roth, J., & Rajagopal, R. (2018). Benchmarking building energy efficiency using quantile regression. *Energy*, *152*, 866–876. https://doi.org/10.1016/j.energy.2018.02.108

Rotondo, J., Johnson, R., Gonzalez, N., Waranowski, A., Badger, C., Lange, N., Goldman, E., & Foster, R. (2016). *Overview of Existing and Future Residential Use Cases for Connected Thermostats*. Report prepared by Energetics Incorporated and Vermont Energy Investment Corporation (VEIC) for the U.S. Department of Energy, Office of Energy Efficiency and Renewable Energy Building Technologies Office.

Rouchier, S., Jiménez, M. J., & Castaño, S. (2019). Sequential Monte Carlo for on-line parameter estimation of a lumped building energy model. *Energy and Buildings*, *187*, 86–94. https://doi.org/10.1016/j.enbuild.2019.01.045

Rouchier, S., Rabouille, M., & Oberlé, P. (2018). Calibration of simplified building energy models for parameter estimation and forecasting: Stochastic versus deterministic modelling. *Building and Environment*, *134*(December 2017), 181–190. https://doi.org/10.1016/j.buildenv.2018.02.043

Rouleau, J., Gosselin, L., & Blanchet, P. (2018). Understanding energy consumption in high-performance social housing buildings: A case study from Canada. *Energy*, *145*, 677–690. https://doi.org/10.1016/j.energy.2017.12.107

Sachs, O., Tiefenbeck, V., Duvier, C., Qin, A., Cheney, K., Akers, C., & Roth, K. (2012). *Field Evaluation of Programmable Thermostats*. U.S. Department of Energy, Building Technologies Program.

Salvalai, G., Sesana, M. M., & Iannaccone, G. (2017). Deep renovation of multi-storey multi-owner existing residential buildings: A pilot case study in Italy. *Energy and Buildings*, *148*, 23–36. https://doi.org/10.1016/j.enbuild.2017.05.011

Salvatier, J., Wiecki, T. V, & Fonnesbeck, C. (2016). Probabilistic programming in Python using PyMC3. *PeerJ Computer Science*, *2*, e55.

Samarripas, S., Dan York, & Lauren Ross. (2017). *More Savings for More Residents: Progress in Multifamily Housing Energy Efficiency*. American Council for an Energy-Efficient Economy.

Särkkä, S., & Solin, A. (2019). *Applied stochastic differential equations* (Vol. 10). Cambridge University Press.

Schaefer, A., & Ghisi, E. (2016). Method for obtaining reference buildings. *Energy and Buildings*, *128*, 660–672. https://doi.org/10.1016/j.enbuild.2016.07.001

Schultz, P. W. (2014). Strategies for Promoting Proenvironmental Behavior. *European Psychologist*, *19*(2), 107–117. https://doi.org/10.1027/1016-9040/a000163

Schultz, P. W., Nolan, J. M., Cialdini, R. B., Goldstein, N. J., & Griskevicius, V. (2007). The Constructive, Destructive, and Reconstructive Power of Social Norms. *Psychological Science*, *18*(5), 429–434. https://doi.org/10.1111/j.1467-9280.2007.01917.x

Scott, J., Brush, A. J. B., Krumm, J., Meyers, B., Hazas, M., Hodges, S., & Villar, N. (2011). PreHeat: Controlling Home Heating Using Occupancy Prediction. *UbiComp '11 Proceedings of the 13th International Conference on Ubiquitous Computing*, 281–290. https://www.microsoft.com/en-us/research/publication/preheat-controlling-home-heating-using-occupancy-prediction/

Siemann, M. J. (2013). *Performance and applications of residential building energy grey-box models*. Ph.D. dissertation, University of Maryland.

Siggelsten, S. (2014). Reallocation of heating costs due to heat transfer between adjacent apartments. *Energy and Buildings*, *75*, 256–263. https://doi.org/10.1016/j.enbuild.2014.02.022

Siggelsten, S., & Olander, S. (2013). Individual metering and charging of heat and hot water in Swedish housing cooperatives. *Energy Policy*, *61*, 874–880. https://doi.org/10.1016/j.enpol.2013.06.083

Simon, D. (2006). *Optimal state estimation: Kalman, H infinity, and nonlinear approaches*. John Wiley & Sons.

Smith, B. A., Wong, J., & Rajagopal, R. (2012). A Simple Way to Use Interval Data to Segment Residential Customers for Energy Efficiency and Demand Response Program Targeting. *ACEEE Summer Study on Energy Efficiency in Buildings*.

Soltanaghaei, E., & Whitehouse, K. (2018). Practical occupancy detection for programmable and smart thermostats. *Applied Energy*, *220*(October 2017), 842–855. https://doi.org/10.1016/j.apenergy.2017.11.024

Sparn, B., Frank, S. M., Earle, L., & Scheib, J. G. (2017). *Innovation Incubator: Whisker Labs Technical Evaluation*. National Renewable Energy Laboratory. https://doi.org/10.2172/1374964

Stan Development Team. (2020a). *Stan Reference Manual Version 2.23 - 10.6 Ordered Vector*. https://mc-stan.org/docs/2_23/reference-manual/ordered-vector.html

Stan Development Team. (2020b). *Stan User's Guide Version 2.23 - 5 Finite Mixtures*. https://mc-stan.org/docs/2_23/stan-users-guide/mixture-modeling-chapter.html

Storvik, G. (2002). Particle filters for state-space models with the presence of unknown static parameters. *IEEE Transactions on Signal Processing*, *50*(2), 281–289. https://doi.org/10.1109/78.978383

Strengers, Y. (2014). Smart Energy in Everyday Life: Are You Designing for Resource Man? *Interactions*, *21*(4), 24–31. https://doi.org/10.1145/2621931

Sussman, R., & Chikumbo, M. (2016). *Behavior Change Programs: Status and Impact*. American Council for an Energy-Efficient Economy.

U.S. Department of Energy. (2016). Advanced Metering Infraestructure and Customer Systems - Results from the Smart Grid investment grant program. In *Results from the Smart Grid investment grant program* (p. 98). U.S. Department of Energy, Office of Electricity Delivery and Energy Reliability. https://www.energy.gov/sites/prod/files/2016/12/f34/AMI Summary Report_09-26-16.pdf

U.S. Department of Energy. (2018). *Weatherization Works!* U.S. Department of Energy, Office of Energy Efficiency and Renewable Energy.

U.S. Department of Energy. (2020). *Building Energy Use Benchmarking*. https://www.energy.gov/eere/slsc/building-energy-use-benchmarking

U.S. Department of Energy. (2021a). *EnergyPlus™ Version 9.5.0 Documentation - Engineering Reference*. U.S. Department of Energy, Building Technologies Program.

U.S. Department of Energy. (2021b). *EnergyPlus™ Version 9.5.0 Documentation - Input Output Reference*.

U.S. Energy Information Administration. (2018). *Commercial Buildings Energy Consumption Survey (CBECS)*. U.S. Department of Energy.

Ueno, T., & Meier, A. (2020). A method to generate heating and cooling schedules based on data from connected thermostats. *Energy and Buildings*, *228*, 110423. https://doi.org/10.1016/j.enbuild.2020.110423

von Bomhard, T., Wörner, D., & Röschlin, M. (2016). Towards smart individual-room heating for residential buildings. *Computer Science - Research and Development*, *31*(3), 127–134. https://doi.org/10.1007/s00450-014-0282-8

Walter, T., & Sohn, M. D. (2016). A regression-based approach to estimating retrofit savings using the Building Performance Database. *Applied Energy*, *179*, 996–1005. https://doi.org/10.1016/j.apenergy.2016.07.087

Wang, J., Tang, C. Y., Brambley, M. R., & Song, L. (2019). Predicting home thermal dynamics using a reduced-order model and automated real-time parameter estimation. *Energy and Buildings*, *198*, 305–317. https://doi.org/10.1016/j.enbuild.2019.06.002

Wang, S., & Xu, X. (2006). Parameter estimation of internal thermal mass of building dynamic models using genetic algorithm. *Energy Conversion and Management*, *47*(13), 1927–1941. https://doi.org/https://doi.org/10.1016/j.enconman.2005.09.011

West, M. (1993). Approximating Posterior Distributions by Mixtures. *Journal of the Royal Statistical Society: Series B (Methodological)*, *55*(2), 409–422. https://doi.org/10.1111/j.2517-6161.1993.tb01911.x

Wörner, D., von Bomhard, T., Röschlin, M., & Wortmann, F. (2014). Look Twice: Uncover Hidden Information in Room Climate Sensor Data. *4th International Conference on the Internet of Things*, 6. https://www.alexandria.unisg.ch/245734/

Yang, R., & Newman, M. W. (2012). Living with an Intelligent Thermostat: Advanced Control for Heating and Cooling Systems. *Proceedings of the 2012 ACM Conference on Ubiquitous Computing*, 1102–1107. https://doi.org/10.1145/2370216.2370449

Yang, R., Newman, M. W., & Forlizzi, J. (2014). Making Sustainability Sustainable: Challenges in the Design of Eco-interaction Technologies. *Proceedings of the SIGCHI Conference on Human Factors in Computing Systems*, 823–832. https://doi.org/10.1145/2556288.2557380

Yang, R., Pisharoty, D., Montazeri, S., Whitehouse, K., & Newman, M. W. (2016). How Does Eco-Coaching Help to Save Energy? Assessing a Recommendation System for Energy-Efficient Thermostat Scheduling. *Proceedings of the 2016 ACM International Joint Conference on Pervasive and Ubiquitous Computing*, 1176–1187. https://doi.org/10.1145/2971648.2971698

Yang, Z., Roth, J., & Jain, R. K. (2018). DUE-B: Data-driven urban energy benchmarking of buildings using recursive partitioning and stochastic frontier analysis. *Energy and Buildings*, *163*, 58–69. https://doi.org/10.1016/j.enbuild.2017.12.040

York, D., Relf, G., & Waters, C. (2019). *Integrated Energy Efficiency and Demand Response Programs*. American Council for an Energy-Efficient Economy.

Yoshino, H., Hong, T., & Nord, N. (2017). IEA EBC annex 53: Total energy use in buildings—Analysis and evaluation methods. *Energy and Buildings*, *152*(March 2013), 124–136. https://doi.org/10.1016/j.enbuild.2017.07.038

VITA

Sang woo Ham

Ph.D., Lyles School of Civil Engineering, Purdue University (2016 – 2021)

M.S., Department of Architectural Engineering, Hanyang University (2016)

B.S., Department of Civil Engineering, Hanyang University (2014)

PUBLICATIONS

Journal papers:

1. Ham, S. woo, Karava, P., Bilionis, I., & Braun, J. (2021). A data-driven model for building energy normalization to enable eco-feedback in multi-family residential buildings with smart and connected technology. Journal of Building Performance Simulation, 14(4), 343–365.
2. Ham, S. woo, Karava, P., Bilionis, I., & Braun, J. (2021). Real-time model for unit-level heating and cooling energy use prediction in multi-family residential buildings for eco-feedback design, Submitted to Journal of Building Performance Simulation.

Conference papers:

1. Ham, S.-W., and Karava, Panagiota., Online Building Energy Model to Evaluate Heating and Cooling-related Behavior Changes for Eco-feedback in a Multifamily Residential Building, Proceedings of the 16th IBPSA Building Simulation Conference, Rome, Italy, Sept. 2-4, 2019, Page 2379-2387.
2. Ham, S.-W., and Karava, Panagiota., Identifying Peer Groups in a Multifamily Residential Building for Eco-Feedback Design, 2018 International High Performance Buildings Conference, Paper 319.